Data Collection Optimization for UAV-Assisted Wireless Sensor Networks

Mengyu Chen

A thesis submitted for the degree of

Doctor of Philosophy of

The Australian National University

May 2023

Except where otherwise indicated, this thesis is my own original work.

Mengyu Chen

1 May 2023

To my dear family who always respect my decisions and unconditionally support me to pursue my dreams.

Declaration

This thesis is a presentation of the original work except where otherwise stated. I completed this work jointly with Professor Weifa Liang. My contribution to the work is around 90%.

Mengyu Chen

1 May 2023

Acknowledgments

This thesis becomes a reality with the generous help and support from many individuals. I would like to extend my sincere gratitude to all of them.

Works in this thesis are conducted and completed under the supervision of my former supervisor, Professor Weifa Liang. I started my research career under the guidance of Prof. Liang since my honour year at the Australian National University. Without the dedicated support and guidance of Prof. Liang, I can not continue my study as a Ph.D. student and my achievement during my Ph.D. would not be possible. Words can not express my gratitude to Prof. Liang for his patience, dedication and professional supervision to enlighten me on the promising study field, while showing us a role model to be an open-minded, diligent, dedicated and independent researcher.

This endeavor would not have been possible without the encouragement, support and guidance of my supervisor Dr. Zhenchang Xing. I'm extremely grateful to Dr. Xing for his significant support in guiding me to continue my Ph.D. study. Honestly speaking, I felt stressed about changing topics and learning from scratch in the third year of my Ph.D. which was caused by the unexpected issues. However, the great patience and professional guidance of Dr. Xing significantly improved my confidence to conquer difficulties. His insight and professional knowledge with thoughtful recommendations steered me in the right direction to develop my technical skills and research ability to conduct pioneering and impactful research.

I am grateful to the Australian National University (ANU), which gave me the opportunity to conduct my Ph.D. research. I also appreciate for the ANU Ph.D. Scholarship (international) and the HDR Fee Remission Merit Scholarship provided by the Australian National University to financially support me to pursue my Ph.D. degree. I am also thankful for the staff in the Research School of Computer Science at the Australian National University, for their generous help and assistance in various aspects. Hanna Kurniawati deserves to be especially appreciated for promptly addressing my candidature issues with considerate plans.

I am deeply indebted to my family for the unconditional love. I am so lucky to have a giving and caring family that fills my heart with strength, joy and love. Like a sturdy and well-laid foundation, my family allows me to grow and flourish with great courage and confidence to handle difficulties in my life. They always respect my decisions and support me to pursue my dreaming life. My gratitude to my family is infinite and endless.

Finally, I would like to express my sincere appreciation to my fantastic friends. With the company and support of my friends, I feel a strong sense of safety and belonging. I appreciate all of the time together, with laughs, help and unforgettable memories. My friends are my light in the darkness and I feel so grateful that I always have shoulders of my friends to lean on when times are tough. They bring tremendous positive energy to me and definitely nourish my soul.

Publications

Conference

[1] Mengyu Chen, Weifa Liang, Yuchen Li. Data collection maximization for UAV-enabled wireless sensor networks. In *Proceedings of the International Conference on Computer Communications and Networks* (ICCCN), pp. 1–9, IEEE, 2020.

[2] Mengyu Chen, Weifa Liang, Sajal K. Das. Data collection utility maximization in wireless sensor networks via efficient determination of UAV hovering locations. In *Proceedings of the 2021 IEEE International Conference on Pervasive Computing and Communications* (PerCom), pp. 1-10, IEEE, 2021.

[3] Mengyu Chen, Weifa Liang, Jing Li. Energy-efficient data collection maximization for UAV-assisted wireless sensor networks. In *Proceedings of IEEE Wireless Communications and Networking Conference* (WCNC), pp. 1-7, IEEE, 2021.

[4] Jing Li, Weifa Liang, Mengyu Chen, Zichuan Xu. Mobility-aware dynamic service placement in D2D-assisted MEC environments. In *Proceedings of IEEE Wireless Communications and Networking Conference* (WCNC), pp. 1-6, IEEE, 2021.

Abstract

The last decade witnessed rapid advancement of digital technology, such as the Internet of Things (IoT), having enormous applications in various domains. Wireless Sensor Networks (WSNs) play a central role in the context of IoT for providing a massive amount of data captured by ubiquitous sensors. Thus, data collection becomes crucial to feed fresh data into IoT services while avoiding data overwritten due to limited storage capacities of IoT sensors. With high agility, mobility and flexibility, the Unmanned Aerial Vehicles (UAVs) have recently received considerable attention for data collection in WSNs.

In this thesis, we investigated novel problems for optimizing the data collection efficiency in UAV-assisted WSNs. We conducted studies to maximize data collection volume via UAV hovering duration allocation. Furthermore, we studied the maximization of the data collection utility by jointly considering the UAV hovering location recognition and the UAV hovering duration allocation. We also investigated the design for UAV data collection trajectory, with the consideration of the UAV energy consumption on both hovering and mechanical movement, where the variation of the data transmission rate is also considered.

We firstly address the UAV hovering duration allocation problem, which is a fundamental but crucial issue for data collection optimization. For WSNs with a special deployment, we develop an optimal algorithm which guarantees the maximized volume of collected data. For general cases, we devise an efficient algorithm with a provable approximation ratio, which significantly

improves the data collection efficiency.

We secondly deal with the UAV hovering location identification problem. It is widely considered to be intractable to precisely determine the UAV's hovering locations from infinitely many potential ones jointly with the data collection. Most existing studies either neglect this critical issue or discretize the UAV serving area into small regions with a given size, which results in the inevitable utility loss of data collection. To tackle this problem, we propose a novel algorithm to precisely determine the UAV's potential hovering locations and devise an efficient approximation algorithm with guaranteed data collection performance.

We thirdly explore the UAV traveling trajectory designing problem, which focuses on both the hovering location identification of the UAV and the UAV traveling path designing for improving data collection efficiency in WSNs. We consider the energy consumption of the UAV on both hovering and mechanical movement together with the variation of sensors' data transmission rate, and develop a promising algorithm to find a closed UAV data collection tour for maximizing the data collection volume.

We finally evaluate the performance of all proposed algorithms in this thesis through experimental simulations. Simulation results show that the proposed algorithms significantly outperform existing algorithms.

Contents

List of Figures

Chapter 1

Introduction

1.1 Internet of Things and Wireless Sensor Networks

The momentous developments of digital technology over the last decade enable the breakthrough of Internet of Things (IoT), which is progressively acts as a vital part of our daily life. With communications among smart devices and sensors through internet, IoT delivers solutions for numerous challenges related to business, governmental and public/private industries across the world [Sfar et al., 2017]. In recent years, IoT products have been increasingly popular, such as home automation devices, wearable health monitors and smart vehicles, which significantly enhances living standards of individuals in various domains including healthcare [Mavrogiorgou et al., 2019], education [Al-Emran et al., 2020], transportation [Sutar et al., 2016] and public safety [Fraga-Lamas et al., 2016]. Fig. 1.1 shows an illustrative example of some IoT devices for Smart Home. IoT also brings unneglectable benefits when applied to industries, enhancing productivity, improving agility while saving overall costs [Chowdhury and A Raut, 2019].

Regarded as one of the five essential IoT technologies, Wireless Sensor Networks (WSNs) play a crucial role in developing IoT-based products and

Figure 1.1: An illustrative example of some IoT devices for Smart Home.

services [Lee and Lee, 2015] by providing a massive amount of data captured by sensors.

WSNs are employed in a variety of monitoring and control applications including environmental monitoring [Othman and Shazali, 2012], health caring [Alemdar and Ersoy, 2010], military surveillance [Đurišić et al., 2012] and smart home [Li and Lin, 2015]. Fig. 1.2 and Fig. 1.3 show illustrative examples of WSNs for monitoring wildlife and equipment in factory respectively.

As the core components of WSNs, spatial or densely dispersed sensors are exploited to sense and collect data from their surroundings. Each sensor node is a tiny device, equipped with a miniaturized on-board storage with limited capacities. Sensory data are continuously generated and temporarily stored at each sensor. Constrained by the on-board storage capacity, data at sensors are likely to be overwritten if the sensing data cannot be collected in time.

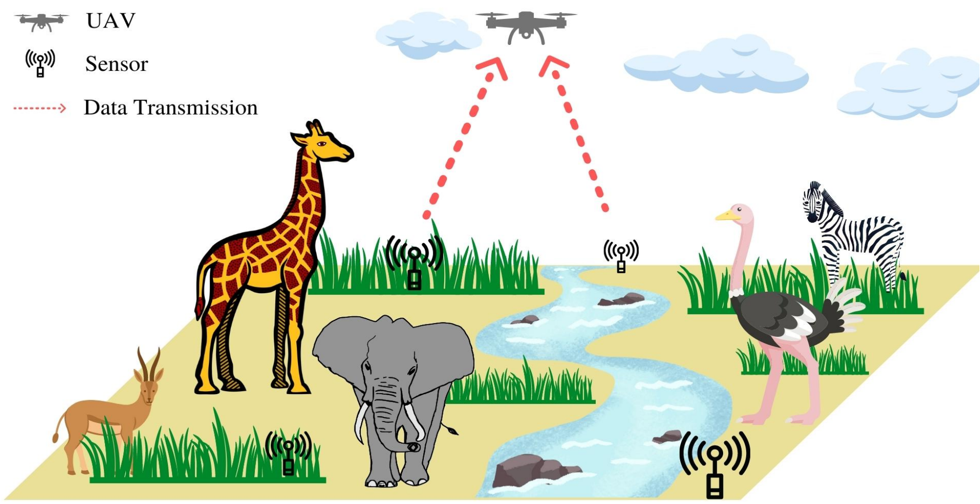

Figure 1.2: An illustrative example of wireless sensor networks for monitoring wildlife.

1.2 Data Collection in Wireless Sensor Networks

Conventionally, data collection is achieved in WSNs through multi-hop transmissions scheme, where sensors transmit their data to a data station via many other sensors according to a pre-defined protocol. Under this scheme, data are only transmitted when two sensors are within the communication range of each other, which requires considerate deployment of sensors. For monitoring regions that are isolated from others in a WSN, a large number of additional sensors should be employed into the WSN for conducting data transmission tasks from the monitoring area to the data station, which brings extra cost for the WSNs. In addition, the energy consumption of sensors on data transmission is not neglectable. Sensors which are communicating with many other sensors are easily going out of power. Once a sensor breaks down, not only can it continue sensing, but also the multi-hop network disconnects, resulting in failures in data transmission to the data station [Gong et al., 2018b]. Owing to the limited storage of sensors, data that cannot be

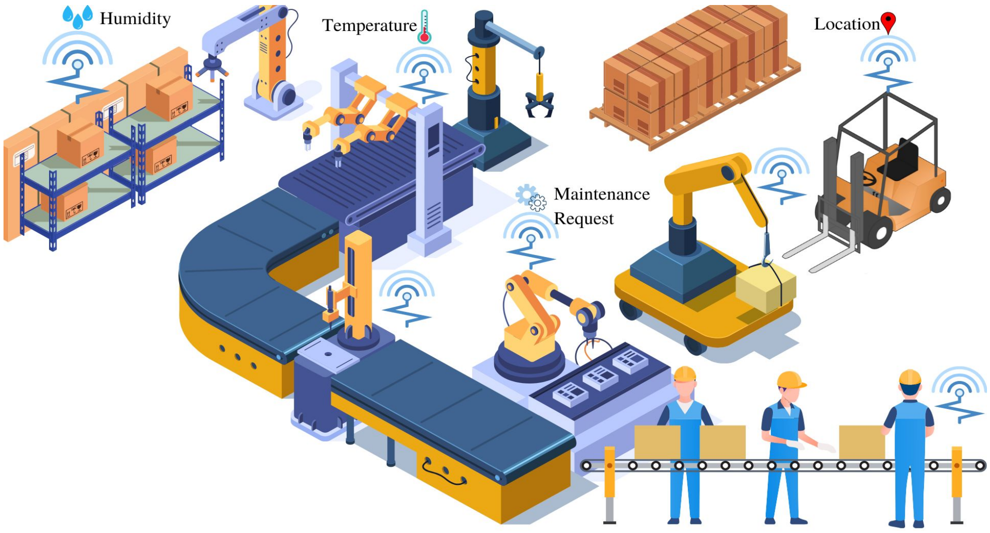

Figure 1.3: An illustrative example of wireless sensor systems in factory.

transmitted in time are likely to be overwritten by newly captured data.

To avoid data collection failures caused by the multi-hop transmission scheme, mobile vehicles are utilized for data collection in WSNs. Mobile data collection agents travel on the ground, sojourn at or nearby sensors and receive data transmitted from target sensors. Compared with the multi-hop transmission scheme, sensors are not required for transmitting data for other sensors, which enables more energy of the limited battery capacity to be spent on sensing missions. Besides, data collection from a sensor is not affected by energy exhaustion of other sensors in WSNs.

With high agility, mobility and flexibility, the Unmanned Aerial Vehicles (UAVs) have recently received considerable attention for data collection [Samir et al., 2019; Liang et al., 2018; Khochare et al., 2021]. Compared with land vehicles, UAVs can support WSNs in more complicated terrains such as towers, cliffs and other tall structures, which may be not accessible for land vehicles. When planning a data collection tour, the obstacle is also a crucial issue that limits the serving area of the data collection agents. The

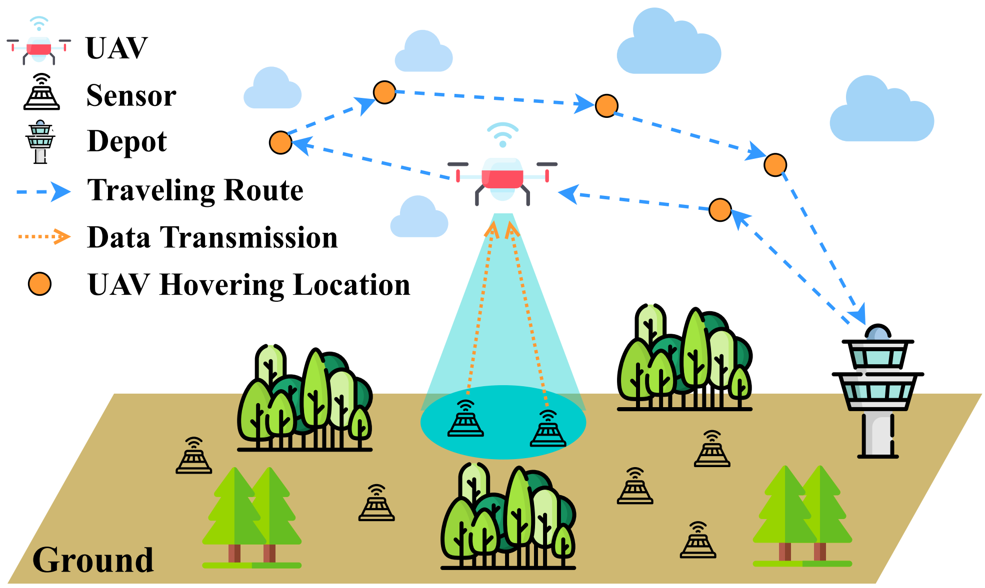

Figure 1.4: An illustrative example of data collection in a UAV-enabled WSN.

adjustability of UAV flying altitude enables more flexible traveling space for data collection service, instead of bypassing the obstructed sensors.

One or a fleet of UAVs departs from a depot, travels over a WSN and hovers at pre-defined hovering locations to collect data from sensors. After completing the data collection mission, UAVs travel to a data station, where the collected data will be stored and processed. In many scenarios, the depot is collocated with the data station.

1.2.1 Data Collection in UAV-Assisted WSNs

Many existing works investigated data collection in UAV-assisted WSNs. For example, Gong *et al.* [Gong et al., 2018a] investigated in the scenario where sensors are located on a straight line, with the objective to minimize the total aviation time of a UAV to collect a certain volume of data from each sensor. In this paper, only one sensor is served at each time.

Low-altitude UAVs are utilized by Nazib *et al.* [Nazib and Moh, 2021] to reduce the energy consumption of WSNs. They developed an energy-efficient and fast data collection scheme in UAV-aided WSNs for hilly areas to deploy a UAV as a data mule. They proposed a central bias hybrid energy-efficient distributed clustering algorithm for grouping the sensors and optimized the UAV position by applying a modified tabu search algorithm for data collection. They also developed a traveling salesman problem and solved it by utilizing a modified genetic algorithm.

Samir *et al.* [Samir et al., 2019] explored the maximization of the network throughput from time-constrained devices via a single UAV, where each device had a data uploading deadline. Khelifi *et al.* [Khelifi et al., 2018] developed a localization method to reduce the power utilization of complete network while enhancing the network lifetime, depending upon the weighted centroid localization module. Jia *et al.* [Jia et al., 2021] considered the Low Earth Orbit (LEO) satellite-assisted UAV data collection for the Internet of Remote Things (IoRT) sensors. They studied two transmission modes for the delay-tolerant and the delay-sensitive scenarios respectively, where for the delay-tolerant scenario, the carry-store mode of UAVs to Earth is leveraged and for the delay-sensitive, the UAV-satellite network is leveraged to transmit data to Earth.

Sun *et al.* [Sun et al., 2021] focused on the temporal value of collected data, with the Age of Information (AoI) as a performance metric to quantify the temporal correlation among data packets consecutively sampled by the Internet of Things (IoT) devices. They explored an AoI-energy-aware data collection scheme, with the objective to minimize the weighted sum of expected average AoI, the UAV propulsion energy, and IoT devices' transmission energy, by jointly optimizing the UAV flight speed, hovering locations, and bandwidth allocation for data collection. Yi *et al.* [Yi et al., 2020] also explored the freshness of collected data. They studied the fresh data collection problem in UAV-assisted IoT networks, where the UAV travels to collect status update packets from sensors within a given duration under the energy constraint. With the aim of minimizing the weighted sum of the age of information (AoI), they focused on finding the optimal flight trajectory of the UAV and transmission scheduling of the sensors. They also developed an algorithm with reinforcement learning to overcome the curse of dimensionality.

Cao *et al.* [Cao et al., 2017] investigated event-related issues of data collection, and proposed a cloud-assisted data gathering strategy in the light of emerging events. They also developed a cloud-assisted approach for delivering the optimal traveling and data gathering sequence of a WSN cluster for the UAV.

Poudel*et al.* [Poudel and Moh, 2021] investigated the hybrid path planning for efficient data collection in UAV-aided WSNs for emergency applications, where timely data collection from sensor nodes and data transmission to the base station (BS) is a prime requisite. They also considered the environment comprising various obstacles, where the path should be ensured to efficiently reach the target point.

Both the Orthogonal Frequence Division Multiple Access (OFDMA) technique [Mozaffari et al., 2016] and the power-domain Non-Orthogonal Multiple Access (NOMA) protocol [Farajzadeh et al., 2019] supports for One-to-many data collection scheme. By adopting OFDMA or NOMA, multiple sensors can transmit data to the deployed UAV simultaneously as long as the Euclidean distance between the sensor and the UAV is no greater than the data transmission range of the sensor, which significantly improves the data collection efficiency. For example, with the assumption that IoT devices can utilize the OFDMA technique, Mozaffari *et al.* [Mozaffari et al., 2016] studied the minimization of the transmission energy consumption of ground IoT devices, in terms of finding an optimal trajectory for each of multiple UAVs, where the UAV can collect data from multiple sensors simultaneously. In [Farajzadeh et al., 2019], NOMA protocol is adopted for data collection from long-range backscatter devices via UAV.

1.3 Research Topics

A UAV hovering location is a location at the UAV flying altitude, where the UAV hovers to collect data from sensors. Based on the UAV hovering location, a data collection trajectory is a sequence of UAV hovering locations that the UAV visits in order during a data collection tour. The UAV hovering duration is the corresponding hovering time for the UAV when it hovers at a certain hovering location. The data collection volume is the amount of data that the UAV collects from sensors. We use data collection utility to describe the profit from data collection.

Since the energy of UAV is constrained by its battery capacity, the UAV may not be able to collect all data from a WSN before it goes out of power. Unlike other data collection agents serving on the ground, UAV suffering from energy exhaustion will crash and may lose the data collected among the tour, the planning about the UAV working tour before its departure thus is crucial. There are many factors that impact data collection efficiency at each tour.

In this thesis, we study data collection planning for UAV in terms of UAV hovering duration allocation, UAV hovering location identification and data collection trajectory designing, with the objective to optimize the data collection performance.

Specifically, we will address three main issues to optimize the data collection performance: (1) given a hovering budget and a finite set of hovering location candidates for the UAV, which hovering location candidates should be selected and how long the UAV should sojourn at each selected location; (2) without pre-defined hovering location candidates, how to identify hovering locations for the UAV from infinitely many potential ones to maximize the data collection utility; and (3) how to plan a closed data collection tour for the UAV including a sequence of selected hovering locations with corresponding hovering duration at each selected one.

Due to the energy constraint of the UAV, the identification of hovering locations of UAV, the hovering duration determination at each selected location and the location visiting sequence determination significantly impact the data collection efficiency in the scheme where a UAV is able to collect data from multiple sensors simultaneously, the aforementioned three topics thus are requisites for data collection performance optimization in UAV-assisted WSNs.

Solutions to topic (1) provide the duration allocation at each selected hovering location, with the assumption that a finite set of location candidates are pre-defined. As a prerequisite for solutions to topic (1), topic (2) is to identify a finite set of hovering location candidates from infinitely many ones, with a further complicated task to maximize the data collection utility.

Both topic (1) and topic (2) are studied under the scenario where data at each sensor can be partially collected. To be specific, it is allowed to have remaining data uncollected from each sensor. However, there are some scenarios where data from a sensor should be fully collected. For example, for certain sensors of WSNs in wild fields which have captured traces of targeting animals, the UAV cannot distinguish the portion of data which covers the activities of animals. If the UAV is not required to fully collect data from sensors, it is very likely to collect the data without animals and leave the desired data behind. To deal with this problem, topic (3) explores another common situation where data at each sensor are required to be fully collected. Solutions to topic (3) deliver a closed data collection tour for the UAV, which includes not only the duration allocation at each selected hovering location, but also the visiting order of each selected location. The impacts of the variation of the data transmission rate of each sensor are also considered in topic (3).

1.3.1 UAV Hovering Duration Allocation for Data Collection Maximization

Under the one-to-many data collection scheme, the UAV can collect data from multiple sensors simultaneously as long as these sensors are located within the data collection range of the UAV. In the situation where the data transmission rate of each sensor is identical, the volume of collected data at each time slot by the UAV is determined by the number of the sensors within the UAV's data collection range, whose data have not been fully collected. The hovering duration allocation over UAV hovering location candidates thereby significantly impacts the data collection volume during each data collection tour. To optimize the UAV data collection performance, we thus firstly explored a fundamental topic about the UAV hovering duration allocation.

To be specific, given a hovering duration budget for the UAV, which hovering location candidates should be selected and how long the UAV should hover at each selected hovering location to maximize the volume of collected data during a data collection tour. To enhance the data collection volume, we allow the UAV to partially collect data from sensors, and data at each sensor can be collected for multiple times.

1.3.2 Hovering Location Identifications for Utility Maximization

For the sake of tractability, most of the existing approaches discretize the UAV serving area into different regions with certain sizes, where each region is regarded as a potential UAV hovering spot. However, the locations in a discretized region cannot be distinguished from each other, which results in the inevitable utility loss of data collection. Moreover, the time complexity of discretization-based approaches highly depends on the size of the network monitoring area, making the data collection inefficient, especially for large-scale WSNs.

To address the aforementioned challenges, we consider the UAV hovering location determination jointly with data collection utility maximization, under the one-to-many data collection scheme, where the total hovering duration of the UAV is constrained by a given budget. Tackling this problem poses many challenges. For example, to avoid the utility loss caused by discretizations, determining precise hovering locations for the UAV from the infinitely many potential ones is non-trivial. Moreover, jointly considering the hovering location determination and the data collection utility maximization, while separating the computational complexity from the network size, makes the problem further complex. Finally, the allocation of UAV hovering budget at each selected hovering location also impacts the data collection utility significantly.

1.3.3 UAV Trajectory Designing for Data Collection Maximization

The designing of the UAV data collection tour is quite challenging considering the energy consumption of the UAV on both mechanical movement and hovering, with an energy constraint for the UAV. Since the mechanical movement of the UAV consumes energy, it is intuitive to enable the UAV to spend a smaller percentage of energy on traveling while spending a larger percentage of energy on hovering, the hovering locations which are relatively close to the depot thus are preferred.

However, considering the data collection efficiency in the one-to-many data collection scheme, it is likely that the UAV can collect the largest amount of data from hovering locations which are relatively far away from the depot in a certain period. How to balance the trade-off between the energy consumed on hovering and traveling for the UAV thus is crucial to maximizing the data collection volume. The variation of the data transmission rate makes the related problems further complicated. To be specific, the data collection rate from a sensor is non-identical when the UAV hovers at different locations, which is dependent on the Euclidean distance between the sensor and the UAV. There are infinitely many potential hovering locations in the UAV serving area and each location is corresponding to different data collection rates for the set of sensors, the identification of a finite set of hovering locations for the UAV thus impacts the data collection efficiency significantly.

1.4 Thesis Contributions

The main contributions of this thesis are to systematically study data collection maximization problems in UAV-assisted WSNs under the one-to-many data collection scheme, by formulating non-trivial optimization problems, showing the NP-hardness of the proposed problems and developing efficient approximation or heuristic algorithms to the problems. The maximization of data collection is studied in terms of the UAV hovering duration allocation, the UAV hovering location identification and the UAV data collection trajectory designing. Specifically, the main contributions of this thesis are as follows.

- Unlike most existing studies that the data from all sensors within the data reception range of the UAV must be fully collected, in Chapter 2, we assume that the data stored at a sensor can be partially collected and can be collected through multiple times by the UAV per tour. The UAV duration allocation problem over a finite set of hovering location candidates for UAV is firstly studied in Chapter 2, via an energy-constrained UAV under the one-to-many data collection scheme with the aim to maximize the volume of collected data. Contributions to this topic include: (1) a novel multi-sensor data collection optimization problem to maximize the volume of data collected is formulated, under the assumption that the UAV can collect data from multiple sensors simultaneously, with the proof of the NP-hardness of the proposed problem; (2) a special case of the proposed problem is investigated with the constraint on the deployment of hovering location candidates, and an optimal algorithm for the special case is developed and empirically evaluated; (3) a variant of the proposed problem is explored and an efficient algorithm with guaranteed performance for the variant is devised; and (4) a novel approximation algorithm with provable approximation ratio is devised and empirically evaluated for the proposed problem without the requirement on the deployment of hovering location candidates.

- Although there exists works on data collection in UAV-enabled WSNs, it is challenging to identify the hovering locations for UAVs in the one-to-many data collection scheme. To be specific, the data collection efficiency under this scheme massively relies on the hovering locations of the UAV and the hovering duration at each such location. However, efficient determination of UAV hovering locations is widely considered to be intractable as there are infinitely many potential hovering locations in the UAV serving area. For the sake of tractability, most of the existing approaches discretize the UAV serving area into different regions with certain sizes, where each region is regarded as a potential UAV hovering spot. However, the locations in a discretized region cannot be distinguished from each other, which results in the inevitable utility loss of data collection. Moreover, the time complexity of discretization-based approaches highly depends on the size of the network monitoring area, thus making the data collection inefficient, especially for large-scale WSNs. To address the aforementioned challenges, in Chapter 3, we secondly significantly extend Chapter 2 by jointly considering the UAV hovering location positioning and the data collection utility maximization problem under the one-to-many data collection scheme, where the total hovering duration of the UAV is constrained by a given budget. To the best of our knowledge, we are the first to focus on enhancing UAV hovering location positioning to improve data collection utility in WSNs. Contributions involved in the Chapter 3 are as follows: (1) we formulate a novel data collection utility maximization problem to maximize the utility of data collection under the one-to-many data collection scheme and show that the problem is NP-hard; (2) we address the widely considered intractable UAV hovering location positioning problem by proposing a novel algorithm to precisely determine the UAV's potential hovering locations, which improves the data collection utility significantly, where we jointly consider the UAV hovering location positioning and data collection utility maximization; (3) we devise an approximation algorithm for the proposed problem with approximation ratio $(1 - \frac{1}{e})$ for the UAV hovering location positioning problem, where e is the base of the natural logarithm; and (4) we design and conduct simulation experiments to evaluate the performance of proposed algorithms, which demonstrates that the developed algorithms are promising.

- In Chapter 4, we study a more challenging data collection maximization problem considering the energy constraint on a UAV, where the UAV consumes energy on both hovering and mechanical movement. We also consider the identification of hovering locations for the UAV from infinitely many potential ones corresponding to the different data collection rates of sensors. The identification of hovering locations for the UAV from infinitely many potential ones makes the data collection tour finding more difficult, as different locations correspond to different data collection rates of sensors, which impacts significantly on the data collection efficiency. Besides, we consider the fluctuation of data transmission ranges of sensors caused by the different Euclidean distances between sensors and the UAV. Contributions in Chapter 4 includes: (1) a novel UAV trajectory designing problem with the objective to maximize the data collection volume is formulated and proved to be NP-hard; (2) the variation of the data transmission rate of each sensor affected by the distance from the UAV is jointly considered; (3) the energy consumption of the UAV on both hovering and mechanical movement are considered; and (4) an efficient algorithm to find a closed data collection tour for the problem is developed and empirically evaluated.

1.5 Thesis Outline

The remainder of the thesis is organized as follows. Chapter 2 studies a novel UAV hovering duration allocation problem to maximize the volume of collected data by distributing the UAV hovering budget over pre-defined hovering location candidates. Chapter 3 addresses the UAV hovering location identification problem to determine precise hovering locations for the UAV from the infinitely many potential ones, while maximizing the data collection utility. Chapter 4 explores the impacts of fluctuation of data transmission rates to data collection efficiency, and devises the data collection trajectory with the consideration of the UAV energy consumption on both hovering and mechanical movement, with the constraint that data at each sensor should be fully collected. Chapter 5 summarizes the thesis and proposes future works.

Chapter 2

UAV Hovering Duration Allocation for Data Collection Maximization

2.1 Introduction

Wireless Sensor Networks (WSNs) play important roles in data acquisition, including industrial monitoring [Guo et al., 2019], healthcare [Luo et al., 2019], underwater monitoring [Di Valerio et al., 2019] and smart homes [Kodeswaran et al., 2016]. Each sensor in WSNs is a tiny device with limited energy battery and storage. With the fast deployment of 5G networks, the data generated from various sensor devices will grow exponentially, which will help governments, businesses and organizations for smart management and business decision-making. However, collecting fresh sensing data in WSNs becomes crucial to avoid data loss and data overwritten. The unmanned aerial vehicle (UAV) has emerged as a promising technology for data collection in WSNs, due to its autonomy and flexibility. However, the UAV is required to be replenished quite often, due to its limited energy capacity, which poses many challenges. For example, the energy supply of a UAV may not be able to collect data from all sensors in a monitoring region, then which sensors' data should the UAV collect? To maximize the volume of the collected data, at which locations should the UAV hover and how long should it stay at each hovering location? In this chapter we will address these challenges.

Extensive studies of data collection in WSNs have been conducted in the past. For example, Zhan *et al.* [Zhan et al., 2017] jointly considered working states of sensors and the trajectory of the UAV by utilizing a fading channel model for the senor-UAV links to minimize the maximum energy consumption of sensors. Binol *et al.* [Binol et al., 2018] aimed at finding a time-optimal path for each of multiple UAVs for data collection from roadside units. These studies of data collection are based on the one-to-one data collection scheme, in which a UAV can collect sensing data from one sensor only at each time. On the other hand, there are several other studies under the one-to-many data collection scheme where a UAV can collect sensing data from multiple sensors simultaneously as long as the UAV is within the transmission ranges of the sensors. For example, Mozaffari *et al.* [Mozaffari et al., 2016] assumed that IoT devices can transmit their data by adopting the Orthogonal Frequency Division Multiple Access (OFDMA) technique, such that a UAV can support multiple IoT devices simultaneously. They dealt with the finding of an optimal trajectory for each of multiple UAVs to minimize the transmission energy consumption of ground IoT devices. Ghorbel *et al.* [Ghorbel et al., 2018] focused on the identification of optimal locations for a single UAV to collect data from a cluster of sensors with the aim of minimizing the energy consumption of the UAV. Samir *et al.* [Samir et al., 2019] considered a scenario where a UAV is dispatched for data collection from time-constrained devices and each device had a data uploading deadline, aiming at maximizing the network throughput. Li *et al.* [Li et al., 2020] considered data collection in WSNs by taking into account both hovering energy and traveling energy consumptions of an energy-constrained UAV, and developed efficient approximation and heuristic algorithms for the problem. Unlike most aforementioned studies that the data from all sensors within the data reception range of the UAV must be fully collected, in this chapter we assume that the data stored at a sensor can be partially collected and can be collected through multiple times by the UAV per tour. We study data collection in WSNs via an energy-constrained UAV [Lin et al., 2019] under one-to-many data collection scheme with the aim to maximize the volume of collected data.

This study is focused on investigating a specific scenario where a single UAV is deployed for data collection, with a limitation of energy for hovering during each tour. The sensors employed in the WSN are uniform and stationary, with an identical data transmission range and bandwidth. The UAV employs the one-to-many data collection mode, allowing for simultaneous data collection from multiple sensors. The height of the UAV's flight is constant, and the energy consumed during travel is not considered. Moreover, the UAV is required to hover at predetermined locations during the data collection process. These limitations should be taken into account while analyzing the results and drawing conclusions from the study.

The novelties of this study lie in that a novel data collection problem via the use of UAV is formulated and a performance-guaranteed approximation algorithm for the problem is devised.

The main contributions of the chapter are as follows.

- We formulate a novel Multi-sensor data collection Optimization Problem (MOP) to maximize the volume of data collected under the assumption that the UAV can collect data from multiple sensors simultaneously, and show that the problem is NP-hard.

- We devise an approximation algorithm with a $(1 - \frac{1}{e})$ approximation ratio for the problem.

- We evaluate the performance of the proposed algorithm through extensive experimental simulations. Simulation results demonstrate that the proposed algorithm is promising.

The remainder of the chapter is organized as follows. Section 2.2 introduces the UAV data collection model for WSNs and defines the problems. The NP-hardness of the defined problems is also shown in this section. Section 2.4 deals with a special case of the MOP and an optimal algorithm for this special case is proposed. Section 2.5 studies the MOP, and an approximation algorithm for it is devised. Section 2.6 evaluates the performance of the proposed algorithms, and Section 2.7 concludes the chapter.

2.2 Preliminaries

In this section, we first introduce the system and data collection models. We then define the problem precisely. We finally show the NP-hardness of the defined problem.

2.2.1 System Model

We consider a WSN, where $\mathcal{V} = \{v_i \mid 1 \leq i \leq N\}$ is a set of homogeneous sensor nodes deployed over a two-dimensional region on the ground. Let $(x_i, y_i, 0)$ denote the location of sensor v_i. We assume that each sensor node v_i has a fixed data transmission range R and an identical data transmission bandwidth B, with a volume D_i of data stored locally to be collected. A UAV is deployed for sensory data collection in the WSN, with a fixed hovering

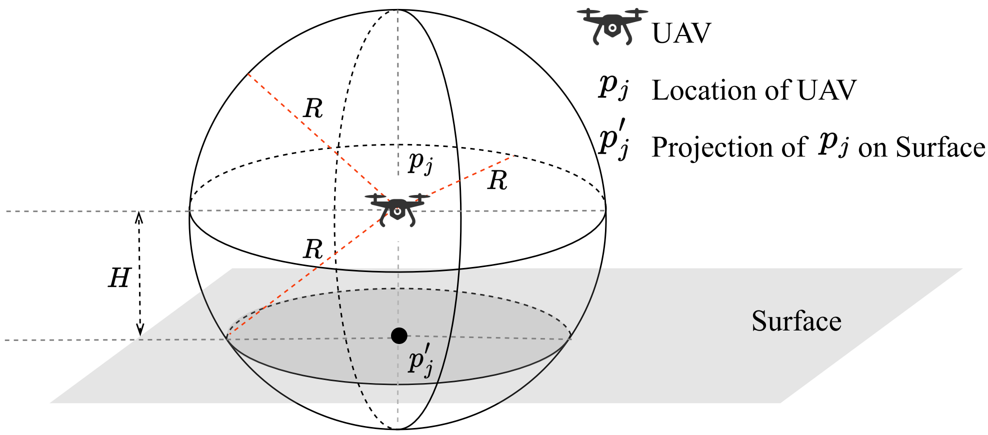

Figure 2.1: The sphere O_j with center p_j and radius R, where $p_j = (X_j, Y_j, H)$ is one of the predefined UAV hovering locations; $p'_j = (X_j, Y_j, 0)$ is the projection of p_j on the ground. The flying height of the UAV is H. Data from sensors within the sphere O_j can be collected when the UAV hovers at p_j.

altitude H. Considering the energy capacity constraint of the UAV, we assume that the maximum number of hovering (equal) time slots of the UAV per tour is Γ. Supported by OFDMA technique [Mozaffari et al., 2016], the UAV is able to collect data from multiple sensors simultaneously.

2.2.2 The Data Collection Model

We assume that a set $\mathcal{P} = \{p_j = (X_j, Y_j, H) \mid 1 \leq j \leq M\}$ of potential hovering locations is given, where the UAV can only hover at locations in $\mathcal{P}$ for data collection. Under the one-to-many data collection scheme, where each sensor has an identical data transmission range R, it is equivalent to regard the UAV to be with a data reception range R. As shown in Fig. 2.1, for each given location $p_j = (X_j, Y_j, H)$, a sphere O_j with center p_j and radius R can be obtained. When the UAV hovers at p_j, a location (x, y, z) is within the data reception range of the UAV, if and only if it locates within the space of O_j

(including the surface of O_j), i.e.,

$$(x - X_j)^2 + (y - Y_j)^2 + (z - H)^2 \leq R^2. \tag{2.1}$$

Denote by p'_j the projection of p_j on the ground, i.e., $p'_j = (X_j, Y_j, 0)$. If a location $(x, y, 0)$ on the ground is within the data reception range of the UAV, it is equivalent to say, the Euclidean distance between the location and p'_j is no greater than $\sqrt{R^2 - H^2}$. For a given location $p_j \in P$, its *data collection sensor set* S_j is a subset of sensors in $\mathcal{V}$, whose Euclidean distance from p'_j is no greater than $\sqrt{R^2 - H^2}$, i.e.,

$$S_j = \{v_i \mid (x_i - X_j)^2 + (y_i - Y_j)^2 \leq R^2 - H^2,\ v_i \in \mathcal{V}\}. \tag{2.2}$$

For a given sensor $v_i \in V$, its *data collection location set* L_i is a subset of locations in $\mathcal{P}$, in which each location p_j is within the data transmission range of sensor $v_i \in \mathcal{V}$, i.e.,

$$\begin{aligned} L_i = \{p_j \mid (x_i - X_j)^2 + (y_i - Y_j)^2 \leq R^2 - H^2,& \\ p_j \in \mathcal{P}\}.& \end{aligned} \tag{2.3}$$

Under the one-to-many data collection scheme, the UAV can collect sensory data from all sensors in S_j simultaneously when it hovers at location p_j. In other words, the data of sensor v_i can be collected by the UAV when the UAV hovers at any location in L_i. We thus have $v_i \in S_j$ if and only if $p_j \in L_i$. Fig. 2.2 is an example to illustrate the relationships between the data collection sensor set S_j and the data collection location set L_i.

Although the one-to-many data collection scheme can significantly im-

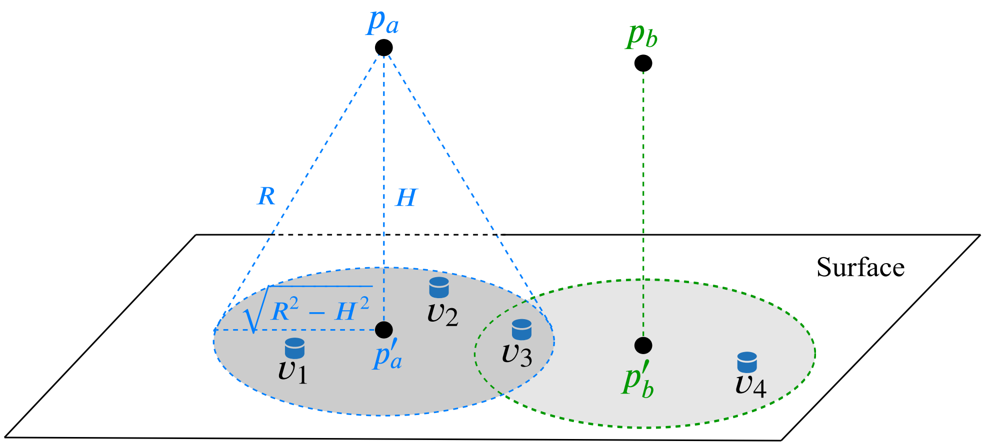

Figure 2.2: p'_a and p'_b are projections of p_a and p_b on the ground. We have that $S_a = \{v_1, v_2, v_3\}$, $S_b = \{v_3, v_4\}$, $L_1 = \{p_a\}$, $L_2 = \{p_a\}$, $L_3 = \{p_a, p_b\}$, $L_4 = \{p_b\}$.

prove data collection efficiency, an energy-constrained UAV usually cannot collect all sensory data from a large-scale WSN, due to its energy capacity constraint. In this chapter, we refer to the energy capacity constraint on the UAV as the maximum hovering duration of the UAV per tour, and we further divide the hovering duration of the UAV per tour into Γ equal *time slots* with each having length τ [Lin et al., 2019]. Denote by $\mathcal{T} = \{T_j \mid T_j \geq 0,\ p_j \in \mathcal{P}\}$ a set of hovering durations (in terms of time slots) of the UAV at different locations $p_j \in \mathcal{P}$. The total hovering duration of the UAV per tour thus is no greater than Γ time slots, i.e.,

$$\sum_{T_j \in \mathcal{T}} T_j \leq \Gamma. \tag{2.4}$$

Denote by C_i the total amount of data collected from sensor v_i by the UAV at hovering locations in L_i, which can be calculated as follows.

$$C_i = \sum_{p_j \in L_i} B \cdot \tau \cdot T_j. \tag{2.5}$$

As each sensor v_i has a data volume D_i initially, the total volume of data collected by the UAV per tour thus is

$$\sum_{v_i \in \mathcal{V}} \min\{C_i,\ D_i\}. \tag{2.6}$$

2.2.3 Problem Definitions

In the following we define two novel data collection optimization problems under the one-to-many data collection scheme.

The *Multi-sensor data collection Optimization Problem (MOP)*: Given a WSN with a set $\mathcal{V} = \{v_i \mid 1 \le i \le N\}$ of sensors on the ground, a UAV with the maximum number of hovering time slots Γ per tour is deployed for data collection in the WSN under the one-to-many data collection scheme. Each sensor $v_i \in \mathcal{V}$ has a volume D_i of data to be collected, assuming that each sensor has a data transmission range R with transmission bandwidth B. A set $\mathcal{P} = \{p_j = (X_j, Y_j, H) \mid 1 \le j \le M\}$ of potential hovering locations with altitude H for the UAV is given, where the UAV can only hover at the locations in $\mathcal{P}$ for data collection. The problem is to identify which locations in $\mathcal{P}$ will be the hovering locations of the UAV, and to determine the hovering duration at each identified hovering location under the energy constraint of the UAV, such that the total volume of data collected from sensors is maximized, subject to Γ time slots per tour, i.e.,

$$maximize \sum_{v_i \in \mathcal{V}} min\{C_i,\ D_i\}. \tag{2.7}$$

$$s.t. \sum_{T_j \in \mathcal{T}} T_j \leq \Gamma, \tag{2.8}$$

$$0 \leq T_j \leq \Gamma, \tag{2.9}$$

$$Eq.\ (2.3),\ (2.5). \tag{2.10}$$

We now define the *Multi-sensor data collection Optimization with hovering location Constraint Problem (MOCP)*, which is a special case of the defined MOP, where the Euclidean distance $DIS(p_a,\ p_b)$ between any two hovering locations p_a and p_b in $\mathcal{P}$ is strictly larger than $2\sqrt{R^2 - H^2}$, i.e., $DIS(p_a,\ p_b) > 2\sqrt{R^2 - H^2}$.

To tackle the MOP, in this chapter we first study one of its variants – the *Maximum Coverage with Height problem (MCH)* defined as follows.

Given a vertex set $\mathcal{V} = \{v_i \mid 1 \leq i \leq N\}$ and an integer $K \geq 1$, let $\mathcal{S} = \{S_j \mid 1 \leq j \leq M\}$ be a collection of subsets on $\mathcal{V}$. Associated with each vertex $v_i \in \mathcal{V}$, there is a height h_i with the initial value $h_i^0 \geq 0$, and the value of h_i is updated to $\max\{h_i - 1,\ 0\}$ if a set S_j containing v_i is chosen. To be specific, denote by h_i' and h_i'' the heights of v_i before and after selecting S_j respectively. Then, the decrement of the height of v_i caused by the selection of S_j is

$$h_i' - h_i'' = \begin{cases} 1, & \text{if } v_i \in S_j \text{ and } h_i' \geq 1 \\ h_i', & \text{if } v_i \in S_j \text{ and } h_i' < 1 \\ 0, & \text{otherwise.} \end{cases} \tag{2.11}$$

The MCH is to select K subsets from $\mathcal{S}$ such that the total height decrement of vertices in $\mathcal{V}$ is maximized.

2.3 NP Hardness of Problems

In the following we show that both MCH and MOP are NP-hard.

Theorem 1 *The Maximum Coverage with Height problem (MCH) is NP-hard.*

Proof We prove the NP-hardness of the MCH through a reduction from a well-known NP-hard problem - the *maximum coverage problem* (MCP). An instance of the MCP can be reduced to an instance of the MCH, where each vertex $v_i \in \mathcal{V}$ in MCH has an initial height $h_i^0 = 1$. In the case when $h_i^0 = 1$, the MCH problem is to find the maximum number of covered nodes by selecting K subsets, which is the definition of the MCP. It can be seen that a solution to the MCH returns a solution to the MCP, and the reduction is polynomial. The theorem thus follows. □

Theorem 2 *The Multi-sensor data collection Optimization Problem (MOP) is NP-hard.*

Proof We show the NP-hardness of the MOP through a reduction from the MCH.

For each instance M_1 of the MCH, it can be reduced to an instance M_2 of the MOP as follows. Let $\Gamma = K$, then the number K of selected sets of M_1 correspond the number $\Gamma = K$ of hovering time slots of UAV in M_2. The set $\mathcal{V}_1$ in M_1 corresponds to a set $\mathcal{V}_2$ of sensors in M_2, while each set S_j in M_1 corresponds to a potential hovering location p'_j with the data collection sensor set S'_j, such that for each vertex $v_i \in S_j$ with height h_i, there exists a corresponding sensor $v'_i \in S'_j$, with $D'_i = h_i \cdot B \cdot \tau$ volume of data to be collected, where B is the data transmission bandwidth and τ is the length of each time slot.

The MOP is to maximize the volume of collected data by selecting the hovering locations in $\mathcal{P}$ with durations for the UAV, subject to Γ $(= K)$ hovering time slots. It can be seen that a solution to M_2 returns a solution to M_1, and the reduction is polynomial. The theorem thus follows. $\square$

2.4 An Optimal Algorithm for the MOCP

In this section, we consider the special case MOCP of the MOP, where the Euclidean distance between any two locations in $\mathcal{P}$ is strictly larger than $2\sqrt{R^2 - H^2}$, for which we propose an optimal algorithm as follows.

2.4.1 Profit Function

Following the definition of the MOCP, the Euclidean distance $DIS(p_a, p_b)$ between any two locations $p_a,\ p_b \in \mathcal{P}$ is

$$DIS(p_a, p_b) > 2\sqrt{R^2 - H^2}, \tag{2.12}$$

where $\mathcal{P} = \{p_j \mid 1 \leq j \leq M\}$ is the set of potential hovering locations. Fig. 2.3 provides an illustrative example of the MOCP.

Under this assumption, there is no overlapping between S_a and S_b when the UAV hovers at locations p_a and p_b with $p_a \neq p_b$, respectively, i.e.,

$$S_a \cap S_b = \emptyset, \quad \forall p_a,\ p_b \in \mathcal{P}. \tag{2.13}$$

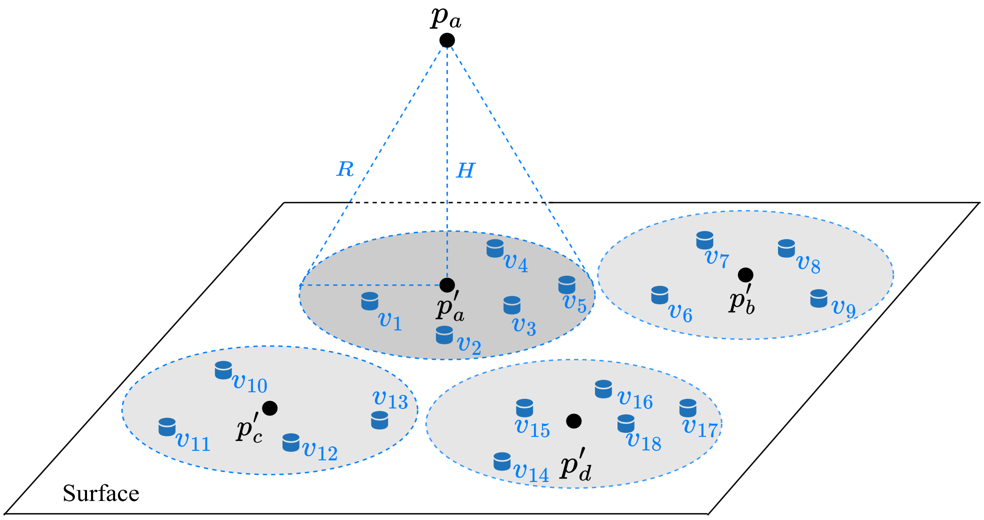

Figure 2.3: An illustration of the special case MOCP, where p'_a, p'_b, p'_c and p'_d are projections of hovering locations p_a, p_b, p_c and p_d on the ground respectively. The Euclidean distance between any two locations in $\mathcal{P}$ is strictly larger than $2\sqrt{R^2 - H^2}$. The data collection sensor set $S_a = \{v_1, v_2, v_3, v_4, v_5\}$, $S_b = \{v_6, v_7, v_8, v_9\}$, $S_c = \{v_{10}, v_{11}, v_{12}, v_{13}\}$ and $S_d = \{v_{14}, v_{15}, v_{16}, v_{17}, v_{18}\}$. There is no overlapping between any two data collection sensor sets from S_a, S_b, S_c and S_d.

Without loss of generality, we assume that $\cup_{j=1}^{M} S_j = \mathcal{V}$. Then, for each sensor $v_i \in \mathcal{V}$, there is exactly one hovering location $p_j \in \mathcal{P}$ within the data transmission range of v_i, i.e.,

$$|L_i| = 1, \quad \forall v_i \in \mathcal{V}, \tag{2.14}$$

$$L_i = \{p_j\}, \quad \text{if } v_i \in S_j. \tag{2.15}$$

A *p_j-located time slot* is referred as a time slot when the UAV hovers at p_j. Recall that T_j is the number of time slots when the UAV hovers at location p_j, which indicates that the hovering duration of the UAV at p_j consists of T_j p_j-located time slots. In the following, we focus on the volume of data collected with the tth p_j-located time slot, where $1 \leq t \leq T_j$.

Denote by $u_j(t)$ the *profit function* as the volume of data collected at the

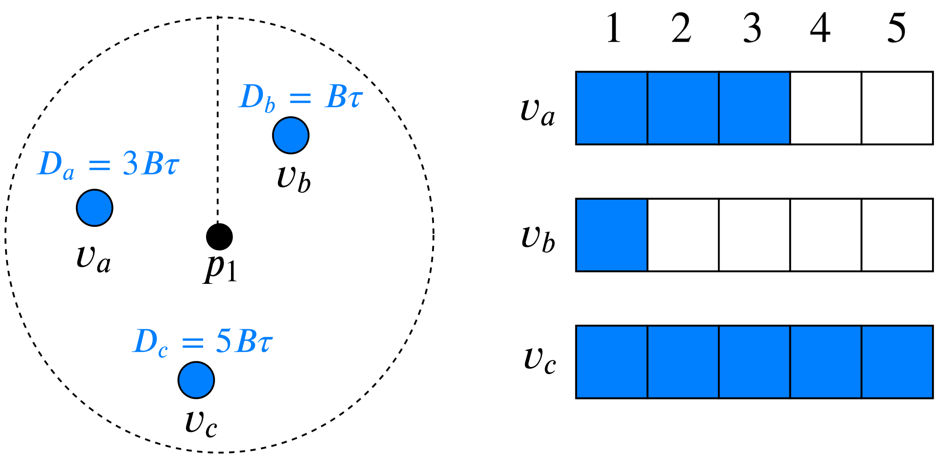

Figure 2.4: An illustration of data collected by the UAV at location p_1, where the number 1 to 5 is the time slot index. $S_1 = \{v_a, v_b, v_c\}$ is the set of sensors from which data can be collected when the UAV hovers at p_1. The data volume stored at each sensor is $D_a = 3B\tau$, $D_b = B\tau$ and $D_c = 5B\tau$ respectively. The volume of data collected at the first 5 time slots when the UAV hovers at p_1 is $3B\tau$, $2B\tau$, $2B\tau$, $B\tau$, and $B\tau$ respectively, i.e., $u_1(1) = 3B\tau$, $u_1(2) = 2B\tau$, $u_1(3) = 2B\tau$, $u_1(4) = B\tau$ and $u_1(5) = B\tau$.

tth p_j-located time slot. In the following, we show an example of $u_j(t)$ in Fig. 2.4, where $S_1 = \{v_a, v_b, v_c\}$ and the data volume stored at each sensor is $D_a = 3B\tau$, $D_b = B\tau$ and $D_c = 5B\tau$ respectively. It can be seen that, at the first $(t = 1)$ p_1-located time slot, the UAV can collect data from sensors v_a, v_b and v_c, with the data volume $u_1(1) = 3B\tau$ of collected data; at the second $(t = 2)$ and third $(t = 3)$ p_1-located time slots, data from sensors v_a and v_c are collected with $u_1(2) = 2B\tau$ and $u_1(3) = 2B\tau$, while for the p_1-located time slots with $t = 4$ and $t = 5$, we have that $u_1(4) = B\tau$ and $u_1(5) = B\tau$.

Denote by l_i the maximum number of time slots when the UAV can collect all data from v_i, i.e.,

$$l_i = \frac{D_i}{B\tau}. \tag{2.16}$$

Note that, since τ can be set properly, for the sake of convenience, we assume that l_i is an integer.

Denote by $f_i(t)$ a binary variable indicating whether sensor v_i still has remaining data to be collected at the tth p_j-located time slot when the UAV hovers at location p_j in L_i:

$$f_i(t) = \begin{cases} 1, & 0 \le t \le l_i, \\ 0, & \text{otherwise.} \end{cases} \tag{2.17}$$

The profit function $u_j(t)$ of the UAV at the tth p_j-located time slot is

$$u_j(t) = B \cdot \tau \sum_{v_i \in S_j} f_i(t). \tag{2.18}$$

An example of the profit function $u_j(t)$ is shown in Fig. 2.5. For the case in Fig. 2.4, the value of the derived profit function is $u_1(1) = 3B\tau$, $u_1(2) = 2B\tau$, $u_1(3) = 2B\tau$, $u_1(4) = B\tau$, $u_1(5) = B\tau$. When t is greater than 5, $u_1(t) = 0$. An illustration is shown in Fig. 2.6.

Let $l_{max} = \max\{l_i \mid v_i \in S_j\}$. We define *a drop point* d_k as a time slot where $u_j(d_k) > u_j(d_k + 1)$ with $0 < d_k \le l_{max}$, where k indicates that d_k is the kth drop point of the value of $u_j(t)$. Denote by $d_{K_{max}}$ the drop point with $u_j(d_{K_{max}} + 1) = 0$, where $d_{K_{max}} = l_{max}$.

Theorem 3 *The defined profit function $u_j(t)$ has the following properties for all t with $1 \le t \le l_{max}$.*

1. *$u_j(t)$ is non-increasing. For any $0 < a < b \le l_{max}$, where a, $b \in \mathbb{N}^+$, $u_j(a) \ge u_j(b) > 0$.*

2. *$u_j(t)$ is a piecewise constant function. The value of $u_j(t)$ is in a finite set $\{u_j(d_k) \mid 1 \le k \le K_{max}\}$ with $u_j(d_k + \Delta) = u_j(d_{k+1})$, where $1 \le \Delta \le$*

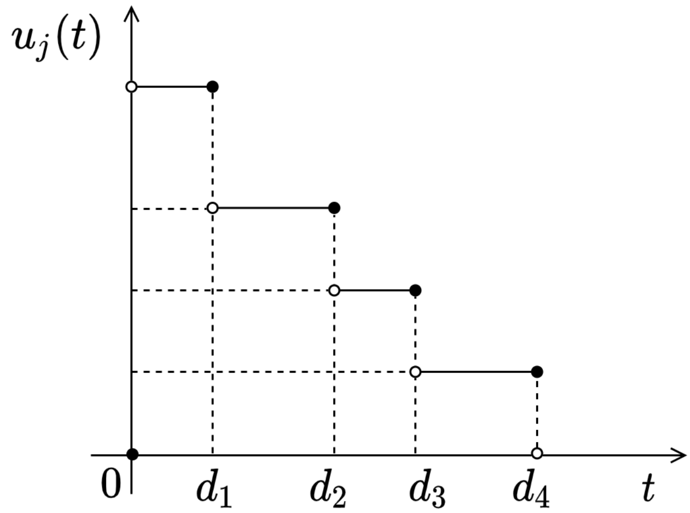

Figure 2.5: An instance of the profit function $u_j(t) = B \cdot \tau \sum_{v_i \in S_j} f_i(t)$, where t is the time slot index and $u_j(t)$ is value for the profit function at the tth p_j-located time slot.

$d_{k+1} - d_k$, $k+1 \leq K_{max}$, $\Delta \in \mathbb{N}^+$.

3. *The decrement at a drop point is determined by the number of sensors in S_j which finish their data transmission at the drop point, i.e., $u_j(d_k) - u_j(d_k + 1) = \sum_{v_i \in S_j}(f_i(d_k) - f_i(d_k+1)) \cdot B \cdot \tau$, with $1 \leq k \leq K_{max}$, $k \in \mathbb{N}^+$, where $\sum_{v_i \in S_j}(f_i(d_k) - f_i(d_k+1))$ is the number of sensors in S_j that finish their data transmission at the d_kth p_j-located time slot.*

4. *The number of time slots between two consecutive drop points in $u_j(t)$ is determined by the minimum remaining data of sensors in S_j at the previous drop point. For two consecutive drop points d_k and d_{k+1}, denote by D_k^{min} the minimum remaining data among sensors in S_j at d_k, then $d_{k+1} - d_k = \frac{D_k^{min}}{B\tau}$, where $1 \leq k \leq K_{max} - 1$, $k \in \mathbb{N}^+$.*

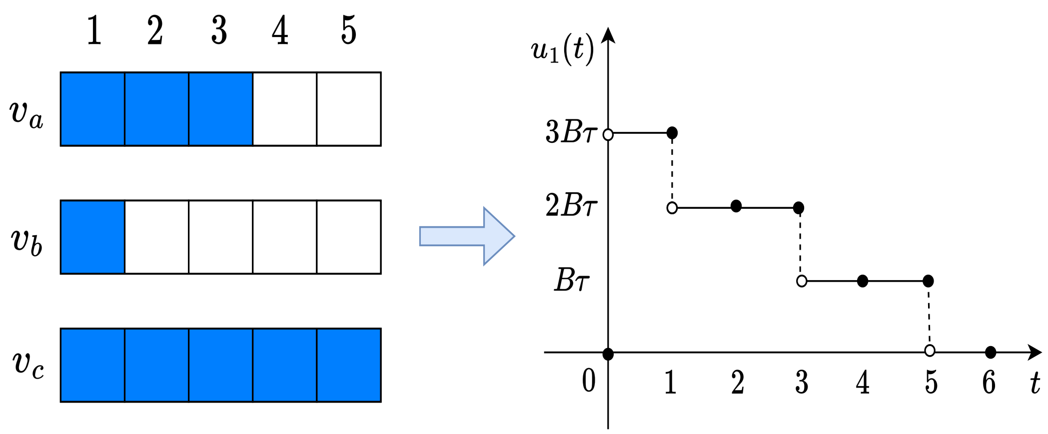

Figure 2.6: An example of the profit function, which is derived from the example in Fig. 2.4.

2.4.2 Optimal Algorithm

We propose a time-slot-based algorithm for the MOP by utilizing the defined profit function. The detailed algorithm is shown in `Algorithm 1`.

We first calculate the profit function of each potential charging location in $\mathcal{P}$. As mentioned before, l_{max} indicates the maximum number of time slots when the UAV can collect data at location p_j, where $u_j(l_{max}) > 0$ and $u_j(l_{max}+1) = 0$. Note that once the value of a profit function at a hovering location is determined, the value would not change later (Step 2 to Step 5 in the proposed algorithm). The hovering duration at each location in $\mathcal{P}$ is initialized as 0. The algorithm then proceeds iteratively, and there are Γ iterations. Within each iteration, a time slot is allocated to a location in $\mathcal{P}$. T_j is the number of iterations so far when p_j has been selected as a hovering location.

Then, at the current iteration, we allocate a time slot to a location that a maximum profit gain can be achieved, i.e., a location $p_{j^{max}} \in \mathcal{P}$ with the maximum value of $u_j(T_j+1)$ is chosen, and a time slot is allocated at location $p_{j^{max}}$, by increasing its hovering duration $T_{j^{max}}$ by 1 (Step 6 to Step 9 of the proposed algorithm).

Finally, any location p_j in $\mathcal{P}$ with $T_j > 0$ is identified as one of the hovering locations of the UAV during a data collection tour, and the UAV will hover at location $p_j \in \mathcal{F}$ for $T_j > 0$ time slots, before moving to the next hovering location.

Algorithm 1 Algorithm for the MOCP

Input: A set $\mathcal{V} = \{v_i \mid 1 \le i \le N\}$ of sensors;
a set $\mathcal{P}$ of potential hovering locations for the UAV;
a family $\mathcal{S} = \{S_j \mid p_j \in \mathcal{P}\}$ of data collection sensor sets for the set $\mathcal{P}$ of locations;
the maximum number of hovering time slots Γ for the UAV per tour.

Output: $\mathcal{F} = \{(p_j, T_j) \mid p_j \in \mathcal{P},\ T_j \ge 1\}$: a set of selected hovering locations for the UAV and the corresponding hovering durations;

```
F ← ∅;
for each p_j ∈ P do
    l_max ← max{l_i | v_i ∈ S_j}; /* find the maximum value among sensors in S_j */
    for t ← 1 to l_max + 1 do
        u_j(t) ← Bτ · Σ_{v_i∈S_j} f_i(t);
T ← {T_j ← 0 | p_j ∈ P};
for I ← 1 to Γ do
    Identify a hovering location p_{j^max} s.t. j^max ← argmax_{p_j∈P} u_j(T_j + 1);
    T_{j^max} ← T_{j^max} + 1;
for each p_j ∈ P do
    if T_j ≥ 1 then
        F ← F ∪ {(p_j, T_j)};
return F
```

2.4.3 Algorithm Analysis

The rest is to show that `Algorithm 1` delivers an optimal solution for the MOCP.

Lemma 1 *Denote by $\mathcal{T}^* = \{T_j^* \mid 0 \le T_j^* \le \Gamma,\ p_j \in \mathcal{P}\}$ the set of durations for locations in $\mathcal{P}$ delivered by* `Algorithm` *1. Then, $u_a(T_a^*) \ge u_b(T_b^* + 1)$ for any pair* *of locations $p_a,\ p_b \in \mathcal{P}$ with $T_a^* \geq 1$.*

Proof We prove the claim by contradiction.

Assume that there exist T_a^* and T_b^* such that $u_a(T_a^*) < u_b(T_b^*+1)$.

Following `Algorithm` 1, assume at iteration t', T_a^* increases from T_a^*-1 to T_a^* when $T_b = T_b' \leq T_b^*$, we then have $u_b(T_b') \geq u_b(T_b^*) \geq u_b(T_b^*+1)$, since $u_b(t)$ is a non-increasing function, by Theorem 3.

On the other hand, assuming $u_a(T_a^*) < u_b(T_b^*+1)$, we have $u_b(T_b') \geq u_b(T_b^*) \geq u_b(T_b^*+1) > u_a(T_a^*)$.

By Step 7 to Step 9 of `Algorithm` 1, T_b should increase from T_b' to $T_b'+1$, instead of that T_a increases from T_a^*-1 to T_a^*. This results in a contradiction. □

Lemma 2 *For any hovering duration set $\mathcal{T} = \{T_j \mid 0 \leq T_j \leq \Gamma,\ p_j \in \mathcal{P}\}$, where $u_a(T_a) \geq u_b(T_b+1)$ for any $T_a,\ T_b \in \mathcal{T}$ with $T_a > 0$ and $\sum_{T_j \in \mathcal{T}} T_j = \Gamma$, it leads to a maximum volume of data collected by the UAV when it hovers at the locations in $\mathcal{P}$ with the hovering durations in $\mathcal{T}$ greater than zeros.*

Proof We consider a general case where not all sensory data in a WSN can be fully collected, due to the energy capacity on the UAV. It is to collect as much data as possible by the UAV, the total UAV hovering duration of the optimal solution thus must be exactly Γ time slots.

In the following, we prove the claim by contradiction.

Assume that there exists a hovering duration set $\mathcal{T}' = \{T_j' \mid p_j \in \mathcal{P}\}$ with $\sum_{T_j \in \mathcal{T}} T_j = \Gamma$, in which there exist $T_a' \geq 1$ and T_b' with

$$u_a(T_a') < u_b(T_b'+1), \tag{2.19}$$

which results in an optimal solution.

Denote by U' the total volume of data collected by the scheduling $\mathcal{T}'$, i.e.,

$$U' = \sum_{t=0}^{T'_a} u_a(t) + \sum_{t=0}^{T'_b} u_b(t) + \Big(\sum_{p_j \in \mathcal{P}} \sum_{t=0}^{T'_j} u_j(t) - \sum_{t=0}^{T'_a} u_a(t) - \sum_{t=0}^{T'_b} u_b(t)\Big) \tag{2.20}$$

Let $\mathcal{T}'' = \{T''_j \mid p_j \in \mathcal{P}\}$ denote a hovering duration set with $T''_a = T'_a - 1$, $T''_b = T'_b + 1$ and $T''_j = T'_j$ for $j \neq a,\ b$. Denote by U'' the total volume of collected data by $\mathcal{T}''$, i.e.,

$$U'' = \sum_{t=0}^{T'_a-1} u_a(t) + \sum_{t=0}^{T'_b+1} u_b(t) + \Big(\sum_{p_j \in \mathcal{P}} \sum_{t=0}^{T'_j} u_j(t) - \sum_{t=0}^{T'_a} u_a(t) - \sum_{t=0}^{T'_b} u_b(t)\Big) \tag{2.21}$$

Then, we have

$$\begin{aligned} U'' - U' &= \sum_{t=0}^{T'_a-1} u_a(t) + \sum_{t=0}^{T'_b+1} u_b(t) - \Big(\sum_{t=0}^{T'_a} u_a(t) + \sum_{t=0}^{T'_b} u_b(t)\Big) && (2.22)\\ &= -u_a(T'_a) + u_b(T'_b + 1) && (2.23)\\ &> 0 \quad \text{(by 2.19)} && (2.24) \end{aligned}$$

It can be seen that the volume of data collected by $\mathcal{T}''$ is larger than the one by $\mathcal{T}'$, which contradicts the assumption that $\mathcal{T}'$ will lead to an optimal solution. The lemma thus follows. □

Theorem 4 `Algorithm` *1 for the MOCP delivers an optimal solution.*

Proof Denote by $\mathcal{T}^* = \{T^*_j \mid 0 \leq T^*_j \leq \Gamma,\ p_j \in \mathcal{P}\}$ the hovering duration set delivered by `Algorithm` 1. Since there are Γ iterations in `Algorithm` 1, a time slot is allocated to a hovering location in $\mathcal{P}$ at each iteration, and we have $\sum_{T^*_j \in \mathcal{T}^*} = \Gamma$ time slots to be allocated.

By Lemma 1, it has shown that for any two hovering durations $T^*_a \geq 1$

and T_b^* in $\mathcal{T}^*$ delivered by `Algorithm` 1, $u_a(T_a^*) \geq u_b(T_b^* + 1)$. Meanwhile, by Lemma 2, for any hovering duration set $\mathcal{T} = \{T_j \mid p_j \in \mathcal{P}\}$ where $u_a(T_a) \geq u_b(T_b + 1)$ for any $T_a,\ T_b \in \mathcal{T}$ with $T_a \geq 1$ and $\sum_{T_j} = \Gamma$, it will lead to an optimal solution.

Thus, the hovering duration at each location in the solution delivered by `Algorithm` 1 will result in the maximum volume of data collected, and the solution is optimal. □

2.5 Approximation Algorithm for the MOP

In this section, we investigate the MOP, by devising an approximation algorithm for it. We start with an approximation algorithm for its variant - the MCH first. We then show how to extend the proposed algorithm to solve the MOP.

2.5.1 Approximation Algorithm for the MCH

Recall in the definition of MCH in Section 2.2.3, each vertex v_i in $\mathcal{V}$ has a variable height h_i, which is likely to reduce if a set S_j covering v_i is selected.

The MCH is to maximize the total height decrement of vertices in $\mathcal{V}$ by choosing K sets where K is given in advance. The algorithm for the MCH proceeds iteratively. Within iteration k with $1 \leq k \leq K$, a set S^k is selected. Denote by h_i^k the height of v_i after S^k is selected, then

$$h_i^k = \begin{cases} \max\{h_i^{k-1} - 1,\ 0\}, & \text{if } v_i \in S^k, \\ h_i^{k-1}, & \text{otherwise,} \end{cases} \tag{2.25}$$

where h_i^0 is the initial height of v_i. The MCH thus is to identify a collection of sets $\{S^1, S^2, ..., S^K\}$ such that $\sum_{v_i \in \mathcal{V}}(h_i^0 - h_i^K)$ is maximized.

In the following we develop an approximation algorithm with a provable $(1 - \frac{1}{e})$ ratio for the MCH.

The core idea behind the proposed algorithm proceeds iteratively. Let $\mathcal{Y}$ be the collection of chosen sets so far. With each iteration k with $1 \le k \le K$, a set from the collection $\mathcal{S} \setminus \mathcal{Y}$ is chosen such that the accumulative height decrement of sensors in iteration k is maximized, i.e., a set with index j^{max} will be chosen where

$$j^{max} = \text{argmax}_{S_{j^{max}} \in \mathcal{S} \setminus \mathcal{Y}} \sum_{v_i \in S_{j^{max}}} (h_i^{k-1} - h_i^k). \tag{2.26}$$

By Eq. (2.25), Eq. (2.26) can be rewritten as

$$j^{max} = \text{argmax}_{S_{j^{max}} \in \mathcal{S} \setminus \mathcal{Y}} \sum_{v_i \in S_{j^{max}}} \min\{h_i^{k-1},\ 1\}. \tag{2.27}$$

The detailed algorithm for the MCH is given in `Algorithm` 2.

2.5.2 Approximation Algorithm for the MOP

The basic idea of an algorithm for the MOP is similar to the one for the MCH, which also proceeds iteratively.

There are Γ iterations (as there are Γ time slots per tour of the UAV). Within iteration k, a set S^k is chosen. The rest is how to modify `Algorithm` 2 for the MOP. To this end, the sensor heights and the formation of sets should be given as follows.

Sensor Height Determination: Denote by h_i^k the height of sensor v_i after

Algorithm 2 Algorithm for the MCH

Input: A set $\mathcal{V} = \{v_i \mid 1 \le i \le N\}$, where each vertex $v_i \in \mathcal{V}$ has a initial height h_i^0;
a collection of vertex sets $\mathcal{S} = \{S_j \mid 1 \le j \le M\}$;
a fixed K, which is the number of sets to be selected from $\mathcal{S}$.
Output: The K chosen sets.

```
U ← S;
Y ← ∅; /* the solution */
for k ← 1 to K do
    j^max ← argmax_{S_{j^max} ∈ U} Σ_{v_i ∈ S_{j^max}} min{h_i^{k-1}, 1};
    S^k ← S_j^max;
    Y ← Y ∪ {S^k};
    U ← U \ {S^k};
    for each v_i ∈ V do
        if v_i ∈ S^k then
            h_i^k ← max{h_i^{k-1} − 1, 0};
        else
            h_i^k ← h_i^{k-1};
return Y
```

a set S^k is selected, where the initial height of v_i is $h_i^0 = l_i = \frac{D_i}{B \cdot \tau}$. Given h_i^{k-1} and the selected set S^k, the value of h_i^k can be calculated by Eq. (2.25).

Sensor Set Virtualization: Denote by $l_j^{max} = \max\{l_i \mid v_i \in S_j\}$ the maximum value among sensors in S_j. A collection $\mathcal{A}_j = \{A_j^m \mid 1 \le m \le l_j^{max}\}$ of virtual sets of S_j is then formed, where each element A_j^m in $\mathcal{A}_j$ contains exactly identical sensors as in S_j and the cardinality of $\mathcal{A}_j$ is l_j^{max}.

Now, each sensor v_i can be regarded as a vertex v_i with the initial height $\frac{D_i}{B \cdot \tau}$, and the union $\cup_{p_j \in \mathcal{P}} \mathcal{A}_j$ can be regarded as the collection of sets in the MCH.

Following `Algorithm` 2, within iteration k with $1 \le k \le \Gamma$, a set $S_{j^{max}}$ with the maximum value of $\sum_{v_i \in S_{j^{max}} \setminus \mathcal{Y}} min\{h_i^{k-1}, 1\}$ is selected from $\cup_{p_j \in \mathcal{P}} \mathcal{A}_j$.

Consequently, the identified hovering locations for the UAV are the locations in $\mathcal{P}$ whose virtual set is selected in any iteration, while the hovering duration (in terms of time slots) at each selected location p_j is equal to the number of selected virtual sets of S_j during the Γ iterations.

The detailed algorithm for the MOP is given in `Algorithm` 3. Fig. 2.7 presents an illustrative example of virtual set selection and sensor height decrease.

2.5.3 Analysis of the Approximation Ratio

In the following, we analyze the approximation ratios of `Algorithm` 2 and `Algorithm` 3.

We use OPT to denote the value of the optimal solution of the MCH. `Algorithm` 2 consists of K iterations, and within each iteration a set with the maximum height decrements is chosen. Denote by p_k and q_k the sum of height decrements at the kth iteration and the total height decrements up to the kth iteration (including the kth iteration), i.e., $q_k = \sum_{m=1}^{k} p_m$. Let g_k be the value difference with OPT after the kth iteration, i.e., $g_k = OPT - q_k$.

Lemma 3 *1.* $p_{k+1} \geq \frac{g_k}{K}$, *for* $k = 0, 1, \ldots, K-1$, *where* $p_0 = q_0 = 0$, *and* $g_0 = OPT$.

2. $g_{k+1} \leq (1 - \frac{1}{K})^{k+1} \cdot OPT$, *for* $k = 0, 1, \ldots, K-1$.

Proof 1) g_k is the value difference from OPT after iteration k with $1 \leq k \leq K$. By the Pigeonhole Principle, one of the K iterations in the optimal solution must be at least $\frac{g_k}{K}$. Since p_{k+1} is the maximum one at time slot $k+1$, we have $p_{k+1} \geq \frac{g_k}{K}$, for $k = 0, 1, \ldots, K-1$.

2) We show this claim by induction. For the base case where $k = 0$, we need to show $g_1 \leq (1 - \frac{1}{K}) \cdot OPT$.

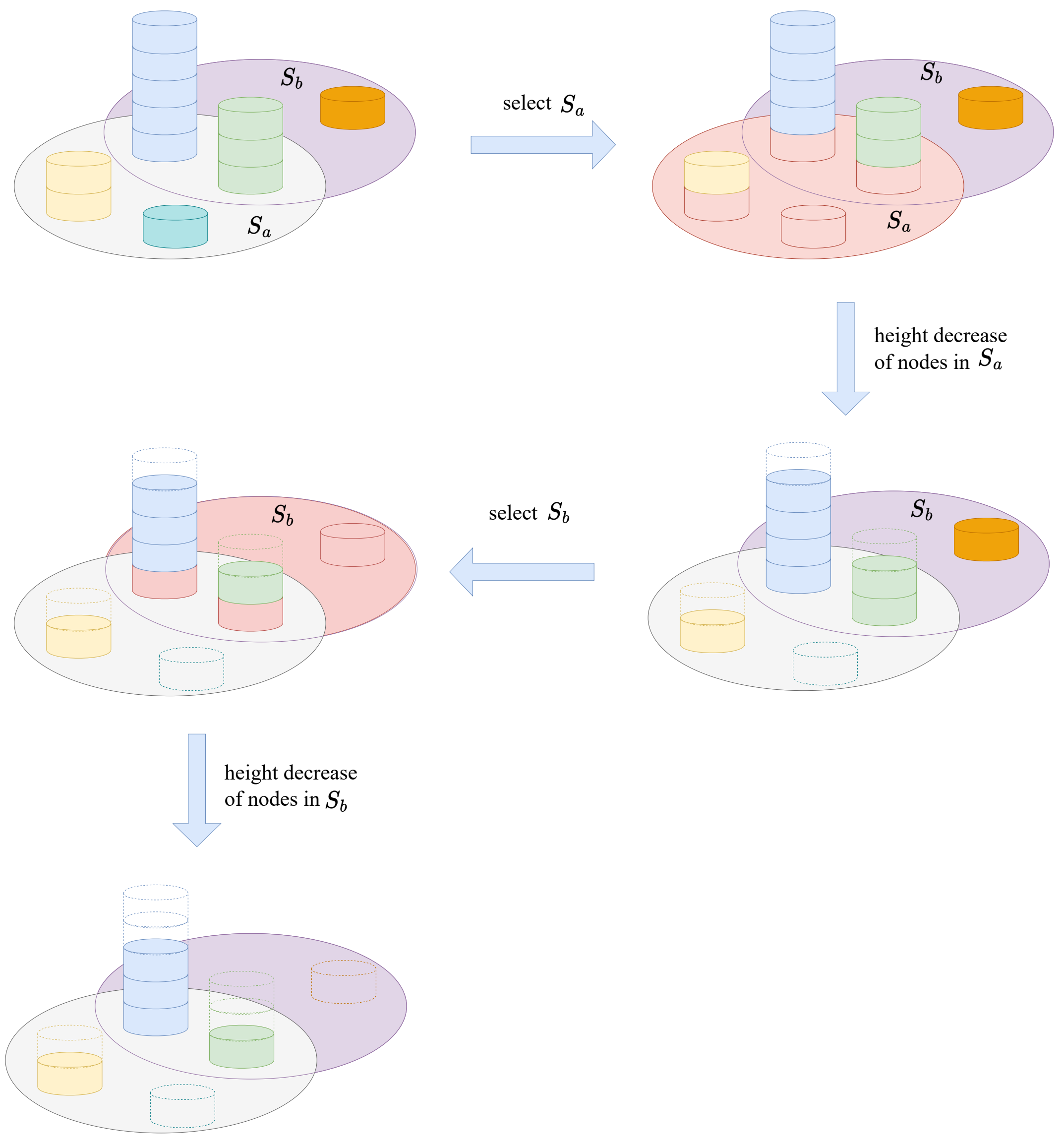

Figure 2.7: An illustrated example of virtual set selection and sensor height decrease referred to in `Algorithm` 3.

Since $g_k = OPT - q_k$, we have

$$g_1 \leq OPT - q_1 = OPT - p_1 \tag{2.28}$$
$$\leq OPT - \frac{g_0}{K} \quad \text{by Lemma 3(1)} \tag{2.29}$$
$$= OPT - \frac{OPT}{K} \tag{2.30}$$
$$= (1 - \frac{1}{K}) \cdot OPT \tag{2.31}$$

We then show that $g_{k+1} \leq (1 - \frac{1}{K})^{k+1} \cdot OPT$, based on the following inductive hypothesis, that is,

$$g_k \ \leq \ (1 - \frac{1}{K})^k \cdot OPT \tag{2.32}$$

By induction,

$$g_{k+1} \ = \ g_k - p_{k+1} \tag{2.33}$$
$$\leq \ g_k - \frac{g_k}{K} \quad \text{by Lemma 3(1)} \tag{2.34}$$
$$= \ g_k(1 - \frac{1}{K}) \tag{2.35}$$
$$\leq \ (1 - \frac{1}{K})^k \cdot OPT \cdot (1 - \frac{1}{K}) \quad \text{by (2.32)} \tag{2.36}$$
$$= \ (1 - \frac{1}{K})^{k+1} \cdot OPT \tag{2.37}$$

□

Theorem 5 *The approximation ratio of* `Algorithm` *2 for the MOP is* $(1 - \frac{1}{e})$.

Proof By Lemma 3, we have shown $g_K \leq (1 - \frac{1}{K})^K \cdot OPT$.

Since $(1 - \frac{1}{K})^K \approx \frac{1}{e}$, we have $g_K \leq \frac{OPT}{e}$.

Then,

$$q_K = OPT - g_K \;\geq\; OPT - \frac{OPT}{e} \;\geq\; OPT(1 - \frac{1}{e}) \tag{2.38}$$

where q_K is the profit after the Kth iteration of `Algorithm` 2.

We thus conclude that the approximation ratio of `Algorithm` 2 is $(1 - \frac{1}{e})$.
□

Theorem 6 *The approximation ratio of* `Algorithm` *3 for the MOP is* $(1 - \frac{1}{e})$.

Proof Since the sensor height determination and sensor set virtualization never change the volume of data collected at each location in $\mathcal{P}$, the approximation ratio of `Algorithm` 3 is determined by the selection of hovering locations (Step 11 to Step 19 in `Algorithm` 3), which is same as `Algorithm` 2. Therefore, the approximation ratio of `Algorithm` 3 is also $(1 - \frac{1}{e})$ according to Theorem 5. □

2.6 Performance Evaluation

In this section, we evaluate the performance of the proposed algorithm by experimental simulations. We also investigate the impact of parameters on the algorithm performance.

2.6.1 Experimental Environment Settings

We consider a WSN deployed within $1,000 \times 1,000$ square meters, in which sensors are randomly distributed [Li et al., 2020].

The data transmission range and bandwidth of each sensor are set at 150 meters and 1 MB/s [Theunissen et al., 2018], respectively. The data volume

D_i of each sensor v_i is randomly drawn from $(0,\ 1000]MB$. We employ one UAV for data collection [Liang et al., 2018], hovering at the altitude 100 meters [Gong et al., 2018b]. The total hovering time of the UAV is set as $1,800$ seconds [dji], with the length of each time slot 1 second. Unless otherwise specified, these parameters will be adopted in the default setting.

The MOP is a new problem, where existing algorithms in literature are unlikely to be adopted directly due to different data collection models. To evaluate the performance of `Algorithm 1` and `Algorithm 3`, we propose the following benchmark heuristics.

- *Greedy*. It iteratively selects a hovering location p_{max} for the UAV with the maximum volume of collected data, and the UAV hovers at p_{max} until all data from the sensors in S_{max} are collected. This procedure continues until the accumulative hovering duration of the UAV reaches Γ.

- *NSearch*. The UAV firstly hovers at a location p_{max_1} with the maximum volume of collected data, where it collects all data from the sensors in S_{max_1}. It then selects a location p_{max_2} from the neighbors of p_{max_1} (sensors no larger than 225 meters away from location p_{max_1}) where data is also fully collected. The procedure of neighbor selection continues until the UAV runs out of power.

- *UCollect*. The UAV collects data at each hovering location in $\mathcal{P}$ with equal duration, i.e., $\frac{\Gamma}{|\mathcal{P}|}$ number of time slots at each $p_i \in \mathcal{P}$.

- *WCollect*. Denote by $\mathcal{D} = \sum_{p_j \in \mathcal{P}} \sum_{v_i \in S_j} D_i$ the sum of data from all data collection sensor sets (not as same as the total volume of data in the

WSN). The hovering duration of the UAV at p_j is decided by the ratio of the volume of data from S_j to $\mathcal{D}$, i.e., $T_j = \Gamma \cdot \frac{\sum_{v_i \in S_j} D_i}{\mathcal{D}}$.

Each value in figures is the mean result by applying each mentioned algorithm to 50 network instances with the same size. The running time of all mentioned experimental simulations is obtained from a desktop with 2.7 GHz Intel Core i5 CPU and 8 GB RAM.

2.6.2 Performance Evaluation of Different Algorithms

We first investigate the performance of `Algorithm 1` (denoted by *Alg01*) against heuristics `Greedy`, `NSearch`, `UCollect` and `WCollect` for the MOCP, with 25 randomly distributed potential hovering locations (since the distance between any two locations is required to be strictly larger than $2 \cdot \sqrt{150^2 - 100^2} \approx 225$ meters, the maximum number of potential hovering locations we can generate is around 25).

Fig. 2.8(a) shows that `Alg01` significantly outperforms other heuristics, due to the fact that `Alg01` can always deliver an optimal solution. Fig. 2.8(b) plots the running time curves of the comparison algorithms.

We then evaluate the performance of `Algorithm 3` (denoted by *Alg03*) against heuristics `Greedy`, `NSearch`, `UCollect` and `WCollect` for the MOP, by varying the number of sensors from 100 to $1,000$, with 100 potential hovering locations. Fig. 2.9(a) demonstrates that the volume of collected data by all mentioned algorithms is proportional to the network size, due to the fact that with the increase on the number of sensors, more data is generated in the WSN, such that the UAV is able to collect more data at each hovering location. It can also be seen that, the volume of collected data by `Alg03` is

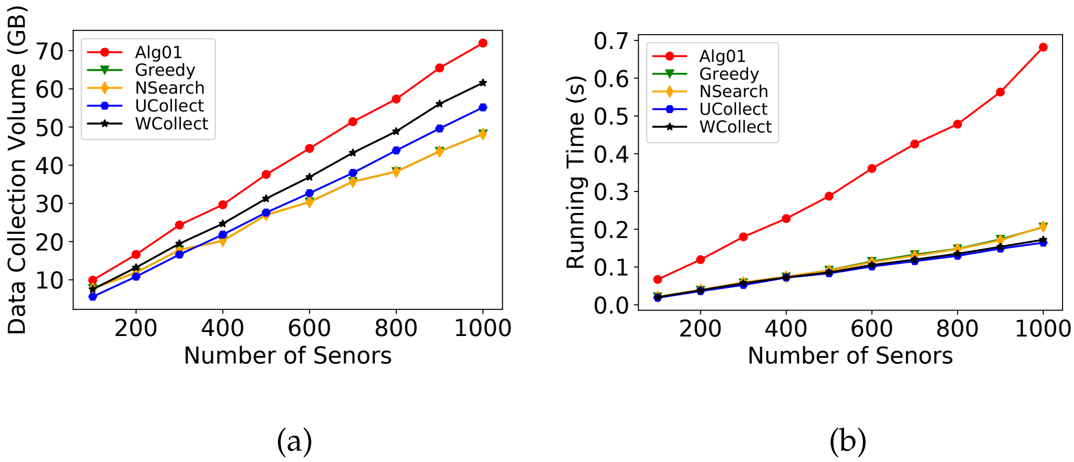

Figure 2.8: Performance of `Alg01`, `Greedy`, `NSearch`, `UCollect` and `WCollect` in WSNs consisting of sensors from 100 to 1,000.

approximately 129% of the one by `WCollect`, and 145% of the ones by other heuristics. Fig. 2.9(b) depicts the time curves of the proposed algorithms.

Note that, `Algorithm 2` just serves as a bridge to solve the MOP. We instead evaluate the performance of `Algorithm 3` directly.

2.6.3 Impact of Parameters on the Performance of Algorithms

The rest is to investigate the impact of the UAV hovering durations and the data transmission range on the performance of the mentioned algorithms, with 1,000 sensors randomly deployed in the monitoring field.

We first investigate the impact of the UAV hovering duration on the performance of different algorithms, where the number of hovering time slots of the UAV varies from 1,500 to 2,500, with length of 1 second. Fig. 2.10(a) depicts that the volume of collected data delivered by the mentioned algorithms grows rapidly against the hovering time of the UAV, as the UAV is able to collect more data with longer hovering durations. Besides, `Alg03` significantly outperforming others in any cases, where the result of `Alg03` is approximately

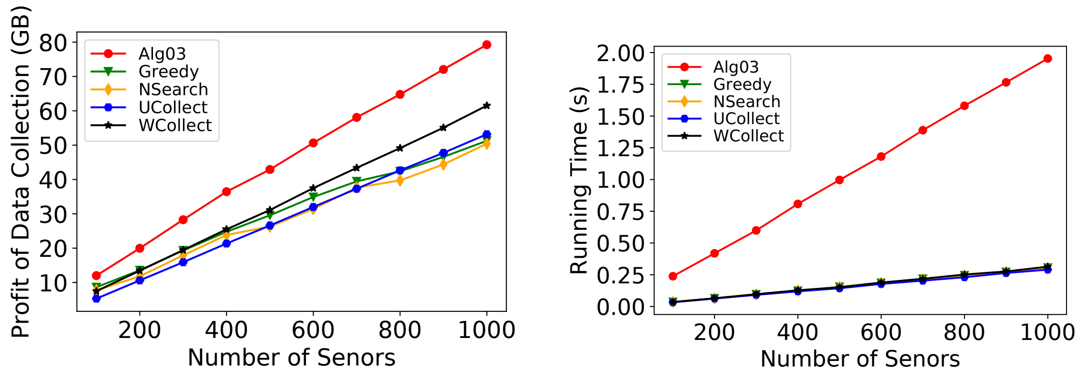

(a) (b)

Figure 2.9: Performance of `Alg03`, `Greedy`, `NSearch`, `UCollect` and `WCollect` in WSNs consisting of sensors from 100 to 1,000.

123% of `WCollect`. From Fig. 2.10(b), the running time of `Alg03` also grows against the number of hovering time slots of the UAV, due to that the number of iterations of `Alg03` is determined by the number of UAV hovering time slots.

We then investigate the impact of the data transmission range of sensors on the performance of the mentioned algorithms, by increasing the transmission range from 120 meters to 220 meters (since the transmission range should be larger than the height of the UAV), with 1,000 sensors randomly deployed in the network. Fig. 2.11(a) plots that the volume of collected data delivered by different algorithms rises against the data transmission range, due to the fact that the UAV can collect more data with a larger data transmission range of sensors. It also can be seen that the performance gaps between `Alg03` and other heuristics become increasingly larger with the growth on the data transmission range. Fig. 2.11(b) plots the running time curves of the mentioned algorithms. It can be seen from Fig.2.10 and Fig.2.11 that the data collection of `Alg03` is proportional to the UAV hovering duration and the data trans-

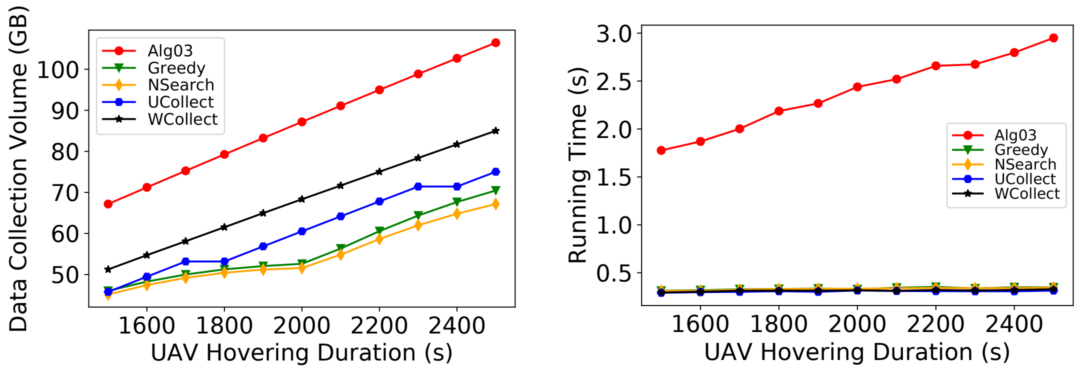

(a) (b)

Figure 2.10: Performance of `Alg03`, `Greedy`, `NSearch`, `UCollect` and `WCollect` with UAV hovering duration from 1,500 to 2,500.

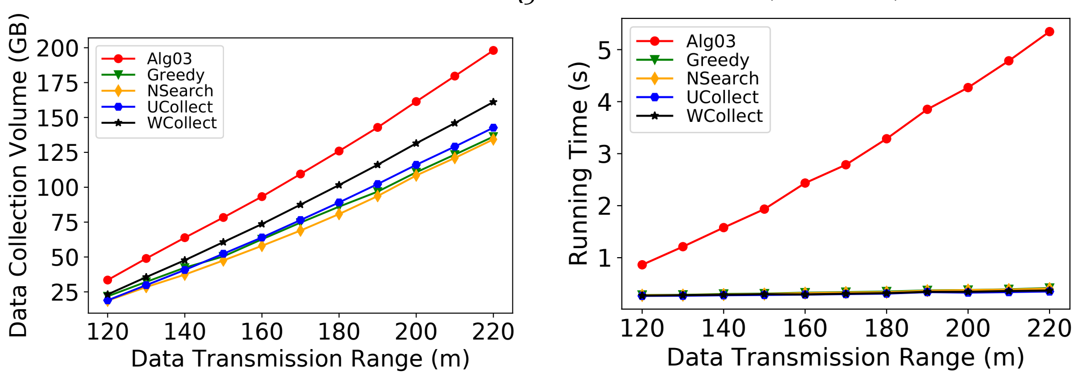

(a) (b)

Figure 2.11: Performance of `Alg03`, `Greedy`, `NSearch`, `UCollect` and `WCollect` by varying the data transmission range of sensors from 120 meters to 220 meters.

mission range of sensors.

2.7 Summary

In this chapter, we studied data collection in a WSN, using an energy-constrained UAV, where data from multiple sensors can be collected simultaneously by the UAV at any hovering location. We first formulated a novel multi-sensor data collection optimization problem and showed that the problem is NP-hard. We then devised an efficient approximation algorithm with a constant approximation ratio for it. We finally evaluated the proposed algorithm through experimental simulations. Simulation results demonstrate that the proposed algorithm is promising, and outperforms other heuristics significantly.

Algorithm 3 Approximation Algorithm for the MOP

Input: A set $\mathcal{V} = \{v_i \mid 1 \leq i \leq N\}$ of sensors;
a set $\mathcal{P}$ of potential hovering locations for the UAV;
a family $\mathcal{S} = \{S_j \mid p_j \in \mathcal{P}\}$ of data collection sensor sets for the set $\mathcal{P}$ of locations;
the maximum number of hovering time slots Γ for the UAV per tour.

Output: $\mathcal{F} = \{(p_j,\ T_j) \mid p_j \in \mathcal{P},\ T_j \geq 1\}$: a set of selected hovering locations for the UAV and the corresponding hovering durations;

$\mathcal{F} \leftarrow \emptyset$;
$\mathcal{Q} \leftarrow \emptyset$;
$\mathcal{T} \leftarrow \{T_j \leftarrow 0 \mid p_j \in \mathcal{P}\}$;
for each $v_i \in \mathcal{V}$ **do**
  $l_i \leftarrow \frac{D_i}{B\tau}$;
  $h_i^0 \leftarrow l_i$;
for each $p_j \in \mathcal{P}$ **do**
  $l_j^{max} \leftarrow \max_{v_i \in S_j}\{l_i\}$;
  A collection of virtual sets $\mathcal{A}_j \leftarrow \{A_j^m \mid 1 \leq m \leq l_j^{max}\}$ by duplicating S_j;
  $\mathcal{Q} \leftarrow \mathcal{Q} \cup \mathcal{A}_j$;
for $k \leftarrow 1$ to Γ **do**
  Select a $G_{j^*}^m \in \mathcal{Q}$ with maximum $\sum_{v_i \in G_{j^*}^m} \min\{h_i^{k-1},\ 1\}$;
  $T_{j^*} \leftarrow T_{j^*} + 1$;
  $\mathcal{Q} \leftarrow \mathcal{Q} \setminus \{G_{j^*}^m\}$;
  for each $v_i \in \mathcal{V}$ **do**
    if $v_i \in G_{j^*}^m$ **then**
      $h_i^k \leftarrow \max\{h_i^{k-1} - 1,\ 0\}$;
    else
      $h_i^k \leftarrow h_i^{k-1}$;
for each $p_j \in \mathcal{P}$ **do**
  if $T_j \geq 1$ **then**
    $\mathcal{F} \leftarrow \mathcal{F} \cup \{(p_j,\ T_j)\}$;
return $\mathcal{F}$.

Chapter 3

UAV Hovering Location Identification for Utility Maximization

3.1 Introduction

The last decade witnessed rapid advancement of digital technology, such as the Internet of Things (IoT), having enormous applications in various domains that include wearables [Ometov et al., 2016; Gu et al., 2017], smart homes [Dorri et al., 2017] and smart cities [Roy et al., 2019; Cabrera et al., 2020]. Wireless Sensor Networks (WSNs) play a central role in the context of IoT for providing a massive amount of data captured by ubiquitous sensors [Ghosal et al., 2020]. Thus, data collection becomes crucial to feed fresh data into IoT services while avoiding data overwritten due to limited storage capacities of IoT sensors [Choi et al., 2012; Di Francesco et al., 2011; Gao et al., 2010; Wang et al., 2010; Navarra et al., 2015; Imon et al., 2014; Chen et al., 2021]. With high agility, mobility and flexibility, the Unmanned Aerial Vehicles (UAVs) have recently received considerable attention for data collection [Samir et al., 2019; Liang et al., 2018; Khochare et al., 2021]. In UAV-enabled WSNs, one or multiple UAVs fly over the network monitoring area, hover at certain locations to collect data from sensors wirelessly, and deliver the collected data to a base station for further processing [Li et al., 2020].

In the literature, extensive efforts have been made to explore UAV-enabled WSNs in recent years. For example, in [Liu et al., 2018] the age-optimal trajectory for a UAV is studied to collect data from sensors with different priorities. The authors in [Zhang et al., 2021] investigated the data collection tour for multiple UAVs to ensure data freshness. In [Trotta et al., 2019] the quality of collected data is optimized by taking into account the data requirements and energy issues, where UAVs are able to wake up sensors through energy transmissions. The above works follow one-to-one data collection scheme, where data from only one sensor can be collected by the UAV at any time instant.

The advancements of wireless communication technologies have led to the emergence of one-to-many data collection scheme as a promising approach, where a UAV is able to simultaneously collect data from multiple sensors, significantly improving the data collection efficiency. For instance, in [Mozaffari et al., 2016], optimal trajectories for multiple UAVs are developed to minimize energy consumption of IoT devices, by adopting the Orthogonal Frequency Division Multiple Access (OFDMA) technique. In [Farajzadeh et al., 2019], data collection is investigated from long-range backscatter devices via UAV, adopting the power-domain Non-Orthogonal Multiple Access (NOMA) protocol, which outperforms OFDMA in many scenarios. The authors in [Caillouet et al., 2018] considered the coverage problem in UAV-enabled WSNs aiming to minimize the deployment cost of UAVs, where a fleet of UAVs are deployed to continuously monitor the network and transmit the collected data to a fixed base station.

In Chapter 2, we studied a one-to-many data collection scenario where a set of potential hovering locations for the UAV are determined in advance. Based on pre-defined potential hovering locations, we developed an efficient approximation algorithm by allocating the time slot budget to the given potential hovering locations, intending to maximize the total volume of collected data. In this chapter, we will study a more complicated scenario where the set of potential hovering locations is not given. Instead, any location within the UAV working area at its flying height could be a potential hovering location. As a result, the number of potential hovering locations for the UAV is infinite. Furthermore, we study the maximization of data collection utility instead of the data collection volume in Chapter 2. The profit function is a non-decreasing and submodular function, which indicates that the data collection profit at the different time slot from a sensor (when there are data remaining at the sensor) is not necessarily equal as we studied in Chapter 2.

Although there exists works on data collection in UAV-enabled WSNs, it is challenging to identify the hovering locations for UAVs in the one-to-many data collection scheme. To be specific, the data collection efficiency under this scheme massively relies on the hovering locations of the UAV and the hovering duration at each such location. However, efficient determination of UAV hovering locations is widely considered to be intractable as there are infinitely many potential hovering locations in the UAV serving area.

For the sake of tractability, most of the existing approaches discretize the UAV serving area into different regions with certain sizes, where each region is regarded as a potential UAV hovering spot. However, the locations in a discretized region cannot be distinguished from each other, which results in the inevitable utility loss of data collection. Moreover, the time complexity of discretization-based approaches highly depends on the size of the network monitoring area, thus making the data collection inefficient especially for large-scale WSNs.

To address the aforementioned challenges, this chapter significantly extends our previous work [Chen et al., 2020] by jointly considering the UAV hovering location positioning and the data collection utility maximization problem under the one-to-many data collection scheme, where the total hovering duration of the UAV is constrained by a given budget. Tackling this problem poses many challenges. For example, to avoid the utility loss caused by discretizations, determining precise hovering locations for the UAV from the infinitely many potential ones is non-trivial. Moreover, jointly considering the hovering location determination and the data collection utility, while separating the computational complexity from the network size, makes the problem further complex. Finally, the allocation of UAV hovering time budget at each selected hovering location also impacts the data collection utility significantly.

To the best of our knowledge, we are the first to focus on enhancing UAV hovering location positioning to improve data collection utility in WSNs. To this end, we propose an efficient algorithm to precisely identify a finite set of potential hovering locations for the UAV from the infinitely many ones, which significantly improves the data collection utility as compared with four baseline heuristics.

The main contributions of this chapter are summarized below.

- We formulate a novel data collection Utility Maximization Problem (UMP) to maximize the utility of data collection under the one-to-many data collection scheme. We also show that the problem is NP-hard.

- We devise an efficient algorithm to precisely determine the UAV's potential hovering locations, thus improving the data collection utility significantly, where we jointly consider the UAV hovering location positioning and data collection utility maximization.

- We devise an approximation algorithm for UMP with approximation ratio $(1 - \frac{1}{e})$ for the problem, where e is the base of the natural logarithm.

- We evaluate the performance of the proposed algorithms through extensive simulation experiments, demonstrating the superiority of the proposed algorithms.

The scope of this work focuses on maximizing the UAV data collection utility of each tour, with the deployment of a single UAV constrained by its energy capacity, where the pre-determined utility function should be non-decreasing and submodular. The WSN consists of homogeneous and static sensors, with identical data transmission range and bandwidth. The UAV's one-to-many data collection mode enables it to simultaneously collect data from multiple sensors. The consumption of energy during the UAV's travel is not considered in this study. Compared with Chapter 2, the UAV is able to hover at any location on its working sphere at a constant height, with no hovering location predefined. These limitations should be taken into account while analyzing the results and drawing conclusions from the study.

The rest of the chapter is organized as follows. Section 3.2 introduces the system model, data collection tour model, data collection utility model, and the problem definition. Section 3.3 studies the defined problem and designs an approximation algorithm. Section 3.4 analyzes the approximation ratio of the proposed algorithm. Section 3.5 reports the performance results of the proposed algorithms via simulation study. Section 3.6 concludes the chapter.

3.2 Preliminaries

In this section, we first introduce various models such as the system model, and data collection tour and utility models. We then formulate the data collection utility maximization problem in WSNs and show that it is NP-hard.

3.2.1 System Model

We consider a wireless sensor network (WSN) serving a two-dimensional region of length $\mathcal{L}$ and width $\mathcal{W}$. A set $\mathcal{V} = \{v_i \mid 1 \leq i \leq N\}$ of homogeneous sensors are deployed in the region, where each sensor v_i has a unique location, denoted by $(x_i, y_i, 0)$. Assume the sensors perform environmental monitoring continuously, acquire and store a huge amount of data. Let D_i denote the volume of data at sensor $v_i \in \mathcal{V}$.

To avoid data loss or being overwritten at each sensor, a UAV is dispatched periodically for data collection from the sensors. The UAV departs from a depot, hovers on certain locations to collect data from the sensors, and then delivers the collected data to a data center for further processing. Fig. 3.1 shows an illustrative example. For safety considerations imposed by regulatory authorities, the UAV is assumed to travel at a fixed altitude H above the ground[Samir et al., 2019]. In this chapter, we assume that the depot is co-located with the data center, unless otherwise stated.

Supported by the OFDMA technique, the UAV is able to collect data simultaneously from multiple sensors, whose Euclidean distance from the UAV is no larger than R, with a data transmission bandwidth B from each sensor.

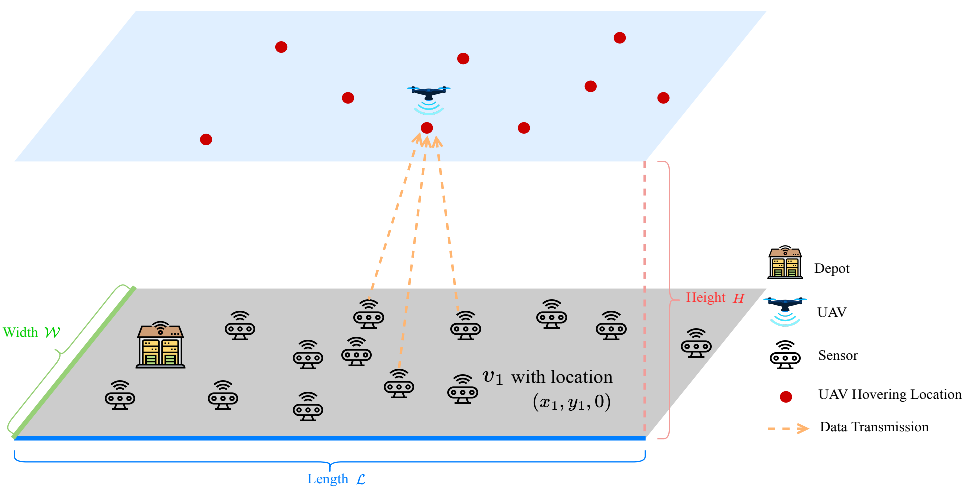

Figure 3.1: An illustrative example of data collection in a UAV-enabled WSN.

3.2.2 Data Collection Tour Model

A *data collection tour* of the UAV is a closed tour starting from and ending at the depot. The tour is a sequence of hovering locations, at altitude H, which the UAV visits one after another for data collection. Since there are infinitely many locations at altitude H, an important challenge for scheduling the data collection tour is to identify a sequence of UAV's hovering locations that improves efficiency of data collection.

Let $\mathcal{H}$ denote a sequence of selected hovering locations for the UAV on a data collection tour, i.e.,

$$\mathcal{H} = (h_1,\ h_2,\ \ldots,\ h_k,\ \ldots,\ h_K), \tag{3.1}$$

where h_k presents the kth hovering location, and K denotes the total number of selected hovering locations on the tour. Under the one-to-many data collection scheme, when hovering at $h_k = (X_k, Y_k, H)$, the UAV is able to collect data from a subset of sensors whose Euclidean distance from the UAV is no greater than a given value R. Let us define the *data collection sensor set*, S_k, as the set of sensors whose data can be collected when the UAV hovers at location h_k, i.e.,

$$S_k = \{v_i \mid (x_i - X_k)^2 + (y_i - Y_k)^2 + H^2 \leq R^2,\ v_i \in \mathcal{V}\}. \tag{3.2}$$

Correspondingly, the data from a sensor v_i can be collected multiple times when the UAV sojourns at different hovering locations of $\mathcal{H}$. Let L_i denote the set of hovering locations of $\mathcal{H}$ which are within the data transmission range of v_i, i.e.,

$$\begin{aligned} L_i = \{h_k \mid (x_i - X_k)^2 + (y_i - Y_k)^2 + H^2 \leq R^2, \\ 1 \leq k \leq K\}. \end{aligned} \tag{3.3}$$

Given the sequence $\mathcal{H}$ of selected hovering locations, the duration T_k for which the UAV sojourns at location h_k is also crucial for the data collection performance. We define the sequence $\mathcal{T}$ of hovering duration corresponding to $\mathcal{H}$ as

$$\mathcal{T} = (T_1,\ T_2,\ \ldots,\ T_k,\ \ldots,\ T_K). \tag{3.4}$$

3.2.3 Data Collection Utility Model

Constrained by its energy capacity, the UAV is unlikely to collect data from all sensors in one tour for a large-scale WSN, it is expected that the UAV is capable to collect data from sensors in important regions in the monitoring area. We consider spatial-temporal correlations among sensors, and model the data collection utility from each sensor by a submodular *utility function*.

Denote by $F_i(t)$ the *utility function* of sensor v_i, which represents the accumulative utility obtained by the UAV when hovering within the data transmission range of v_i for t time units. Denote by $t_i^{max} = \frac{D_i}{B}$ the number of time units required for collecting all data from v_i, where D_i and B are respectively the volume of data at v_i and the data transmission bandwidth. Without loss of generality, we assume that t_i^{max} is an integer. It can be seen that the accumulative utility obtained from v_i increases with the growth of t from 0 to t_i^{max}, and maintains at $F_i(t_i^{max})$ when t is greater than t_i^{max}.

Definition 1 *The defined utility function $F_i(t)$ has the following properties.*

1. *$F_i(t) = 0$ if $t = 0$; $F_i(t) > 0$ if $0 < t \le t_i^{max}$; otherwise $F_i(t) = F_i(t_i^{max})$ if $t > t_i^{max}$, where $t \in \mathbb{N}$.*

2. *$F_i(t)$ is a non-decreasing function, i.e., $F_i(t_1) \le F_i(t_2)$ for $0 \le t_1 < t_2$, where $t_1,\ t_2 \in \mathbb{N}$.*

3. *$F_i(t)$ is a submodular function, where $F_i(t_1 + \Delta) - F_i(t_1) > F_i(t_2 + \Delta) - F_i(t_2)$ for $0 \le t_1 < t_2 \le t_i^{max}$ and $F_i(t_1 + \Delta) - F_i(t_1) = F_i(t_2 + \Delta) - F_i(t_2)$ for $t_i^{max} \le t_1 < t_2$, where $t_1 \in \mathbb{N}$ and $t_2,\ \Delta \in \mathbb{N}^+$.*

To model the utility gain at time unit t when the UAV collects data from a sensor v_i, the *utility margin function* $f_i(t)$ is defined as follows.

$$f_i(t) = \begin{cases} F_i(t) - F_i(t-1), & \text{if } t \in \mathbb{N}^+, \\ 0, & \text{if } t = 0. \end{cases} \tag{3.5}$$

Definition 2 *The defined utility margin function $f_i(t)$ has the following properties.*

1. *$f_i(t_1) > f_i(t_2)$ for $1 \le t_1 < t_2 \le t_i^{max}$ and $t_1,\ t_2 \in \mathbb{N}^+$.*

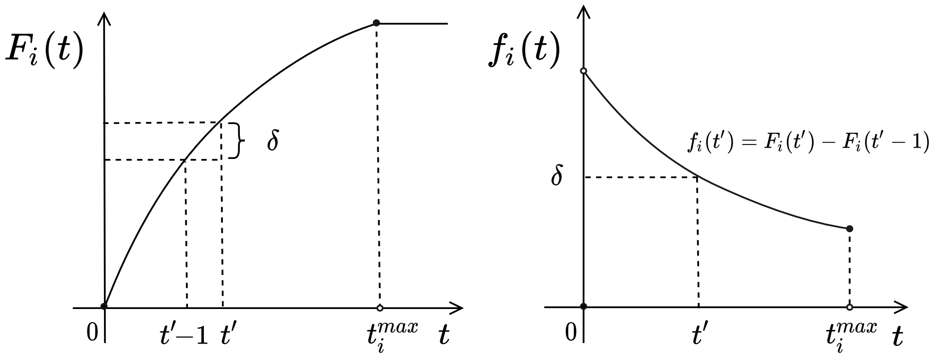

Figure 3.2: An example of utility function $F_i(t)$ and utility margin function $f_i(t)$, where $F_i(t') - F_i(t'-1) = \delta$ and $f_i(t') = \delta$.

2. $f_i(t) = 0$ *for any* $t > t_i^{max}$ *and* $t \in \mathbb{N}^+$.

Fig. 3.2 is an illustrative example of the utility margin function $f_i(t)$ from the utility function $F_i(t)$.

We define u_i as the sum of utility obtained from a sensor v_i during a tour, which is associated with the accumulative duration when the UAV hovers at locations in L_i, i.e.,

$$u_i = F_i(\sum_{h_k \in L_i} T_k), \tag{3.6}$$

recalling that L_i is the set of hovering locations of $\mathcal{H}$ within the data transmission range of v_i, as defined in Eq. (3.3), T_k is the accumulative hovering duration at location h_k.

Denote by U the total data collection utility of a tour, which can be calculated by accumulating the utility u_i obtained from each sensor $v_i \in \mathcal{V}$, i.e.,

$$U = \sum_{v_i \in \mathcal{V}} u_i. \tag{3.7}$$

3.2.4 Data Collection Utility Maximization Problem

We formulate a novel *data collection utility maximization problem* (UMP) in WSNs as follows.

Consider a WSN with a set $\mathcal{V} = \{v_i \mid 1 \leq i \leq N\}$ of sensors deployed in a $\mathcal{L} \times \mathcal{W}$ region. Each sensor $v_i \in \mathcal{V}$ has a data transmission bandwidth B and data transmission range R, with a volume D_i of data to be collected. We assume the utility function $F_i(t)$ of each sensor v_i is pre-defined. A UAV with hovering duration budget Γ travels at a fixed altitude H above the WSN for data collection. Then the UMP is to find a closed data collection tour for the UAV (starting and ending at the depot), which consists of a sequence of hovering locations and hovering duration at each such one, aiming at maximizing the total utility of data collected from the sensors in the WSN.

Formally the problem UMP is formulated as:

$$\text{Maximize} \quad U, \tag{3.8}$$

$$\text{subject to} \quad h_k = (X_k, Y_k, H), \qquad \forall 1 \le k \le K \tag{3.9}$$

$$-R \le X_k \le \mathcal{L} + R, \quad \forall 1 \le k \le K \tag{3.10}$$

$$-R \le Y_k \le \mathcal{W} + R, \quad \forall 1 \le k \le K \tag{3.11}$$

$$T_k \in \mathbb{N}^+, \qquad \forall 1 \le k \le K \tag{3.12}$$

$$\sum_{k=1}^{K} T_k \le \Gamma, \tag{3.13}$$

Constraints (3.10) and (3.11) are used to bound the serving area of the UAV, and assume that the depot is located within the UAV serving area. Constraint (3.13) limits the total hovering duration of the UAV to be no greater than the given hovering budget Γ.

3.2.5 NP Hardness of UMP

Theorem 7 *The data collection utility maximization problem (UMP) is NP-hard.*

Proof We show the NP-hardness of UMP by a reduction from an NP-hard problem – the Robust K-Center problem (RKC) [Charikar et al., 2001]. Given a set V of points in a 2-D plane and K disks with radii r, the decision version of the RKC is to cover at least $M \le |V|$ points by the disks, where M is a given integer. This problem has been shown to be NP-hard [Xiao et al., 2004].

Let I and I_U be the instances of RKC and UMP, respectively. We show that I can be reduced to I_U in polynomial time as follows.

The number K of disks in I corresponds to the number Γ of UAV hovering time units in I_U, i.e., $K = \Gamma$. Denote by V_I the point set in I, which corresponds to the sensor set $\mathcal{V}_U$ in I_U, where there is a corresponding sensor $v_i \in \mathcal{V}_U$ at location $(a_i, b_i, 0)$ of each point with coordinates (a_i, b_i) in I with $1 \le i \le |V|$.

For each disk k with $1 \le k \le K$, there is a corresponding hovering location h_k for the UAV. When the UAV hovers at location h_k, it can collect all data from sensors in S_k within one time unit, assuming that the data volume D_i of each sensor $v_i \in \mathcal{V}_U$ is B, where B is the data transmission bandwidth of v_i. Also, the utility of each sensor v_i is identical by setting $F_i(0) = 0$ and $F_i(t) = 1$ if $t \ge 1$ at each time unit t. The data transmission range of each sensor is $R = \sqrt{H^2 + r^2}$, where r is the radius of each disk in I, and H is the hovering altitude of the UAV in I_U.

Following the reduction from I to I_U, each sensor has an identical utility function with identical volume B of data to be collected, the data of all sensors in S_k can be collected by the UAV at location h_k within one time unit. Also, the accumulative utility obtained at time unit k is determined by the number of sensors in S_k whose data have not been collected yet. Hence, maximizing the data collection utility of I_U is equivalent to covering the maximum number of points in I by the K disks with $K = \Gamma$.

Denote by OPT and $|OPT|$ an optimal solution of I_U and the value of OPT, respectively. A solution for I then can be derived from the solution OPT. Recall that M is the minimum number of points required to be covered in I. If $|OPT| < M$, the maximum number of sensors covered by the K disks is less than M, and there is no feasible solution for I. Otherwise, for the hovering location sequence $\mathcal{H}$ of OPT with $|\mathcal{H}| = K$, we can generate a set of points in I, where for each hovering location (X_j, Y_j, H) of $\mathcal{H}$, there is a corresponding point (X_j, Y_j) on the 2-D plane to the point set that consists of disk locations, which is a feasible solution for I. Thus a feasible solution to

I_U in turn returns a feasible solution to I, and the reduction is in polynomial time. The theorem then follows. □

3.3 Approximation Algorithm for Data collection Utility Maximization

In this section, we study the data collection utility maximization problem (UMP) by proposing an approximation algorithm.

3.3.1 Overview of the Approximation Algorithm

Given the budget of Γ hovering time units, the UMP is to find a closed data collection tour for the UAV containing a sequence of hovering locations, each with a hovering duration, aiming at maximizing the total data collection utility.

The hovering location identification for the UAV is quite challenging since it is impossible to examine every location over the UAV serving area (with infinitely many locations). To tackle this problem, we narrow down the UAV serving area to a finite $\mathbb{M}$-Set, which always contains a location q_t^*, for any time unit t, with the global[1] maximum utility gain. From the identified $\mathbb{M}$-Set, q_t^* is iteratively selected at each time unit t, for $1 \leq t \leq \Gamma$; it is possible that a location is chosen within multiple iterations, i.e., $q_a^* = q_b^*$ where $a \neq b$. Consequently, a sequence L of locations are obtained after Γ iterations. We then regard each distinct location $l \in L$ as a hovering location for the UAV and recognize the number of replications of l contained in L as the

[1]The utility gain for any location q in the UAV serving area is no greater than the utility gain at q_t^* at time unit t.

hovering duration at l. Finally, a data collection tour is obtained by forming a closed circuit visiting the selected hovering locations and the depot, with the corresponding hovering duration. The proposed algorithm for the UMP is an approximation algorithm with a provable approximation ratio of $(1 - \frac{1}{e})$.

3.3.2 Potential Hovering Location Set: $\mathbb{M}$-Set

In the following, we propose to narrow down the UAV serving area to a finite '$\mathbb{M}$-Set' for further processing.

Definition 3 *A potential hovering location set $\mathcal{M}$ is recognized as an $\mathbb{M}$-Set if it has the following two properties:*

1. *$\mathcal{M}$ is a finite hovering location set.*

2. *There always exists a location $q_t^* \in \mathcal{M}$, where the utility gain at q_t^* at time unit t is no less than the utility gain at any other location in the UAV serving area at time unit t, for $1 \leq t \leq \Gamma$.*

By utilizing an $\mathbb{M}$-Set, we can identify q_t^* by finding a location with the largest utility gain in $\mathcal{M}$ at time unit t. In the following, we develop an algorithm to identify an $\mathbb{M}$-Set.

Let (v_a, v_b) be a pair of sensors, where sensors $v_a \in \mathcal{V}$ and $v_b \in \mathcal{V}$ have coordinates $(x_a, y_a, 0)$ and $(x_b, y_b, 0)$, respectively. Denote by $O^s_{a,b}$ such a circle on the ground with a fixed radius $\sqrt{R^2 - H^2}$ that both v_a and v_b are on its circumference with $s \in \{1, 2\}$, and denote by $|v_a v_b|$ the Euclidean distance between v_a and v_b. Then, a pair of sensors can be classified into three cases as follows.

- **Case 1:** $|v_a v_b| > 2\sqrt{R^2 - H^2}$, $O^s_{a,b}$ does not exist.

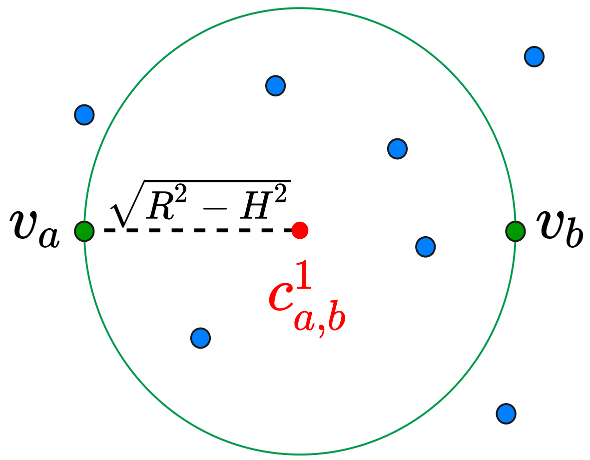

Figure 3.3: Only $O^1_{a,b}$ exists if $|v_a v_b| = 2\sqrt{R^2 - H^2}$, with the center $c^1_{a,b} = (\frac{x_a+x_b}{2}, \frac{y_a+y_b}{2}, 0)$.

- **Case 2:** $|v_a v_b| = 2\sqrt{R^2 - H^2}$. As illustrated in Fig. 3.3, only $O^1_{a,b}$ exists and v_a and v_b on the circumference of the circle. The center of $O^1_{a,b}$ is $c^1_{a,b} = (\frac{x_a+x_b}{2}, \frac{y_a+y_b}{2}, 0)$.

- **Case 3:** $0 < |v_a v_b| < 2\sqrt{R^2 - H^2}$. There are two circles $O^1_{a,b}$ and $O^2_{a,b}$ and v_a and v_b are on their circumferences.

  To obtain $O^1_{a,b}$ and $O^2_{a,b}$, we first form two auxiliary circles O'_a and O'_b centered at v_a and v_b with radius $\sqrt{R^2 - H^2}$ respectively. Denote by $c^1_{a,b}$ and $c^2_{a,b}$ the intersection points of O'_a and O'_b. We can then identify $O^1_{a,b}$ and $O^2_{a,b}$ with radius $\sqrt{R^2 - H^2}$ centering at $c^1_{a,b}$ and $c^2_{a,b}$ respectively. As a result, both v_a and v_b will be on the circumferences of $O^1_{a,b}$ and $O^2_{a,b}$. Fig. 3.4 presents an illustrative example.

  The coordinates of $c^1_{a,b}$ and $c^2_{a,b}$ can be obtained through solving the following equations.

$$\begin{cases} (X_{a,b} - x_a)^2 + (Y_{a,b} - y_a)^2 = R^2 - H^2, \\ (X_{a,b} - x_b)^2 + (Y_{a,b} - y_b)^2 = R^2 - H^2. \end{cases} \tag{3.14}$$

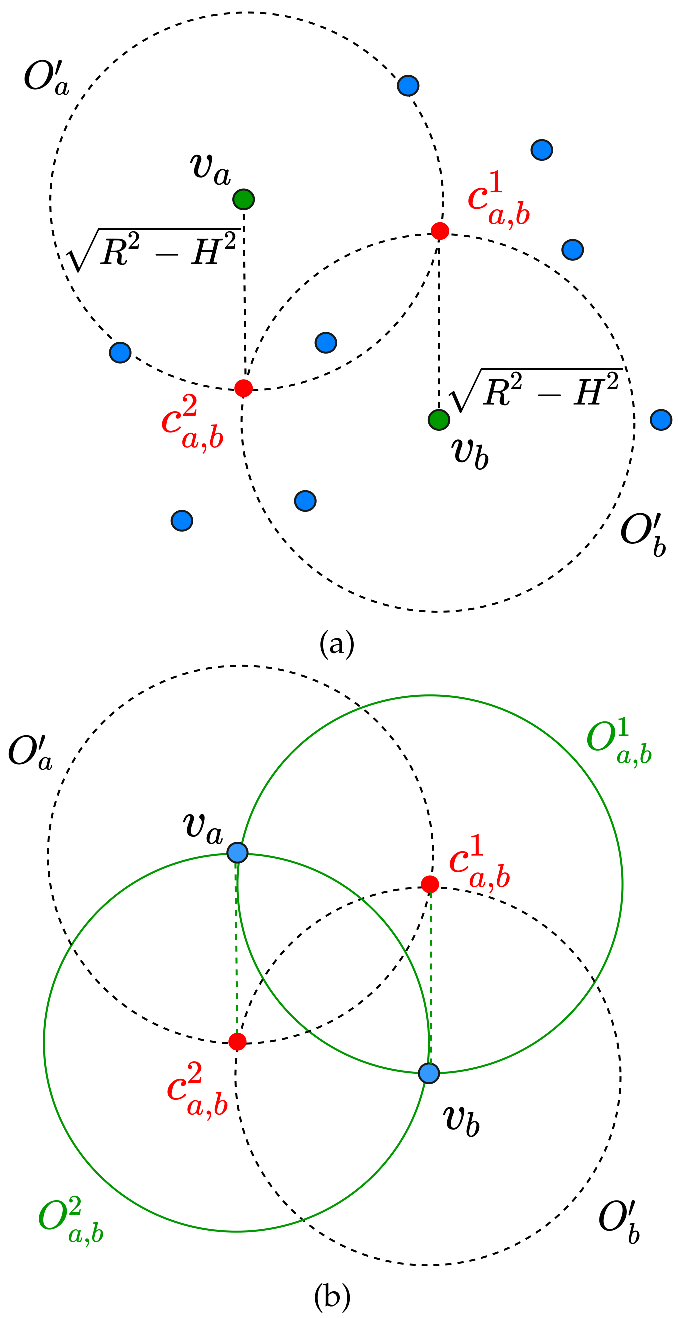

Figure 3.4: An illustrative example to identify $O^1_{a,b}$ and $O^2_{a,b}$ if $0 < |v_a v_b| < 2\sqrt{R^2 - H^2}$. (a) Form O'_a and O'_b with radius $\sqrt{R^2 - H^2}$ centered at v_a and v_b respectively, where $c^1_{a,b}$ and $c^2_{a,b}$ are the intersection points. (b) Centered at $c^1_{a,b}$ and $c^2_{a,b}$ respectively, $O^1_{a,b}$ and $O^2_{a,b}$ are obtained with radius $\sqrt{R^2 - H^2}$, covering both v_a and v_b on their circumferences.

Let $(X^1_{a,b}, Y^1_{a,b})$ and $(X^2_{a,b}, Y^2_{a,b})$ be the solutions of Eqs. (3.14). We then have $c^1_{a,b} = (X^1_{a,b}, Y^1_{a,b}, 0)$ and $c^2_{a,b} = (X^2_{a,b}, Y^2_{a,b}, 0)$.

Following the discussion of the three cases, $O^s_{a,b}$ (if exists) centered at $c^s_{a,b}$ for each pair of sensors v_a and v_b can be found. The projection of $c^s_{a,b}$ at altitude H then can be added to the $\mathbb{M}$-Set $\mathcal{M}$ as a potential hovering location for the UAV. Furthermore, the projection (x_i, y_i, H) of the coordinates of each sensor v_i at altitude H is also added to $\mathcal{M}$.

The detailed algorithm for identifying an $\mathbb{M}$-Set is presented in `Algorithm 4`.

Algorithm 4 Algorithm for identifying an $\mathbb{M}$-Set

Input: A set $\mathcal{V}$ of sensors, data transmission range R of sensors, hovering altitude H of the UAV.

Output: An $\mathbb{M}$-Set;

$\mathcal{M} \leftarrow \emptyset$;
$r \leftarrow \sqrt{R^2 - H^2}$;
for each sensor $v_i \in \mathcal{V}$ **do**
  $\mathcal{M} \leftarrow \mathcal{M} \cup \{(x_i, y_i, H)\}$;
for each sensor pair (v_a, v_b) **do**
  if $|v_a v_b| = 2r$ **then**
    $\mathcal{M} \leftarrow \mathcal{M} \cup \{(\frac{x_a+x_b}{2}, \frac{y_a+y_b}{2}, H)\}$;
  else if $|v_a v_b| < 2r$ **then**
    Find the solutions $(X^{a,b}_1, Y^{a,b}_1)$, $(X^{a,b}_2, Y^{a,b}_2)$ of Eqs. (3.14);
    $\mathcal{M} \leftarrow \mathcal{M} \cup \{(X^{a,b}_1, Y^{a,b}_1, H), (X^{a,b}_2, Y^{a,b}_2, H)\}$;
return $\mathcal{M}$

3.3.3 Approximation Algorithm

Inspired by our previous work [Chen et al., 2020], let us now develop an approximation algorithm for UMP with a provable $(1 - \frac{1}{e})$ ratio by utilizing the $\mathbb{M}$-Set and the defined utility function.

Let L denote a sequence of locations selected for each time unit, i.e.,

$$L \ = < l_1,\ l_2,\ ...,\ l_t,\ ...,\ l_{\Gamma-1},\ l_\Gamma >, \tag{3.15}$$

where l_t is the selected location at time unit t with $1 \leq t \leq \Gamma$.

Due to overlapping between covered sensors of different hovering locations, the data collection utility gain at a location m_j at time unit t is determined by all locations $l_1, l_2, ..., l_{t-1}$ selected so far. Fig. 3.5 provides an illustrative example. For the sake of convenience, we just assume the utility margin function $f_i(t)$ of each sensor appeared on this diagram is $f_i(1) = 1$ and $f_i(t) = 0$ for $t \geq 2$. The utility gain at p_2 for the second time unit is $f_5(1) + f_6(1) = 2$, if p_1 is selected for the first time unit; whereas it is $f_2(1) + f_3(1) + f_4(1) + f_5(1) = 4$ if p_3 is selected for the first time unit. To figure out the utility gain at a location m_j and at time unit t, we thus have to focus on the remaining data at each sensor covered by m_j.

Denote by T_i^t the number of locations within the transmission range of v_i contained in the subsequence of selected locations $< l_1, l_2, \ldots, l_t >$, where $T_i^0 = 0$. Once the hovering location l_{t+1} is identified, the corresponding hovering duration T_i^{t+1} is determined as:

$$T_i^{t+1} = \begin{cases} T_i^t + 1, & \text{if } l_{t+1} \in L_i, \\ T_i^t, & \text{otherwise,} \end{cases} \tag{3.16}$$

where $l_{t+1} \in L_i$ indicates that the selected location l_{t+1} is within the data transmission range of sensor v_i.

We then obtain the utility gain at a hovering location m_j for a certain time unit t by aggregating the utility gain $f_i(T_i^{t-1} + 1)$ at each sensor $v_i \in S_j$, where

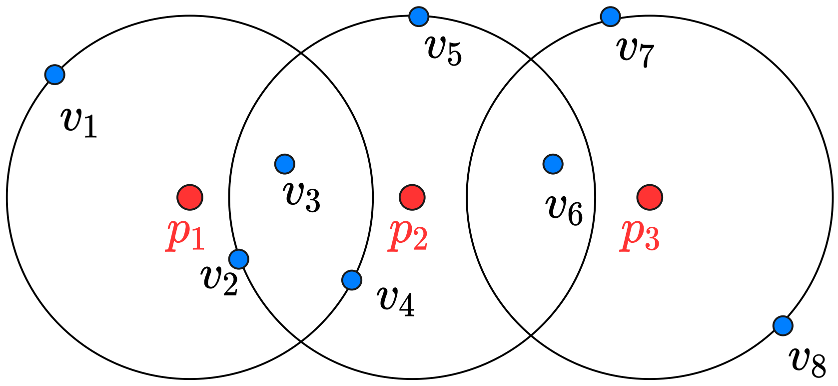

Figure 3.5: An example of the utility gain at a location at a certain time unit affected by the selected locations so far.

$f_i(t)$ is the utility margin function at v_i defined in Eq. (3.5). Recall that S_j is the set of sensors covered by hovering location m_j defined in Eq.(3.2). Denote by $\Lambda_j(t)$ the utility gain at hovering location m_j at time unit t, where $1 \leq t \leq \Gamma$. Thus,

$$\Lambda_j(t) = \sum_{v_i \in S_j} f_i(T_i^{t-1} + 1). \tag{3.17}$$

Having the set $\mathbb{M}$-Set $\mathcal{M}$ and the utility gain $\Lambda_j(t)$ at each location $m_j \in \mathcal{M}$, the proposed algorithm for UMP proceeds as follows.

Initialization. $T_i^0 = 0$ for any sensor $v_i \in \mathcal{V}$.

Identification of the location sequence L. For each t with $1 \leq t \leq \Gamma$, we iteratively select a location $l_t = m_{j^*}$ with the maximum $\Lambda_{j^*}(t)$ from the $\mathbb{M}$-Set $\mathcal{M}$ according to Eq. (3.17), and obtain T_i^t for each $v_i \in \mathcal{V}$ by Eq. (3.16). Consequently, a hovering location sequence L defined in Eq. (3.15) is obtained.

Extraction of hovering duration. Each distinct location in L is a hovering location of the UAV. Note that, there could be multiple duplicates of a hovering location in L, and the number of duplicates of a location m_j is counted as the hovering duration at m_j. For instance, for the case where $L =< p_1, p_4, p_1, p_2, p_1, p_4 >$ with $\Gamma = 6$, the hovering locations for the UAV are p_1, p_2 and p_4 with hovering duration 3, 1 and 2 time units, respectively.

Data collection tour scheduling. With the hovering locations extracted from L, a data collection tour is generated by forming a closed circuit visiting each selected hovering location including the depot, with corresponding hovering duration identified by the previous step.

Algorithm 5 Algorithm for the UMP

Input: A set $\mathcal{V}$ of sensors, data transmission range R of sensors, hovering altitude H of the UAV, the maximum number Γ of hovering time units of the UAV per tour.

Output: A data collection tour $\mathcal{C}$ for the UAV;

An $\mathbb{M}$-Set $\mathcal{M}$ is delivered by calling `Algorithm 4`;
S_j is derived for each location $m_j \in \mathcal{M}$;
$E \leftarrow \{E_j = 0 \mid m_j \in \mathcal{M}\}$; /*$E_j$ is hovering duration at m_j*/
$T \leftarrow \{T_i^t = 0 \mid 0 \le t \le \Gamma,\ v_i \in \mathcal{V}\}$;
for $t \leftarrow 1$ to Γ **do**
    Identify an index j^* such that $j^* \leftarrow \text{argmax}_{m_j \in \mathcal{M}} \Lambda_j(t)$ by Eq. (3.17);
    $E_{j^*} \leftarrow E_{j^*} + 1$;
    for each $v_i \in \mathcal{V}$ **do**
        if $v_i \in S_{j^*}$ **then**
            $T_i^t \leftarrow T_i^{t-1} + 1$;
        else
            $T_i^t \leftarrow T_i^{t-1}$;
for each $m_j \in \mathcal{M}$ **do**
    if $E_j \ge 1$ **then**
        $\mathcal{F} \leftarrow \mathcal{F} \cup \{(m_j, E_j)\}$;
    Find a closed tour $\mathcal{C}$ containing the depot and each location m_j in $\mathcal{F}$, where E_j is the hovering duration when the UAV sojourns at m_j for data collection;
return $\mathcal{C}$

3.4 Algorithm Analysis

In this section, we first show that the hovering location set $\mathcal{M}$ delivered by `Algorithm 4` is consistent with the properties of $\mathbb{M}$-Set in Definition 3. Then we show that the approximation ratio of `Algorithm 5` is $(1-\frac{1}{e})$, where e is the base of natural logarithm.

Denote by $\mathcal{M}_1$ and $\mathcal{M}_2$ the subsets of locations identified from sensor locations (Step 3 and Step 4 of `Algorithm 1`) and sensor pairs (from Step 5 to Step 10 of `Algorithm 1`), respectively. We consider the utility gain at time unit t, where locations $l_1, l_2, \ldots, l_{t-1}$ for the first $(t-1)$ time units have been identified already. Denote by p_{max} the location with the maximum utility gain Λ_{max} over the UAV serving area at time unit t, which is not necessarily contained in $\mathcal{M}$. Denote by S_{max} the data collection sensor set of p_{max}. To show that there exists a location $m \in \mathcal{M}$ with the same utility gain $\Lambda_m = \Lambda_{max}$ at time unit t, we consider $|S_{max}| = 1$ and $|S_{max}| \geq 2$ respectively.

Lemma 4 *If $|S_{max}| = 1$, there exists a location $m \in \mathcal{M}_1$ with the utility gain $\Lambda_m = \Lambda_{max}$ at time unit t.*

Proof Denote by v_{max} the only sensor in S_{max} with location $(x_{max}, y_{max}, 0)$, i.e., $S_{max} = \{v_{max}\}$. In `Algorithm 1`, $m = (x_{max}, y_{max}, H)$ is an element in $\mathcal{M}_1$ according to Step 3 and Step 4. Letting S_m denote the data collection sensor set of m, clearly $v_{max} \in S_m$. Thus $S_{max} \subseteq S_m$ with $\Lambda_{max} \leq \Lambda_m$. Since Λ_{max} is the global maximum utility gain at time unit t, we have $\Lambda_{max} \geq \Lambda_m$, hence $\Lambda_m = \Lambda_{max}$. $\square$

Lemma 5 *If $|S_{max}| \geq 2$, there exists a location $m \in \mathcal{M}_2$, with the utility gain $\Lambda_m = \Lambda_{max}$ at time unit t.*

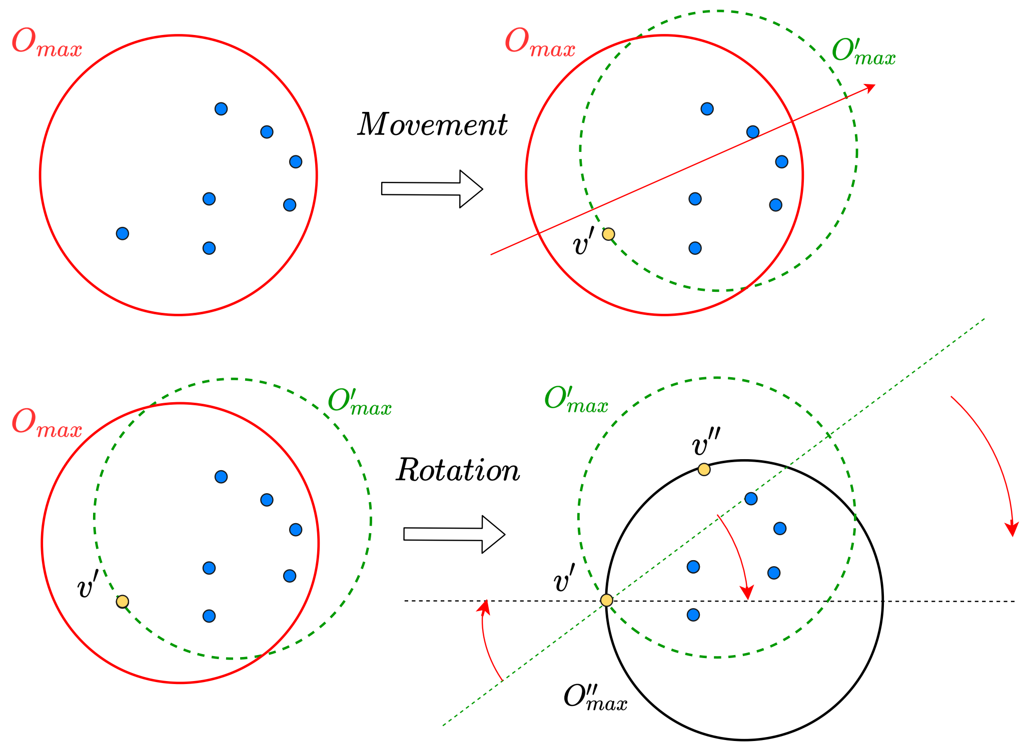

Figure 3.6: An instance of Movement and Rotation.

Proof The claim can be shown as long as a location $m \in \mathcal{M}_2$ with $\Lambda_m = \Lambda_{max}$ can be found. In the following, we show how to identify location m from $\mathcal{M}_2$.

We first find a disk O_{max} on the ground centered at the projection of p_{max} with radius $r = \sqrt{R^2 - H^2}$, where sensors covered by O_{max} (including sensors inside the disk area and sensors on its circumference) are the same as sensors contained in S_{max}. If the number of sensors on the circumference of disk O_{max} is no less than 2, we can obtain a location $m = p_{max}$; otherwise, we find location m by performing operations: *Movement* and *Rotation*. (For an example, see Figure 3.6.)

- *Movement:* If no sensor is on the circumference of disk O_{max}, move the disk in an arbitrary direction until a sensor sits on its circumference.

Denote by O'_{max} and p'_{max} the disk and its center after the `Movement` operation. Note that, it is very likely to have more than one sensor on the circumference of disk O'_{max}. We can identify the location $m = p'_{max}$ if there are at least 2 sensors on the circumference of O'_{max}. Otherwise, we proceed with the `Rotation` operation as follows.

- *Rotation:* Denote by v' the location of the only one sensor on the circumference of disk O'_{max}. Rotate disk O'_{max} about the pivot point v' in either clockwise or anti-clockwise direction until a sensor (other than v') is on its circumference.

Denoting by O''_{max} and p''_{max} the disk and its center after the `Rotation` operation, the location $m = p''_{max}$ can be obtained. It is possible that there are more than two sensors sitting on the circumference of disk O''_{max}.

We conclude that the location m is either p_{max}, p'_{max}, or p''_{max}. Consequently, we find a disk O_{max}, O'_{max} or O''_{max} centered at m with no less than two sensors sitting on its circumference. Let v_a and v_b be any two sensors on the circumference of the disk. By Step 5 to Step 10 in `Algorithm 1`, one or two locations can be identified based on (v_a, v_b), which must contain m. This is due to the fact that with a fixed radius and two nodes on the circumference, at most two circles can be formed. We thus have $m \in \mathcal{M}_2$.

Having identified the location m, we now show that the sensors covered by O_{max} do not change when applying both the `Movement` and `Rotation` operations.

`Movement` starts when no sensor is on the circumference of O_{max}, and ends at O'_{max} when the first sensor is on its the circumference. Let v_a be a sensor on the circumference of O'_{max}. Before v_a is on the circumference, no sensor covered by O_{max} (sensors inside or on the circumference of O_{max}) leaves out of O_{max} during the `Movement` operation. Otherwise, this conflicts with the fact that sensor v_a is the first sensor on the circumference. Denote by Λ'_{max} the utility gain of sensors covered by O'_{max} at time unit t. We then have $\Lambda'_{max} \geq \Lambda_{max}$. Since Λ_{max} is the maximum utility gain at time t over the UAV serving area, i.e., $\Lambda_{max} \geq \Lambda'_{max}$, we have $\Lambda_{max} = \Lambda'_{max}$.

`Rotation` starts with O'_{max} when only one sensor v' is on its circumference, and ends at O''_{max} when the first sensor (other than v') is on the circumference of O''_{max}. Let Λ''_{max} be the utility gain of sensors covered by O''_{max}. Then $\Lambda''_{max} = \Lambda'_{max}$ can be shown similar to the `Movement` operation.

Thus, `Movement` and `Rotation` operations do not change the sensors covered by disk O_{max}. As a result, there must exist a location $m \in \mathcal{M}_2$ with $\Lambda_m = \Lambda_{max}$ if $|S_{max}| \geq 2$. $\square$

Theorem 8 *The hovering location set $\mathcal{M}$ generated by* `Algorithm 4` *is an $\mathbb{M}$-Set by the properties in Definition 3.*

Proof Following Lemma 4 and Lemma 5, there always exists a location $m \in \mathcal{M}$ with the maximum utility gain compared with other locations in the UAV serving area at any time unit. From Step 3 to Step 4, and from Step 5 to Step 10 in `Algorithm 4`, there are at most $|\mathcal{V}|$ and $|\mathcal{V}| \cdot (|\mathcal{V}| - 1)$ locations identified, respectively. The set $\mathcal{M}$ thus is a finite set, and theorem follows. $\square$

We now analyze the approximation ratio of the proposed `Algorithm 5`. A location $l_t = m_{j^*}$ with the maximum utility gain is selected from $\mathbb{M}$-Set at time unit t by Step 6. Denote by z_t the increment of the total utility gain by selecting $l_t = m_{j^*}$, i.e., $z_t = \Lambda_{j^*}(t)$. Denote by Z_t the total utility gain by selecting $l_1, l_2, ..., l_t$ so far, i.e.,$Z_t = \sum_{x=1}^{t} z_x$. Let OPT and g_t denote the total utility gain of the optimal solution, and the difference between OPT and Z_t, i.e., $g_t = OPT - Z_t$.

Lemma 6 *(i)* $z_{t+1} \geq \frac{g_t}{\Gamma}$*, for* $0 \leq t \leq \Gamma - 1$*, where*$z_0 = Z_0 = 0$*, and* $g_0 = OPT$*.*

(ii) $g_{t+1} \leq (1 - \frac{1}{\Gamma})^{t+1} \cdot OPT$*, for* $0 \leq t \leq \Gamma - 1$*.*

Proof (i) Recall that g_t is the difference of the total utility gain between OPT and Z_t. By the Pigeonhole Principle, one of the Γ selections in the optimal solution must have at least $\frac{g_t}{\Gamma}$ amount of utility gain. Note that the utility gain at l_{t+1} at time $t+1$ is no less than the utility gain at other locations in $\mathcal{M}$, which always contains the location with the global maximum utility gain by Theorem 8. Therefore, we have that z_{t+1} is the global maximum utility gain at time unit t, i.e., $z_{t+1} \geq \frac{g_t}{\Gamma}$ for $0 \leq t \leq \Gamma - 1$.

(ii) We show the claim by induction. For the base case $t = 0$, since $g_t = OPT - Z_t$, we have

$$
\begin{aligned}
g_1 &\leq OPT - Z_1 = OPT - z_1 && (3.18)\\
&\leq OPT - \frac{g_0}{\Gamma} \qquad \text{by Lemma 6(i)} && (3.19)\\
&= OPT - \frac{OPT}{\Gamma} = (1 - \frac{1}{\Gamma}) \cdot OPT && (3.20)
\end{aligned}
$$

Assuming that $g_t \leq (1 - \frac{1}{\Gamma})^t \cdot OPT$, we show as follows $g_{t+1} \leq (1 - \frac{1}{\Gamma})^{t+1} \cdot OPT$.

$$
\begin{aligned}
g_{t+1} &= g_t - z_{t+1} \leq g_t - \frac{g_t}{\Gamma} \qquad \text{by Lemma 6(i)} && (3.21)\\
&= g_t(1 - \frac{1}{\Gamma}) && (3.22)\\
&\leq (1 - \frac{1}{\Gamma})^{t+1} \cdot OPT, \text{ by induction hypothesis} && (3.23)
\end{aligned}
$$

□

Theorem 9 *The approximation ratio of* `Algorithm 5` *for the Utility Maximization Problem is* $(1 - \frac{1}{e})$.

Proof By Lemma 6, $g_\Gamma \leq (1 - \frac{1}{\Gamma})^\Gamma \cdot OPT$. Since $(1 - \frac{1}{\Gamma})^\Gamma \approx \frac{1}{e}$, we have $g_\Gamma \leq \frac{OPT}{e}$. Thus,

$$\begin{aligned} Z_\Gamma &= OPT - g_\Gamma \\ &\geq OPT - \frac{OPT}{e} \\ &= OPT(1 - \frac{1}{e}). \end{aligned} \tag{3.24}$$

Hence, the proof follows. □

3.5 Performance Evaluation

In this section, we evaluate the performance of the proposed algorithms by simulation experiments, and investigate the impacts of important parameters on the algorithm performance.

3.5.1 Experimental Settings

We consider a UAV-enabled WSN deployed in an area with $1,000 \times 1,000$ square meters, where sensors are randomly distributed [Chen et al., 2020]. The data transmission range and bandwidth of each sensor v_i are 150 meters and 1 Mbps, respectively [Theunissen et al., 2018]. The utility margin function of each sensor v_i is generated by $f_i(t) = \alpha \times \frac{1}{t^\beta + \gamma}$, where $\alpha \in [1,\ 100]$, $\beta \in$

$[0.1,\ 1]$ and $\gamma \in [1,\ 2]$ are constants. We employ a UAV for data collection, with the hovering altitude $H = 120$ meters. The hovering budget of the UAV is set as $\Gamma = 1,800$ seconds [Chen et al., 2020], where the length of each time unit is one second. These parameters are adopted in the default setting, unless otherwise specified.

3.5.2 Comparison Heuristics

Since the UMP is a new problem, existing algorithms in the literature can not be directly compared with it. To evaluate the performance of `Algorithm 5` for the UMP, we propose the following four baseline heuristics.

D-Gre. It first discretizes the monitoring area into square regions with a side length of 10 meters. It then adopts a *Greedy* algorithm for generating a UAV data collection tour, i.e., a region d_{max} with the maximum utility is selected iteratively, and the UAV hovers at a random location p_{max} within the region d_{max} until all data from sensors in S_{max} are collected. This procedure continues until the accumulative hovering time of the UAV reaches the budget.

R-Gre. It first identifies 100 locations randomly from the UAV serving area as potential hovering locations. It then adopts the *Greedy* algorithm to iteratively select a location p_{max} with the maximum utility from the 100 identified locations.

S-Gre. The projection (x_i, y_i, H) of each sensor v_i at altitude H is regarded as a potential hovering location for the UAV, with *Greedy* adopted for forming a UAV data collection tour.

S-N. The projection of each sensor v_i at altitude H is recognized as a potential hovering location for the UAV. From these identified locations, p_{max_1} with the maximum utility is selected, where the UAV will collect all data from the sensors in S_{max_1}. Then p_{max_2} is selected from the neighbors of p_{max_1} (no larger than 180 meters away from p_{max_1}) where data are also fully collected. The procedure continues until the accumulative hovering time of the UAV reaches the budget.

The value plotted in each figure is the mean of the results out of 50 WSN instances with the same size. The running time of all mentioned simulations is obtained from a desktop with 4.0 GHz Intel Core i7 CPU and 32 GB RAM.

3.5.3 Experimental Results

We first evaluate the performance of `Algorithm 1` that aims to identify potential hovering locations for the UAV in order to maximize the total utility in the end.

Here we propose grid-based four heuristics `D-10`, `D-50`, `D-100` and `D-200` for comparison purposes, which divide the monitoring area of sensors into numbers of square regions with side lengths 10, 50, 100 and 200 meters respectively and adopt Step 2 to Step 17 of `Algorithm 2` for generating a UAV data collection tour.

We evaluate the performance of `Algorithm 1` by comparing the simulation results of `Algorithm 2` (denoted by `Alg02`) against the mentioned four heuristics, where the only difference between them is the set of identified potential hovering locations. The square sizes of the simulated networks vary from 600 meters to $1,500$ meters, with 400 sensors randomly deployed.

Fig. 3.7(a) demonstrates that the data collection utility of `Alg02` significantly outperforms other discretization-based heuristics. With increasing network area, the data collection utility of all such algorithms declines, due to

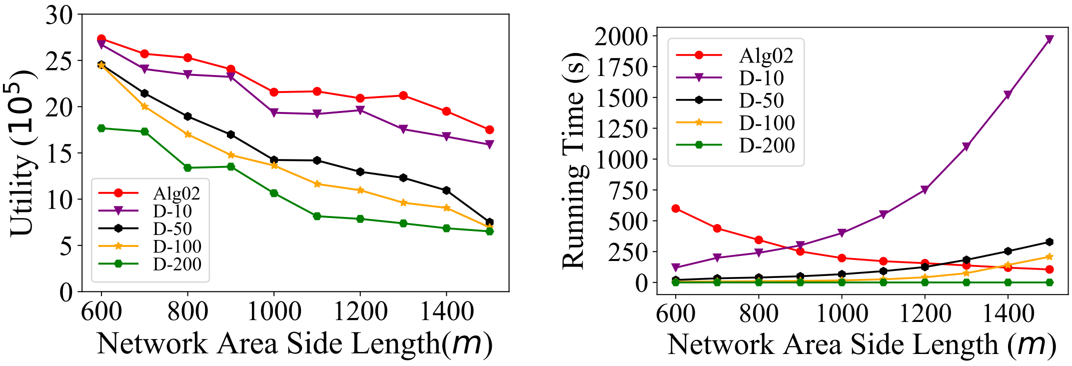

(a) (b)

Figure 3.7: Performance of `Alg02`, `D-10`, `D-50`, `D-100` and `D-200` in WSNs by varying the side length of the network area from 600 meters to $1,500$ meters.

the fact that fewer sensors are located in the data reception range of the UAV in sparser networks. Fig. 3.7(b) plots the running time of `Alg02`, which decreases with the size of the network area, while it increases rapidly for other discretization-based heuristics.

Next we compare the performance of `Algorithm 2` with the aforementioned four heuristics `D-Gre`, `R-Gre`, `S-Gre` and `S-N`, by varying the number of sensors from 100 to $1,000$. Fig.3.8(a) depicts that `Alg02` significantly outperforms the four mentioned heuristics. In particular, the utility delivered by `Alg02` is approximately 149% of that by `D-Gre`, and 170% of the utilities by other heuristics. Fig.3.8(b) plots the running time of the proposed algorithms.

3.5.4 Impacts of Parameters on the Performance

We investigate the impacts of the UAV hovering budget and the data transmission range of sensors on the performance of the algorithms in sensor networks of 400 sensors.

We first study the impact of the UAV hovering budget on the performance

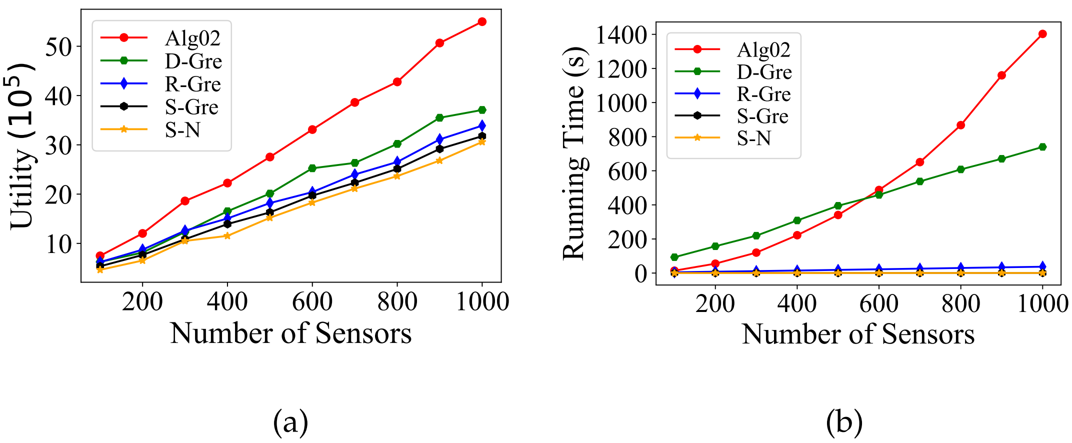

Figure 3.8: Performance of `Alg02`, `D-Gre`, `R-Gre` and `S-Gre`, `S-N` in WSNs consisting of sensors from 100 to 1,000.

of the mentioned algorithms, by varying the UAV hovering budget from 1,000 to 10,000 time units. Fig. 3.9(a) shows that the utilities of different algorithms rapidly grow with the increase on the UAV hovering budget. It can be seen that `Alg02` significantly outperforms the other heuristics in all cases. Fig. 3.9(b) demonstrates that the running time of `Alg02` increases with that of the UAV hovering budget.

We also investigate the impact of the transmission range of sensors on the performance of the mentioned algorithms. Note that the data transmission range of sensors should be no less than the hovering altitude of the UAV; otherwise, the transmitted data from sensors cannot be collected by the UAV.

We evaluate the performance of the proposed algorithms by varying the data transmission range of sensors from 140 meters to 200 meters. It can be seen from Fig. 3.10(a) that the utilities delivered by different algorithms grow with the increase on the data transmission range, due to the fact that more sensors can be covered by the UAV. Fig. 3.10(b) plots the running times of different algorithms.

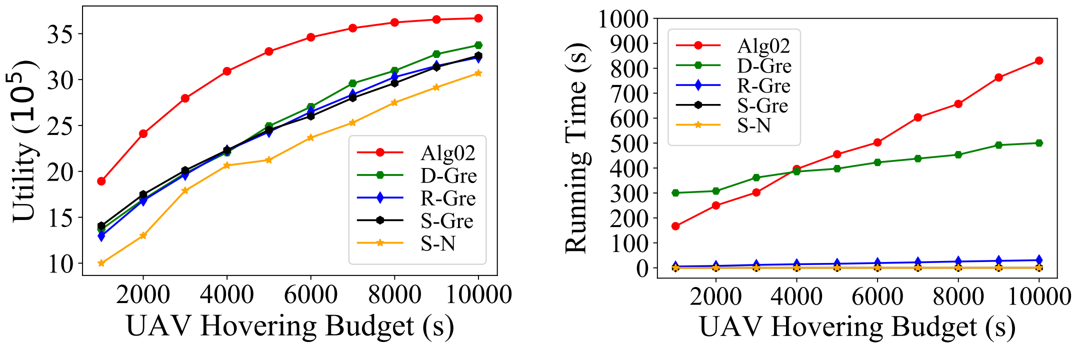

(a) (b)

Figure 3.9: Performance of `Alg02`, `D-Gre`, `R-Gre` and `S-Gre`, `S-N` in WSNs with UAV hovering budgets from 1,000 to 10,000 seconds.

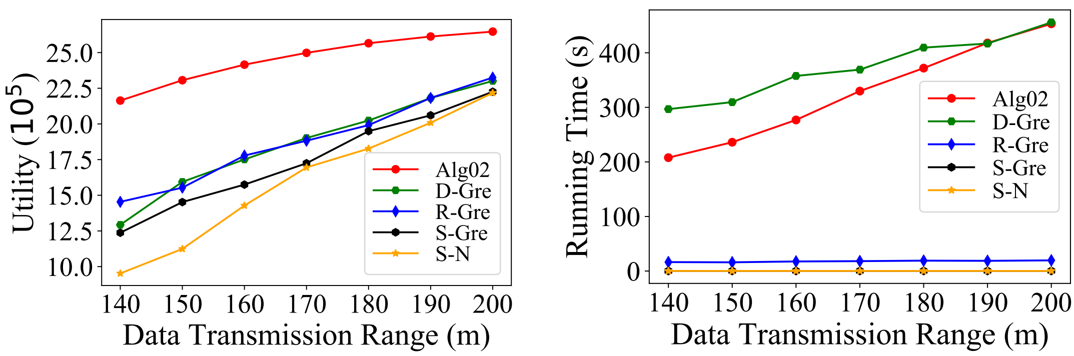

(a) (b)

Figure 3.10: Performance of `Alg02`, `D-Gre`, `R-Gre` and `S-Gre`, `S-N` in WSNs by varying the data transmission range of sensors from 140 meters to 200 meters.

3.6 Summary

In this chapter, we studied the maximization of data collection utility in a UAV-enabled WSN under the one-to-many data collection scheme, where the UAV hovering location positioning and the data collection utility need to be jointly considered. To this end, we first formulated the data collection utility maximization problem (UMP). We then devised an efficient algorithm to identify a finite set of potential hovering locations for the UAV that improves the data collection utility significantly. we further proposed an approximation algorithm for UMP with an approximation ratio of $(1 - \frac{1}{e})$. Finally, we evaluated the proposed algorithm through simulation study and compared with four baseline greedy heuristics. Simulation results demonstrate that the proposed algorithm significantly outperforms the greedy heuristics. As part of future work, we plan to take into consideration the energy consumption of the UAV during the tour for data collection utility maximization in wireless sensor networks.

Chapter 4

UAV Trajectory Designing for Data Collection Maximization

4.1 Introduction

Wireless Sensor Networks (WSNs) play important roles in various applications, including health monitoring [Liu et al., 2011], ocean monitoring [Shahanaghi et al., 2019] and area coverage [Chen et al., 2019]. Massive sensory data are continuously generated by sensors, data collection thus is a crucial issue to avoid data loss and data overwritten in WSNs. With high mobility and flexibility, the Unmanned Aerial Vehicle (UAV) has attracted considerable attention for data collection in recent years. By adopting the Orthogonal Frequency Division Multiple Access (OFDMA) technique, the UAV is capable to collect data from multiple sensors within its communication range simultaneously. This data collection scheme is referred to as the *one-to-many data collection scheme*, which can improve the data collection efficiency significantly, compared with the conventional *one-to-one data collection scheme* where the UAV can only collect the sensory data from one sensor at each time. However, the one-to-many data collection scheme also poses challenges. For example, which sensors' data should be collected during a data collection tour, constrained by the battery capacity of the UAV? Considering that there are infinitely many potential hovering locations for the UAV within its monitoring area, which locations should be chosen as its hovering locations and how long the UAV should sojourn at each chosen hovering location? In this chapter, we will address the challenges.

Extensive studies on data collection in UAV-enabled WSNs have been conducted in past years. For example, Zhang *et al.* [Zhang et al., 2021] considered the freshness of data collection by deploying the minimum number of UAVs and finding data collection tours for the UAVs, where each tour is constrained by a rigid delay. Gong *et al.* [Gong et al., 2018a] investigated the minimization of the total aviation time of a UAV to collect a certain volume of data from each sensor, where sensors are located on a straight line and only one sensor is served at each time. Liu *et al.* [Liu et al., 2018] studied the age-optimal trajectory for a UAV to collect data from sensors with different priorities under the one-to-one data collection scheme. Supported by the OFDMA technique, Mozaffari *et al.* [Mozaffari et al., 2016] focused on optimizing trajectories of multiple UAVs, aiming at minimizing the energy consumption of IoT devices, where data from all sensors are fully collected. Say *et al.* [Say et al., 2016] proposed a framework of data collection in a UAV-enabled WSN with the aim to maximize the network throughput, where sensors within the UAV coverage area can transmit their data to the UAV simultaneously, by assigning higher priorities to sensors in hot spots for their data packet uploading. Li *et al.* [Li et al., 2020] considered the energy consumption of a UAV on both hovering and traveling, aiming to find an optimal trajectory for the UAV to maximize the volume of data collected, assuming that a set of potential hovering locations for a UAV is given in advance.

In Chapter 2 and Chapter 3, we focused on the data collection volume and utility maximization in WSNs via deploying an energy-constrained UAV, where sensory data of sensors can be partially collected at each tour of the UAV. In this chapter, we studied a scenario when data from a sensor should be fully collected. To be specific, under the one-to-many data collection scheme, when the UAV collects data at a hovering location, it can collect data from multiple sensors simultaneously as long as the sensors are within the data collection range of the UAV, as we referred to in Chapter 2 and Chapter 3. The partial data collection mode that is studied in Chapter 2 and 3 allows data to remain at those sensors which have transferred data to the UAV. In contrast, the full data collection mode requires that the UAV cannot fly away until data from sensors within its data collection range are fully collected, without any remaining data at sensors that have contacted the UAV before. Furthermore, in this chapter, we study a challenging data collection maximization problem considering the energy constraint on a UAV, where the UAV consumes energy on both hovering and mechanical movement. We also consider the identification of hovering locations for the UAV from infinitely many potential ones corresponding to the different data collection rates of sensors. The identification of hovering locations for the UAV from infinitely many potential ones makes the data collection tour finding more difficult, as different locations correspond to different data collection rates of sensors, which impacts significantly on the data collection efficiency. Besides, we consider the fluctuation of data transmission ranges of sensors caused by the different Euclidean distances between sensors and the UAV. Fig. 4.1 shows an illustrative example of the UAV data collection tour.

The novelties of this study lie in that a novel data collection maximization problem via the deployment of an energy-constrained UAV is formulated,

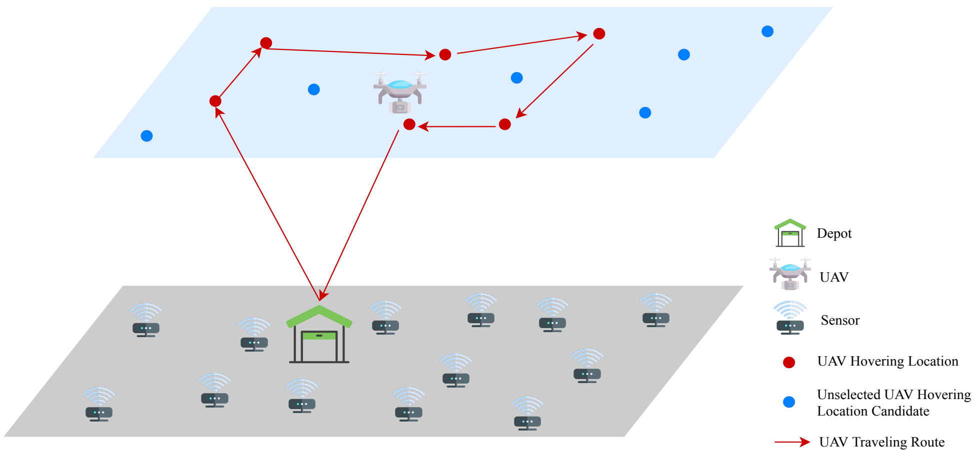

Figure 4.1: An illustrative example of a UAV data collection tour.

and a promising algorithm for the problem is devised, by jointly considering data transmission rates of sensors and hovering locations of the UAV.

The main contributions of the chapter are as follows. We first formulate a novel UAV-enabled data collection maximization problem under the one-to-many data collection scheme and show the NP-hardness of the problem. We then devise an efficient algorithm for the problem, by jointly considering the UAV hovering locations and data transmission rates of sensors. We finally evaluate the performance of the proposed algorithm through extensive experimental simulations. Simulation results demonstrate that the proposed algorithm is promising.

The objective of this research is to maximize the volume of data collected by a single UAV during each tour, while being limited by its energy capacity. The WSN deployed in this study consists of homogeneous and static sensors. The UAV's one-to-many data collection mode enables it to simultaneously collect data from multiple sensors. Moreover, the fluctuation of data transmission rate with the distance between the UAV and each sensor is taken into account. Additionally, this study also considers the energy consumption incurred by the UAV during its mechanical movement. This work is focused on finding a closed data collection tour, which includes sequences of each visited hovering location and the corresponding hovering duration at each location. These limitations should be considered while analyzing the results and drawing conclusions from the study.

The remainder of this chapter is organized as follows. Section 4.2 introduces the system model and the problem definition. Section 4.3 proposes an efficient heuristic algorithm for the problem, and Section 4.4 evaluates the performance of the proposed algorithm. Section 4.5 concludes the chapter.

4.2 Preliminaries

In this section, we first introduce the system model and the energy consumption model of a UAV. We then define the problem precisely.

4.2.1 System Model

Consider a WSN with a set $\mathcal{V} = \{v_i \mid 1 \leq i \leq N\}$ of homogeneous sensors. Denote by $(x_i, y_i, 0)$ the location of sensor $v_i \in \mathcal{V}$. Assume that each sensor v_i with transmission range R has a volume D_i of sensory data stored locally for later collection, where the data from v_i can be transmitted to a data receiver if the Euclidean distance between v_i and the receiver is no greater than R. An OFDMA-applied UAV is adopted to collect sensory data from sensors in the WSN. Guided by a pre-defined data collection schedule, the UAV flies above the monitoring area of the WSN and hovers at certain locations to collect data from multiple sensors simultaneously. It is assumed that the total energy consumption of the UAV per tour is constrained by its energy capacity Γ, which consists of the energy consumptions on its mechanical movement and hovering with the energy consumption rates η_m and η_h, respectively.

Each data collection tour of the UAV is a closed tour that starts from and ends at a depot, and the UAV will visit the hovering locations in the tour one by one with a specified hovering duration at each hovering location. Assume that $\mathcal{H} = (h_1, h_2, \ldots, h_k, \ldots, h_K)$ is the sequence of K hovering locations (excluding the depot) on the tour, where h_k is the kth location. Note that, both h_0 and h_{K+1} refer to the depot, which are excluded in $\mathcal{H}$ for the sake of convenience.

Denote by $V(h_k)$ the set of sensors whose data can be collected when the UAV hovers at location h_k with coordinates (X_k, Y_k, Z_k), then

$$V(h_k) = \{v_i \mid (x_i - X_k)^2 + (y_i - Y_k)^2 \leq R^2 - Z_k^2,\ v_i \in \mathcal{V}\}, \tag{4.1}$$

where Z_k is the hovering altitude of the UAV. In this chapter, we assume that the UAV hovers at a fixed altitude L [Li et al., 2020] that is no greater than R.

Denote by $r_i(h_k)$ the data transmission rate of sensor v_i when the UAV hovers at location h_k. Following the Shannon-Hartley formula [Tse and Viswanath, 2005] [Xiong and Shan, 2018], we have

$$r_i(h_k) = \log\Big(1 + \frac{\sigma_i}{d(v_i, h_k)^\alpha}\Big), \tag{4.2}$$

where $d(v_i, h_k)$ is the Euclidean distance between sensor v_i and hovering location h_k, α is a given path loss exponent with the range between 2 and 6, and σ_i is the transmission power of sensor v_i.

Due to the limited energy capacity imposed on the UAV, it is intuitively to enlarge its energy spending on hovering to improve the data collection efficiency, we thus assume that the UAV hovers at hovering location h_k for a minimum duration until all data from the sensors in $V(h_k)$ are fully collected [Li et al., 2020]. When the UAV hovers at location h_k, the set of sensors whose data to be collected is $V(h_k) \setminus \bigcup_{m=1}^{k-1} V(h_m)$, where $h_1, h_2, \ldots, h_{k-1}$ are the hovering locations visited by the UAV so far prior to the visit to location h_k.

The hovering duration t_k of the UAV at hovering location h_k thus is calculated as follows.

$$t_k = \max_{v_i \in V(h_k) \setminus \bigcup_{m=1}^{k-1} V(h_m)} \{\frac{D_i}{r_i(h_k)}\}, \tag{4.3}$$

where $\frac{D_i}{r_i(h_k)}$ is the time duration of the UAV to fully collect data from v_i. It can be seen that the value of t_k is determined not only by the data volume of sensors in $V(h_k)$ but also by previous hovering locations visited by the UAV: $h_1, h_2, \ldots, h_{k-1}$. Note that, once the sequence of locations in the tour is given, the value of t_k can be calculated by Eq. (4.3) directly. The finding of the data collection tour thus is equivalent to determine a sequence of hovering locations for the UAV, i.e., $\mathcal{H} = (h_1, h_2, \ldots, h_k, \ldots, h_K)$.

Denote by u_k the volume of data collected by the UAV at hovering location h_k, which can be calculated by accumulating the data stored at sensors in $V(h_k) \setminus \bigcup_{m=1}^{k-1} V(h_m)$, i.e.,

$$u_k = \sum_{v_i \in V(h_k) \setminus \bigcup_{m=1}^{k-1} V(h_m)} D_i. \tag{4.4}$$

Denote by $U(\mathcal{H})$ the total volume of data collected during tour $\mathcal{H}$, then

$$U(\mathcal{H}) = \sum_{h_k \in \mathcal{H}} u_k. \tag{4.5}$$

We then define the following operations on a hovering location sequence $(h_1, h_2, \ldots, h_K)$.

- `Append.` Add a new location p' to the end of the sequence, i.e.,

$$(h_1, h_2, \ldots, h_K) + p' = (h_1, h_2, \ldots, h_K, p'). \tag{4.6}$$

- `Replacement.` Replace a location with index α by a new location p, i.e.,

$$(h_1, h_2, \ldots, h_{\alpha-1}, h_\alpha, h_{\alpha+1}, \ldots, h_K)^{h_\alpha \to p} \tag{4.7}$$

$$= (h_1, h_2, \ldots, h_{\alpha-1}, p, h_{\alpha+1}, \ldots, h_K). \tag{4.8}$$

- `Pruning`. Remove a location with index α from the sequence, i.e.,

$$(h_1, h_2, \ldots, h_{\alpha-1}, h_\alpha, h_{\alpha+1}, \ldots, h_K) - h_\alpha \tag{4.9}$$

$$= (h_1, h_2, \ldots, h_{\alpha-1}, h_{\alpha+1}, \ldots, h_K). \tag{4.10}$$

4.2.2 The Energy Consumption Model of the UAV

Denote by $E_h(\mathcal{H})$ the accumulative energy consumption of the UAV on hovering during tour $\mathcal{H}$, which can be expressed as follows.

$$E_h(\mathcal{H}) = \eta_h \cdot \sum_{h_k \in \mathcal{H}} t_k. \tag{4.11}$$

Recall that η_h and t_k are the hovering energy consumption rate of the UAV and the hovering duration at h_k, respectively.

Denote by $E_m(\mathcal{H})$ the accumulative energy consumption of the UAV on its mechanical movement during tour $\mathcal{H}$, i.e.,

$$E_m(\mathcal{H}) = \eta_m \cdot \sum_{k=0}^{|\mathcal{H}|} d(h_k, h_{k+1}). \tag{4.12}$$

Recall that η_m and $d(h_k, h_{k+1})$ are the energy consumption rate of the UAV mechanical movement and the Euclidean distance between h_k and h_{k+1}, respectively. Note that locations h_0 and $h_{|\mathcal{H}|+1}$ represent the same location – the depot.

Denote by $E(\mathcal{H})$ the total energy consumption of the UAV on tour $\mathcal{H}$, then

$$E(\mathcal{H}) = E_h(\mathcal{H}) + E_m(\mathcal{H}), \tag{4.13}$$

which is constrained by the energy capacity Γ of the UAV.

4.2.3 Problem Definition

We here formulate a novel data collection maximization problem by using a UAV under the one-to-many data collection scheme. Given a WSN with a set $\mathcal{V} = \{v_i \mid 1 \leq i \leq N\}$ of homogeneous sensors located on the ground, the *UAV Data Collection Maximization Problem* is to find a closed data collection tour $\mathcal{H}$ for the UAV to maximize the accumulative volume of data collected along the tour, subject to the energy capacity Γ on the UAV.

We formalize the problem as follows.

$$
\begin{aligned}
&\textit{Maximize}\;\; U(\mathcal{H}) && (4.14)\\
&s.t. && (4.15)\\
&\qquad \mathcal{H} = (h_1,\, h_2, \ldots,\, h_K), && (4.16)\\
&\qquad K \in \mathbb{N}^+, && (4.17)\\
&\qquad E(\mathcal{H}) \le \Gamma, && (4.18)\\
&\qquad \text{Eq. } (4.1), (4.2), (4.3), (4.4), (4.5), (4.11), (4.12), (4.13). && (4.19)
\end{aligned}
$$

4.3 Algorithm

In this section, we propose an efficient algorithm for the UAV data collection maximization problem.

4.3.1 Algorithm Overview

The basic idea behind the proposed algorithm is as follows. We first discretize the UAV hovering plane by sets of concentric circles with different radii centered at the projection of each sensor location, where each spot is regarded as a potential hovering location for the UAV. We then find a data collection tour for the UAV in a novel way. That is, based on an initial tour $\mathcal{H}$, each location on $\mathcal{H}$ is iteratively assigned with a substitutive point, and $\mathcal{H}$ is updated by replacing a location with its substitutive point at each iteration. When the number of tour updates exceeds a pre-defined threshold θ, one of the locations on $\mathcal{H}$ will be removed. The algorithm proceeds iteratively until the total energy consumption of the UAV is no greater than its capacity.

4.3.2 Potential Hovering Location Identifications

Inspired by the work in [Fu et al., 2015], in the following we show how to reduce infinitely many potential hovering locations of the UAV to a finite number of potential hovering locations (spots).

For each sensor projection v_i' on the UAV hovering plane, we draw a set of concentric circles centered at v_i' with increasing radii $a_0, a_1, a_2, \ldots, a_M$ with $a_M \leq R$ and $a_{M+1} > R$, such that when the UAV hovers on the circumference of the circle with radius a_m, the data transmission rate $\log(1 + \frac{\sigma_i}{(\sqrt{{a_m}^2 + L^2})^\alpha})$ calculated by Eq. (4.2) is equal to

$$\frac{1}{\Phi^m} \cdot \log(1 + \sigma_i), \tag{4.20}$$

where Φ $(0 < \Phi < 1)$ is a constant between 0 and 1, and $\log(1 + \sigma_i)$ is the data transmission rate of sensor v_i with a unit Euclidean distance away from the UAV. As a result, the data transmission rate between any two conjunctive circles with radii a_m and a_{m+1} is bounded between $\frac{1}{\Phi^m} \cdot \log(1 + \sigma_i)$ and $\frac{1}{\Phi^{m+1}} \cdot \log(1 + \sigma_i)$ respectively, where the values of a_m with $0 \leq m \leq M$ can be calculated by the expression (4.20).

Consequently, the 2-D hovering plane of the UAV is partitioned into a set of small-sized spots by arcs of the circles, as shown in Fig. 4.2(b). We refer to each of the separated spots as a potential hovering location for the UAV, and denote by $\mathcal{P}$ the set of potential hovering locations whose cardinality is bounded, which will be shown later.

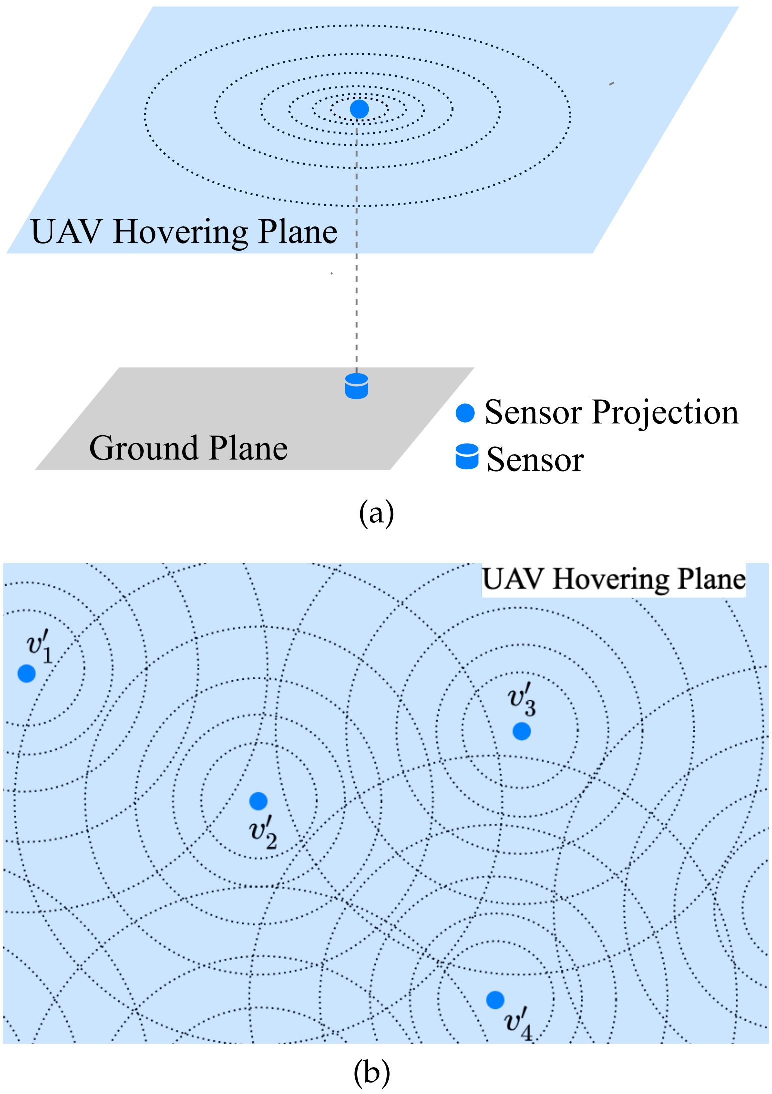

Figure 4.2: Potential hovering location identifications: (a) a set of concentric circles centered at the projection of a sensor. (b) The aerial view of the UAV hovering plane discretized by sets of concentric circles.

4.3.3 Data Collection Tour Scheduling

We find the data collection tour for the UAV by finding a sequence of hovering locations in $\mathcal{P}$.

Given a partial tour $\mathcal{H}$, we define the *Expanding Ratio* $\rho^E(p_j)$ as the ratio of the increment of collected data volume to the increment of the hovering energy cost, by adding p_j into $\mathcal{H}$ as the last hovering location, i.e.,

$$\rho^E(p_j) = \frac{U(\mathcal{H} + p_j) - U(\mathcal{H})}{E_h(\mathcal{H} + p_j) - E_h(\mathcal{H})}. \tag{4.21}$$

Define the *Pruning Ratio* as the ratio of the decrement of the collected data volume to the decrement of the total energy consumption of the UAV, by removing h_α from the tour, i.e.,

$$\rho^P(h_\alpha) = \frac{U(\mathcal{H}) - U(\mathcal{H} - h_\alpha)}{E(\mathcal{H}) - E(\mathcal{H} - h_\alpha)}. \tag{4.22}$$

The algorithm proceeds as follows.

Tour Initialization: Start from an empty tour $\mathcal{H}$, we iteratively expand $\mathcal{H}$ by selecting an unvisited location $p_{j^+} \in \mathcal{P} \setminus \mathcal{P}(\mathcal{H})$ with the maximum $\rho^E(p_{j^+})$, and adding it on $\mathcal{H}$ as the last visited location, i.e.,

$$j^+ = \text{argmax}_{p_j \in \mathcal{P} \setminus \mathcal{P}(\mathcal{H})} \rho^E(p_j), \tag{4.23}$$

where $\mathcal{P}(\mathcal{H})$ denotes the set of hovering locations on $\mathcal{H}$. The tour expanding continues until the total hovering energy $E_h(\mathcal{H})$ exceeds the energy capacity Γ of the UAV.

Tour $\mathcal{H}$ then contains a sequence of visited locations. We then consider another tour $\mathcal{H}^{TSP}$, which is defined as the tour with exactly same visited

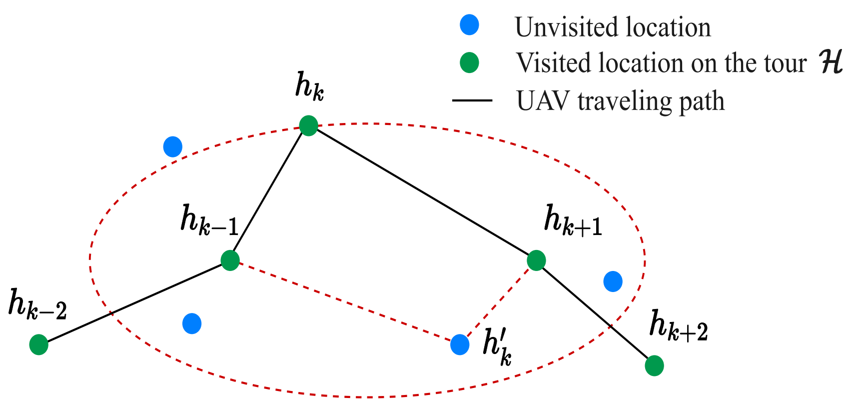

Figure 4.3: With focal points h_{k-1} and h_{k+1}, an ellipse $\mathcal{E}(h_k)$ can be obtained by letting h_k sit on its circumference. h'_k is the chosen substitutive location for h_k, which is inside $\mathcal{E}(h_k)$ and is unvisited by the UAV.

locations as $\mathcal{H}$ but with a minimum closed tour to visit them. It can be seen that $U(\mathcal{H}^{TSP}) = U(\mathcal{H})$ since $\mathcal{P}(\mathcal{H}^{TSP}) = \mathcal{P}(\mathcal{H})$, and $E_m(\mathcal{H}^{TSP}) \leq E_m(\mathcal{H})$ according to the definition of $\mathcal{H}^{TSP}$.

However, as we mentioned before that different visiting orders of a set of visited locations may result in different hovering duration at each location by Eq. (4.3), it is uncertain whether $E_h(\mathcal{H}^{TSP}) < E_h(\mathcal{H})$. In the case where $E_h(\mathcal{H}^{TSP}) < E_h(\mathcal{H})$, we replace $\mathcal{H}$ by $\mathcal{H}^{TSP}$ and continue adding new locations to $\mathcal{H}$ by Eq. (4.23), until both $E_h(\mathcal{H}^{TSP})$ and $E_h(\mathcal{H})$ are greater than Γ. It then proceeds to the operation of `Substitution Selection and Tour Update` as follows.

Substitution Selection and Tour Update: For the partial tour $\mathcal{H}$ delivered so far, we have that $E_h(\mathcal{H}) > \Gamma$ and thus $E(\mathcal{H}) > \Gamma$. In this step, we reduce the mechanical movement energy consumption $E_m(\mathcal{H})$, while mitigating the decrement on the volume of the collected data.

Within each iteration, we find a substitutive location h'_k for each visited location h_k on tour $\mathcal{H}$ in the following ways. As shown in Fig. 4.3, let h_{k-1}

and h_{k+1} on $\mathcal{H}$ be the two focal points (where h_0 and h_{K+1} are the location of the depot), then we can obtain an ellipse $\mathcal{E}(h_k)$ with h_k sitting on the circumference. Note that $\mathcal{E}(h_k)$ is unique since with two focal points and a point on the circumference, only one ellipse can be obtained. Denote by $\mathcal{P}(\mathcal{E}(h_k))$ the subset of potential hovering locations in $\mathcal{P}$ inside $\mathcal{E}(h_k)$ (excluding locations on the circumference), and $\mathcal{P}'(\mathcal{E}(h_k))$ the subset of unvisited potential hovering locations of $\mathcal{P}(\mathcal{E}(h_k))$, i.e., $\mathcal{P}'(\mathcal{E}(h_k)) = \mathcal{P}(\mathcal{E}(h_k)) \setminus (\mathcal{P}(\mathcal{H}) \cap \mathcal{P}(\mathcal{E}(h_k)))$. We then find an unvisited potential hovering location $p_{j'} \in \mathcal{P}'(\mathcal{E}(h_k))$ that satisfies

$$j' = \text{argmin}_{p_j \in \mathcal{P}'(\mathcal{E}(h_k))} U(\mathcal{H}) - U(\mathcal{H}^{h_k \to p_j}). \tag{4.24}$$

Then, $h'_k = p_{j'}$ is the substitutive location for h_k.

With a substitutive location for each location on $\mathcal{H}$, we then update the tour as follows.

We select the hovering location h_{k^*} on $\mathcal{H}$ which satisfies

$$k^* = \text{argmin}_{h_k \in \mathcal{H}} U(\mathcal{H}) - U(\mathcal{H}^{h_k \to h'_k}). \tag{4.25}$$

We replace h_{k^*} by h'_{k^*} on $\mathcal{H}$, and replace $\mathcal{H}$ by $\mathcal{H}^{TSP}$ if $E(\mathcal{H}^{TSP}) < E(\mathcal{H})$.

When the tour $\mathcal{H}$ is updated at each iteration, the mechanical movement energy consumption $E_m(\mathcal{H})$ declines, which will be proved later. The algorithm terminates when the total energy consumption $E(\mathcal{H})$ is no greater than Γ.

However, there is an extreme case where $E(\mathcal{H})$ is not converging, since the replacement with a substitutive location may enlarge $E_h(\mathcal{H})$ and $E(\mathcal{H})$. To deal with this case, we introduce a threshold θ, such that when the number of tour updates exceeds θ, it proceeds to the following `Tour Pruning` operation to further reduce $E(\mathcal{H})$.

Tour Pruning: When the number of tour updates exceeds a predefined threshold θ, we choose a hovering location h_{k^-} on $\mathcal{H}$ with the minimum ρ^P ratio, i.e.,

$$k^- = \text{argmin}_{h_k \in \mathcal{P}(\mathcal{H})} \rho^P(h_k). \tag{4.26}$$

We then remove h_k from the tour and replace tour $\mathcal{H}$ by $\mathcal{H}^{TSP}$ if $E(\mathcal{H}^{TSP}) < E(\mathcal{H})$. It proceeds to the previous step – `Substitution Selection and Tour Update` if $E(\mathcal{H}) > \Gamma$; otherwise, the algorithm terminates.

As a result, $\mathcal{H}$ is the data collection tour of the UAV. The detailed algorithm for finding $\mathcal{H}$ is shown in `Algorithm` 6.

4.3.4 Algorithm Analysis

The rest is dedicated to the theoretical analysis of the proposed algorithm. We first show the NP-hardness of the UAV data collection maximization problem. We then prove that the set of potential hovering locations separated by concentric circles is finite. We finally show that the energy consumption on mechanical movement $E_m(\mathcal{H})$ of the UAV decreases, by replacing a visited location on $\mathcal{H}$ with its substitutive location.

Theorem 10 *The UAV data collection maximization problem is NP-hard.*

Proof We show the claim by a reduction from an NP-hard Robust k-Center (*RKC*) problem [Charikar et al., 2001] [Xiao et al., 2004], which is using k identical disks with radius r to cover at least p points of a given point set V in a 2-D plane, where k, p and r are given.

Algorithm 6 Algorithm for the UAV data collection maximization problem

Input: A set $\mathcal{V} = \{v_i \mid 1 \leq i \leq N\}$ of sensors; data volume D_i of v_i; data transmission range R; the energy capacity Γ for the UAV per tour.

Output: A data collection tour $\mathcal{H}$ for the UAV.

Discretize the UAV hovering plane by sets of concentric circles with different radii based on Eq. (4.20), and form the potential hovering location set $\mathcal{P}$;
$\mathcal{H} \leftarrow \emptyset$; $K \leftarrow 0$; $\mathcal{F} \leftarrow \mathcal{P}$;
while $E_h(\mathcal{H}) \leq \Gamma$ **and** $|\mathcal{F}| > 0$ **do**
    $j^+ \leftarrow \text{argmax}_{p_j \in \mathcal{P} \setminus \mathcal{P}(\mathcal{H})} \rho^E(p_j)$;
    $K \leftarrow K + 1$; $h_K \leftarrow p_{j^+}$; $\mathcal{H} \leftarrow \mathcal{H} + h_K$, $\mathcal{F} \leftarrow \mathcal{F} \setminus \{p_{j^+}\}$;
    if $E_h(\mathcal{H}) > \Gamma$ **and** $E_h(\mathcal{H}) > E_h(\mathcal{H}^{TSP})$ **then**
        $\mathcal{H} \leftarrow \mathcal{H}^{TSP}$;
while $E(\mathcal{H}) > \Gamma$ **do**
    $r \leftarrow 0$; /* number of iterations*/
    while $r \leq \theta$ **do**
        for $k \leftarrow 1$ to K **do**
            Draw an ellipse $\mathcal{E}(h_k)$ with focal points h_{k-1} and h_{k+1}, with h_k on the circumference;
            $j' \leftarrow \text{argmin}_{p_j \in \mathcal{P}'(\mathcal{E}(h_k))} U(\mathcal{H}) - U(\mathcal{H}^{h_k \rightarrow p_j})$;
            $h'_k \leftarrow p_{j'}$;
        $k^* \leftarrow \text{argmin}_{h_k \in \mathcal{H}} U(\mathcal{H}) - U(\mathcal{H}^{h_k \rightarrow h'_k})$;
        $\mathcal{H} \leftarrow \mathcal{H}^{h_{k^*} \rightarrow h'_{k^*}}$; $r \leftarrow r + 1$;
        if $E(\mathcal{H}) > E(\mathcal{H}^{TSP})$ **then**
            $\mathcal{H} \leftarrow \mathcal{H}^{TSP}$;
        if $E(\mathcal{H}) \leq \Gamma$ **then**
            return $\mathcal{H}$
    $k^- \leftarrow \text{argmin}_{h_k \in \mathcal{P}(\mathcal{H})} \rho^P(h_k)$;
    $\mathcal{H} \leftarrow \mathcal{H} - h_{k^-}$;
    if $E(\mathcal{H}) > E(\mathcal{H}^{TSP})$ **then**
        $\mathcal{H} \leftarrow \mathcal{H}^{TSP}$;
return $\mathcal{H}$

Denote by I_R and I_U the instances of the RKC and the UAV data collection maximization problem, respectively. The number of disks of I_R corresponds to the UAV energy capacity in I_U, i.e., $\Gamma = k$ and we further set $\eta_h = 1$ and $\eta_m = 0$ (neglecting the energy consumption of the UAV on mechanical movement).

Denote by V_R and V_U the point set in I_R, and the sensor set in I_U respectively, where for each vertex $v_i = (x_i, y_i)$ and $v_i \in V_R$, there exists a sensor $v'_i \in V_U$ with location $(x_i, y_i, 0)$ and the volume $D_i = 1$ of data stored locally.

For the data transmission rate in Eq. (4.2), it has $\sigma_i = 1$ and $\alpha = 0$, such that for any v_i and h_k, we have $r_i(h_k) = 1$. As a result, the hovering duration of the UAV at any visited location would be exactly 1 time unit. The transmission range of each sensor is $R = \sqrt{L^2 + r^2}$, where r is the radius of disks of I_R, and L is the hovering altitude of the UAV.

It can be seen that a solution to I_U returns a solution to I_R, and the reduction is polynomial. The theorem then follows. □

Theorem 11 *The number of potential hovering locations in $\mathcal{P}$ is at most $|\mathcal{V}|^2M^2 - |\mathcal{V}|M + 2$, where $\mathcal{V}$ is the set of sensors, M is the number of circles centered at each sensor projection.*

Proof According to Eq.(4.20) that $\log(1 + \frac{\sigma_i}{(\sqrt{{a_m}^2+L^2})^\alpha}) = \frac{1}{\Phi^m} \cdot \log(1+\sigma_i)$, we can calculate $a_1, a_2, a_3, \ldots$ by setting $m = 1, 2, 3, \ldots$ respectively, where we can find a constant M satisfying $a_M \leq R$ and $a_{M+1} > R$. Then, M is the number of circles centered at each sensor.

Since the number of sensors on the WSN is $|\mathcal{V}|$, the number of circles on the UAV hovering plane is $|\mathcal{V}| \cdot M$.

By [Mark et al., 2008] and [Fu et al., 2015], the number of regions separated by these circles, which are also referred to as potential hovering locations for the UAV, is at most $|\mathcal{V}|^2M^2 - |\mathcal{V}|M + 2$. □

Theorem 12 *$E_m(\mathcal{H})$ decreases by replacing a visited location h_{k^*} with its substitutive location h'_{k^*}.*

Proof As shown in Fig. 4.3, h'_{k^*} is within $\mathcal{E}(h_{k^*})$. According to the property of ellipses $\mathcal{E}(h_{k^*})$, for any two points p_1, p_2 on the circumference, there is $d(h_{k^*-1}, p_1) + d(p_1, h_{k^*+1}) = d(h_{k^*-1}, p_2) + d(p_2, h_{k^*+1})$, where h_{k^*-1} and h_{k^*+1} are focal points of $\mathcal{E}(h_{k^*})$.

Since h_{k^*} is on the circumference of $\mathcal{E}(h_{k^*})$ and h'_{k^*} is within the circumference of $\mathcal{E}(h_{k^*})$, we have that $d(h_{k^*-1}, h'_{k^*}) + d(h'_{k^*}, h_{k^*+1}) < d(h_{k^*-1}, h_{k^*}) + d(h_{k^*}, h_{k^*+1})$. Due to the fact that h'_{k^*} is selected from unvisited locations, the other visited locations on $\mathcal{H}$ will not be affected.

The theorem then follows. □

4.4 Performance Evaluation

In this section, we evaluate the performance of the proposed algorithm by experimental simulations. We also investigate the impacts of parameters on the algorithm performance.

4.4.1 Experimental Environment Settings

We consider a WSN deployed within $1,000 \times 1,000$ square meters, where sensors are randomly distributed [Chen et al., 2020]. The data transmission range and the transmission power of each sensor are set as 21 m and 330 mW [Xiong

Table 4.1: Experimental Environment Settings

Parameter	Value
Size of the WSN	$1,000 \times 1,000\ m^2$
Data transmission range of each sensor	$21\ m$
Data transmission power of each sensor	$330\ mW$
Data volume range of each sensor	$(0,\ 1024]\ MB$
Number of UAV	1
UAV flying altitude	$5\ m$
Energy capacity of the UAV	$5 \times 10^5\ J$
Energy consumption rate of the UAV on traveling	$10\ J/m$
Energy consumption rate of the UAV on hovering	$150\ J/s$
Threshold θ of numbers of iterations	$5,000$

and Shan, 2018] respectively. The data volume D_i of each sensor v_i is randomly drawn from $(0,\ 1024]\ MB$. We deploy one UAV for the data collection, hovering at an altitude 5 m [Xiong and Shan, 2018]. The energy capacity of the UAV is set as $5 \times 10^5\ J$, and the energy consumption rates on traveling and hovering are 10 J/m and 150 J/s, respectively [Li et al., 2020]. The threshold θ of numbers of iterations in the proposed algorithm is set as $5,000$.

Unless otherwise specified, these parameters will be adopted in the default setting. As the UAV data collection maximization problem is a new problem, existing algorithms in the literature are unlikely to be adopted directly, we here propose the following benchmark heuristics to evaluate the performance of the proposed algorithm.

- *Greedy*. The projection of each sensor on the UAV hovering plane is regarded as a potential hovering location for the UAV. It starts with an empty tour $\mathcal{H}$ and iteratively selects a hovering location p_{max} with the maximum $U(\mathcal{H} + p_{max}) - U(\mathcal{H})$. Then p_{max} is added to $\mathcal{H}$ as the last visited location if $E(\mathcal{H} + p_{max}) < \Gamma$. This procedure continues until $E(\mathcal{H} + p_{max}) > \Gamma$.

- *NGreedy*. The projection of each sensor on the UAV hovering plane is regarded as a potential hovering location for the UAV. The UAV firstly visits a location p_{max_1} with the maximum $U(\mathcal{H} + p_{max_1}) - U(\mathcal{H})$. It then visits a location p_{max_2} from the neighbors of p_{max_1} (potential hovering locations no larger than 50 meters away from p_{max_1}), with the maximum $U(\mathcal{H} + p_{max_2}) - U(\mathcal{H})$ among neighbors of p_{max_1}. The procedure continues until p_{max_m} is found with $E(\mathcal{H} + p_{max_m}) > \Gamma$.

Each value in figures is the mean result by applying each mentioned algorithm to 50 network instances with the same size. The running time of all the mentioned experimental simulations is obtained from a desktop with 2.7 GHz Intel Core i7 CPU and 16 GB RAM.

4.4.2 Performance Evaluation of Different Algorithms

We investigate the performance of the proposed algorithm (denoted by `Alg`) against algorithms `Greedy` and `NGreedy`, by varying the number of sensors from 100 to $1,000$. Fig. 4.4 (a) demonstrates that the performance of `Alg` significantly outperforms the other two heuristics, where the volume of the data collected by `Alg` is approximately 200% of the one collected by `Greedy`, and 300% of the one collected by `NGreedy`.

It can be seen that, the volume of collected data by all mentioned algorithms is proportional to the number of sensors in the network.

4.4.3 Impacts of Parameters on the Performance of Algorithms

The rest is to investigate the impact of the iteration threshold θ on the performance of `Alg`, the UAV energy capacity and the data transmission range on

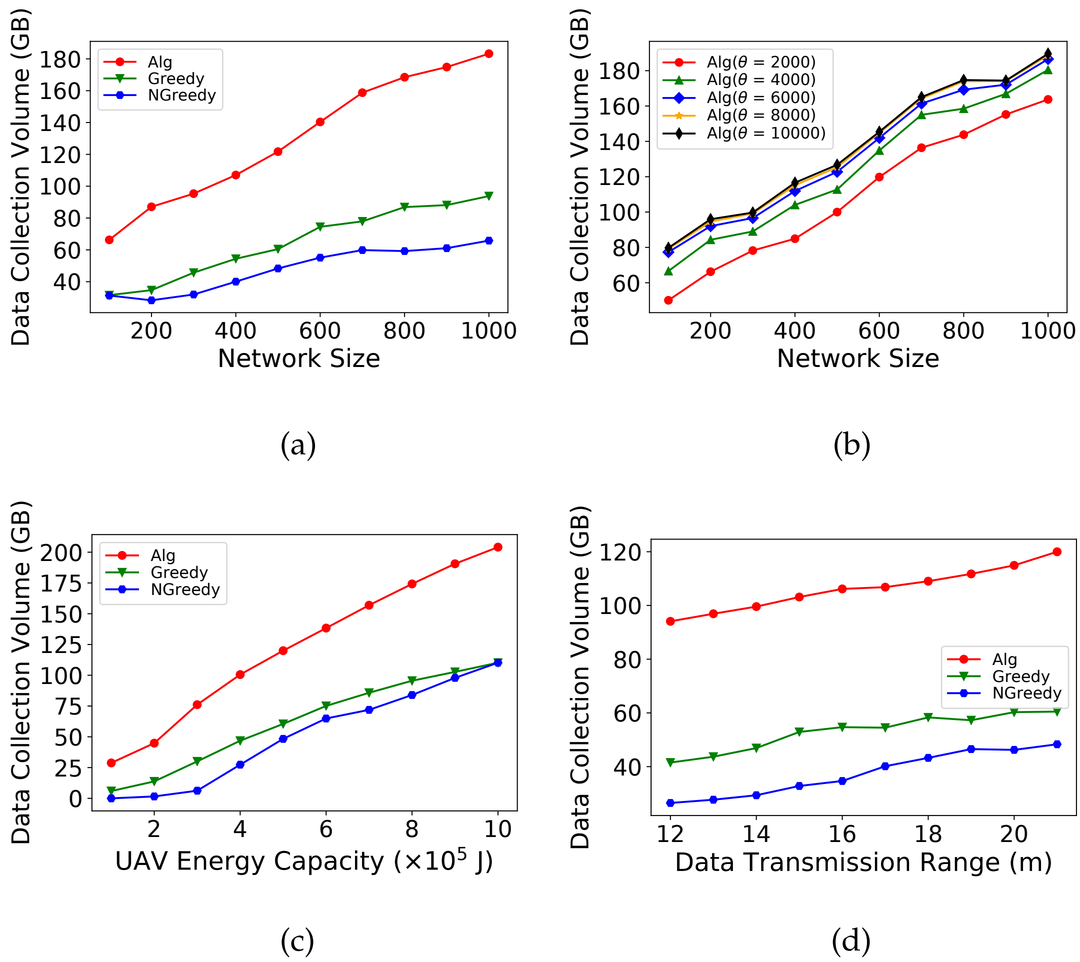

Figure 4.4: Performance of `Alg`, `Greedy` and `NGreedy`: (a) data collection volume of `Alg`, `Greedy` and `NGreedy`; (b) data collection volume of `Alg` with θ values $2,000$, $4,000$, $6,000$, $8,000$ and $10,000$; (c) data collection volume of `Alg`, `Greedy` and `NGreedy` with varying UAV energy capacities; (d) data collection volume of `Alg`, `Greedy` and `NGreedy` with varying data transmission ranges.

the performance of the mentioned algorithms.

We first investigate the impacts of θ, which is the maximum number of iterations in `Substitution Selection and Tour Update` (in step 10 of `Algorithm` 1). We compare the performance of `Alg` with $\theta = 2,000$, $4,000$, $6,000$, $8,000$, $10,000$ respectively, by varying the number of sensors from 100 to $1,000$. Fig. 4.4 (b) depicts that the volume of collected data increases in any size of the network by increasing the value of θ from $2,000$ to $6,000$, but it remains constant when θ varies from $6,000$ to $10,000$.

We then investigate the impacts of the energy capacity Γ of the UAV and the data transmission range R on the performance of the mentioned algorithms, by increasing the energy capacity from $1 \times 10^5 J$ to $10 \times 10^5 J$ and the data transmission range from 12 m to 21 m respectively, with 500 sensors randomly deployed in the network.

Fig. 4.4 (c) depicts that the volume of the data collected by the mentioned algorithms grows rapidly against the energy capacity of the UAV, as the UAV can visit more locations and collect data from more sensors at each visited location.

Fig. 4.4 (d) plots that the volume of the data collected by different algorithms increases against the data transmission ranges, since a larger data transmission range allows data from more sensors to be collected simultaneously. It can be seen that the data collection volume of `Alg` is proportional to the iteration threshold θ, the UAV energy capacity and data transmission ranges of sensors.

4.5 Summary

In this chapter, we studied the data collection maximization problem in a UAV-enabled WSN under the one-to-many data collection scheme, where there are infinitely many hovering locations for the UAV, and the UAV consumes energy on both hovering and mechanical movement. We first formulated a novel UAV data collection maximization problem. We then devised an efficient algorithm for the problem by jointly considering the UAV hovering locations and data transmission rates of sensors. We finally evaluated the proposed algorithm through experimental simulations. Simulation results demonstrate that the proposed algorithm is promising and outperforms the other benchmarks significantly.

Chapter 5

Conclusions and Future Directions

In this chapter, we summarize the contributions we made in this thesis, and discuss potential research topics derived from this work.

5.1 Summary of Contributions

Digital technology such as the IoTs develops rapidly over the last decade, generating enormous applications in various domains. WSNs play a central role in the context of IoT for providing a massive amount of data captured by ubiquitous sensors. Thus, data collection becomes crucial to feed fresh data into IoT services while avoiding data overwritten due to limited storage capacities of IoT sensors. With high agility, mobility and flexibility, UAVs have recently received considerable attention for data collection.

In this thesis, we have systematically studied the data collection planning in UAV-assisted WSNs to optimize the data collection efficiency under one-to-many data collection scheme.

Unlike most existing studies that the data from all sensors within the data reception range of the UAV must be fully collected, in Chapter 2, we assume that the data stored at a sensor can be partially collected and can be collected through multiple times by the UAV per tour. We study data collection in WSNs via an energy-constrained UAV under the one-to-many data collection scheme intending to maximize the volume of collected data. Although there exists work on data collection in UAV-enabled WSNs, it is challenging to identify the hovering locations for UAVs in the one-to-many data collection scheme. To be specific, the data collection efficiency under this scheme massively relies on the hovering locations of the UAV and the hovering duration at each such location. However, efficient determination of UAV hovering locations is widely considered to be intractable as there are infinitely many potential hovering locations in the UAV serving area. For the sake of tractability, most of the existing approaches discretize the UAV serving area into different regions with certain sizes, where each region is regarded as a potential UAV hovering spot. However, the locations in a discretized region cannot be distinguished from each other, which results in the inevitable utility loss of data collection. Moreover, the time complexity of discretization-based approaches highly depends on the size of the network monitoring area, thus making the data collection inefficient, especially for large-scale WSNs. To address the aforementioned challenges, in Chapter 3, we significantly extend Chapter 2 by jointly considering the UAV hovering location positioning and the data collection utility maximization problem under the one-to-many data collection scheme, where the total hovering duration of the UAV is constrained by a given budget. To the best of our knowledge, we are the first to focus on enhancing UAV hovering location positioning to improve data collection utility in WSNs. Furthermore, in Chapter 4, we study a more challenging data collection maximization problem considering the energy constraint on a UAV, where the UAV consumes energy on both hovering and mechanical movement. We also consider the identification of hovering locations for the UAV from infinitely many potential ones corresponding to the different data collection rates of sensors. The identification of hovering locations for the UAV from infinitely many potential ones makes the data collection tour finding more difficult, as different locations correspond to different data collection rates of sensors, which impact significantly on the data collection efficiency. Besides, we consider the fluctuation of data transmission ranges of sensors caused by the different Euclidean distances between sensors and the UAV.

We explored the UAV data collection problems in terms of UAV hovering duration allocation, UAV hovering location identification and UAV travelling trajectory designing. For investigated topics, we defined and formulated novel problems and developed optimization frameworks with efficient algorithms for the proposed problems. We also designed and conducted simulation experiments to evaluate the performance of devised algorithms. The main contributions of the thesis are summarized as follows.

UAV hovering duration allocation is to assign the UAV hovering time slots to a set of pre-defined UAV potential hovering locations under its energy constraint, which is a crucial issue for data collection optimization in the one-to-many data collection scheme, where data at a sensor are allowed to be partially collected. We firstly defined and formulated a novel multi-sensor data collection optimization problem and proved its NP-hardness. We then investigated a special case and the general cases of the proposed problem respectively. For WSNs with a special deployment, we developed an optimal algorithm which guarantees the maximized volume of collected data. For general cases of the WSN deployment, we studied a variant of the proposed problem and devised an efficient algorithm for the variant. We then proposed a novel approach to transform the algorithm for the variant to tackle the original problem, where the delivered algorithm is proved to be with a constant approximation ratio for the original problem.

UAV hovering location identification problem is to precisely determine UAV's hovering locations from infinitely many potential ones jointly optimizing the data collection utility, under the one-to-many data collection scheme, where data at each sensor can be partially collected. This problem is widely considered to be intractable, where many existing studies neglect this critical issue or simply discretize the UAV serving area into small regions with a given size, resulting in the inevitable utility loss of data collection. To this end, we first defined and formulated a data collection utility maximization problem. We then devised an efficient algorithm to identify a finite set of potential hovering locations for the UAV, which improves the data collection utility significantly. We next proposed an approximation algorithm for the data collection utility maximization problem with an approximation ratio of $(1 - \frac{1}{e})$, where e is the base of the natural logarithm.

UAV traveling trajectory designing is to plan the UAV data collection tour considering the energy consumption of the UAV on both hovering and mechanical movement. We firstly formulated a novel UAV data collection maximization problem under the one-to-many data collection scheme with the variation of sensors' data transmission rate, where data at a sensor should be fully collected. We secondly showed the NP-hardness of the proposed problem. We then devised an efficient algorithm for the problem by investigating the impact of UAV hovering location selection on the data collection efficiency.

For devised algorithms, we designed and conducted extensive experiments to evaluate their performance against comparable heuristic algorithms. We also investigated the impact of parameters on the performance. The Experimental results showed that the proposed algorithms outperform the existing ones significantly in terms of maximizing data collection volumes and data collection utility under the one-to-many data collection scheme.

5.2 Future Directions

Although we have intensively investigated critical issues for data collection optimization in UAV-assisted WSNs, there are several potential research topics that are worthwhile for further exploration based on works in this thesis.

Firstly, we will explore obstacle avoidance problems for UAV-assisted data collection in the urban area. Unlike data collection tasks in the plain area where there are a few obstacles and the relatively high flying altitude enables the UAV to be away from barriers on the ground, it is crucial to consider obstacle avoidance when designing tours for UAVs in the urban area. Obstacles such as trees and buildings are common in the urban area, which is likely to let UAVs suffer from crashes. The damage of the UAV caused by crashing into obstacles will not only increase the economic cost of data collection, but also possibly cause the loss of data which have been collected by the broken UAV. Furthermore, falling wreckage of UAVs when crashing into obstacles will bring significant threats to public safety, especially when UAVs work over crowded urban areas. It thus is crucial to consider obstacle avoidance when planning the UAV data collection tour in the urban area.

Secondly, we will further improve the data collection efficiency in WSNs by dispatching a fleet of UAVs. We will investigate the cooperation of multiple UAVs to maximize the data collection efficiency while avoiding collisions of UAVs. For example, for each UAV, which sensor should it collect data from and how to determine the hovering locations to effectively collect data from selected sensors? How long should a UAV stay at each determined hovering location selected for it? Furthermore, how to design the traveling tour for the fleet of UAVs to maximize the data collection utility under their energy constraint while ensuring no collisions between UAVs. These mentioned issues based on works in this thesis will further improve the data collection efficiency.

Thirdly, we will study the data collection for WSNs in 3D scenarios under the one-to-many data collection scheme, where sensors are deployed at complicated terrains such as mountains and cliffs at different altitudes. The UAV is thus allowed to adjust its flying altitude to collect data from multiple sensors simultaneously. How to identify the hovering location for the UAV and how to determine the corresponding hovering duration at each selected hovering spot is crucial for maximizing the data collection efficiency under the constrained energy budget of the UAV.

Finally, we will investigate the privacy issues of UAVs when they conduct data collection tasks. For example, UAVs may visit private spheres such as private yards or private farmlands when they conduct tasks of the image or video captioning, which brings big threats to the privacy. It thus is crucial to bypass private spheres when designing data collection tours. In our future works, we will explore the traveling path designing of the UAV to bypass private spheres while maximizing the data collection efficiency. Furthermore, in the situation where locations of private spheres are not determined previously, we will utilize techniques of computer vision to perform real-time detection of potential private spheres. We will further propose online algorithms to promptly reroute for UAVs to bypass the detected locations of potential private spheres jointly considering the optimization of data collection.

Bibliography

Phantom 4 advanced - product information - dji. https://www.dji.com/au/phantom-4-adv/info. (cited on page 43)

Al-Emran, M.; Malik, S. I.; and Al-Kabi, M. N., 2020. A survey of internet of things (iot) in education: Opportunities and challenges. *Toward social internet of things (SIoT): enabling technologies, architectures and applications*, (2020), 197–209. (cited on page 1)

Alemdar, H. and Ersoy, C., 2010. Wireless sensor networks for healthcare: A survey. *Computer networks*, 54, 15 (2010), 2688–2710. (cited on page 2)

Binol, H.; Bulut, E.; Akkaya, K.; and Guvenc, I., 2018. Time optimal multi-uav path planning for gathering its data from roadside units. In *2018 IEEE 88th Vehicular Technology Conference (VTC-Fall)*, 1–5. IEEE. (cited on page 18)

Cabrera, C.; Palade, A.; White, G.; and Clarke, S., 2020. An urban-driven service request management model. In *2020 IEEE International Conference on Pervasive Computing and Communications (PerCom)*, 1–7. IEEE. (cited on page 51)

Caillouet, C.; Giroire, F.; and Razafindralambo, T., 2018. Optimization of mobile sensor coverage with uavs. In *IEEE INFOCOM 2018-IEEE Conference on Computer Communications Workshops (INFOCOM WKSHPS)*, 622–627. IEEE. (cited on page 52)

Cao, H.; Liu, Y.; Yue, X.; and Zhu, W., 2017. Cloud-assisted uav data collection for multiple emerging events in distributed wsns. *Sensors*, 17, 8 (2017), 1818. (cited on page 7)

Charikar, M.; Khuller, S.; Mount, D. M.; and Narasimhan, G., 2001. Algorithms for facility location problems with outliers. In *SODA*, vol. 1, 642–651. (cited on pages 62 and 100)

Chen, K.; Gao, H.; Cai, Z.; Chen, Q.; and Li, J., 2019. Distributed energy-adaptive aggregation scheduling with coverage guarantee for battery-free wireless sensor networks. In *IEEE INFOCOM 2019-IEEE Conference on Computer Communications*, 1018–1026. IEEE. (cited on page 85)

Chen, M.; Liang, W.; and Li, J., 2021. Energy-efficient data collection maximization for uav-assisted wireless sensor networks. In *2021 IEEE Wireless Communications and Networking Conference (WCNC)*, 1–7. IEEE. (cited on page 51)

Chen, M.; Liang, W.; and Li, Y., 2020. Data collection maximization for uav-enabled wireless sensor networks. In *2020 29th International Conference on Computer Communications and Networks (ICCCN)*, 1–9. IEEE. (cited on pages 54, 68, 77, 78, and 103)

Choi, W.; Ghidini, G.; and Das, S. K., 2012. A novel framework for energy-efficient data gathering with random coverage in wireless sensor networks. *ACM Transactions on Sensor Networks (ToSN)*, 8, 4 (2012), 1–30. (cited on page 51)

Chowdhury, A. and A Raut, S., 2019. Benefits, challenges, and opportunities in adoption of industrial iot. *International Journal of Computational Intelligence & IoT*, 2, 4 (2019). (cited on page 1)

Di Francesco, M.; Das, S. K.; and Anastasi, G., 2011. Data collection in wireless sensor networks with mobile elements: A survey. *ACM Transactions on Sensor Networks (TOSN)*, 8, 1 (2011), 1–31. (cited on page 51)

Di Valerio, V.; Presti, F. L.; Petrioli, C.; Picari, L.; Spaccini, D.; and Basagni, S., 2019. Carma: Channel-aware reinforcement learning-based multi-path adaptive routing for underwater wireless sensor networks. *IEEE Journal on Selected Areas in Communications*, 37, 11 (2019), 2634–2647. (cited on page 17)

Dorri, A.; Kanhere, S. S.; Jurdak, R.; and Gauravaram, P., 2017. Blockchain for iot security and privacy: The case study of a smart home. In *2017 IEEE international conference on pervasive computing and communications workshops (PerCom workshops)*, 618–623. IEEE. (cited on page 51)

Farajzadeh, A.; Ercetin, O.; and Yanikomeroglu, H., 2019. Uav data collection over noma backscatter networks: Uav altitude and trajectory optimization. In *ICC 2019-2019 IEEE International Conference on Communications (ICC)*, 1–7. IEEE. (cited on pages 7, 8, and 52)

Fraga-Lamas, P.; Fernández-Caramés, T. M.; Suárez-Albela, M.; Castedo, L.; and González-López, M., 2016. A review on internet of things for defense and public safety. *Sensors*, 16, 10 (2016), 1644. (cited on page 1)

Fu, L.; Cheng, P.; Gu, Y.; Chen, J.; and He, T., 2015. Optimal charging in wireless rechargeable sensor networks. *IEEE Transactions on Vehicular Technology*, 65, 1 (2015), 278–291. (cited on pages 95 and 102)

Gao, S.; Zhang, H.; and Das, S. K., 2010. Efficient data collection in wireless sensor networks with path-constrained mobile sinks. *IEEE Transactions on mobile computing*, 10, 4 (2010), 592–608. (cited on page 51)

Ghorbel, M. B.; Rodriguez-Duarte, D.; Ghazzai, H.; Hossain, M. J.; and Menouar, H., 2018. Energy efficient data collection for wireless sensors using drones. In *2018 IEEE 87th Vehicular Technology Conference (VTC Spring)*, 1–5. IEEE. (cited on page 18)

Ghosal, A.; Halder, S.; and Das, S. K., 2020. Distributed on-demand clustering algorithm for lifetime optimization in wireless sensor networks. *Journal of Parallel and Distributed Computing*, 141 (2020), 129–142. (cited on page 51)

Gong, J.; Chang, T.-H.; Shen, C.; and Chen, X., 2018a. Aviation time minimization of uav for data collection from energy constrained sensor networks. In *2018 IEEE Wireless Communications and Networking Conference (WCNC)*, 1–6. IEEE. (cited on pages 5 and 86)

Gong, J.; Chang, T.-H.; Shen, C.; and Chen, X., 2018b. Flight time minimization of uav for data collection over wireless sensor networks. *IEEE Journal on Selected Areas in Communications*, 36, 9 (2018), 1942–1954. (cited on pages 3 and 43)

Gu, F.; Niu, J.; Das, S. K.; He, Z.; and Jin, X., 2017. Detecting breathing frequency and maintaining a proper running rhythm. *Pervasive and Mobile Computing*, 42 (2017), 498–512. (cited on page 51)

Guo, J.; Wang, T.; He, Y.; Jin, M.; Jiang, C.; and Liu, Y., 2019. Twinleak: Rfid-based liquid leakage detection in industrial environments. In *IEEE IN-*

FOCOM 2019-IEEE Conference on Computer Communications, 883–891. IEEE. (cited on page 17)

Imon, S. K. A.; Khan, A.; Di Francesco, M.; and Das, S. K., 2014. Energy-efficient randomized switching for maximizing lifetime in tree-based wireless sensor networks. *IEEE/ACM transactions on networking*, 23, 5 (2014), 1401–1415. (cited on page 51)

Jia, Z.; Sheng, M.; Li, J.; Niyato, D.; and Han, Z., 2021. Leo-satellite-assisted uav: Joint trajectory and data collection for internet of remote things in 6g aerial access networks. *IEEE Internet of Things Journal*, 8, 12 (2021), 9814–9826. doi:10.1109/JIOT.2020.3021255. (cited on page 6)

Khelifi, F.; Bradai, A.; Singh, K.; and Atri, M., 2018. Localization and energy-efficient data routing for unmanned aerial vehicles: Fuzzy-logic-based approach. *IEEE Communications Magazine*, 56, 4 (2018), 129–133. (cited on page 6)

Khochare, A.; Simmhan, Y.; Sorbelli, F. B.; and Das, S. K., 2021. Heuristic algorithms for co-scheduling of edge analytics and routes for uav fleet missions. In *IEEE INFOCOM 2021-IEEE Conference on Computer Communications*, 1–10. IEEE. (cited on pages 4 and 51)

Kodeswaran, P.; Kokku, R.; Mallick, M.; and Sen, S., 2016. Demultiplexing activities of daily living in iot enabled smarthomes. In *IEEE INFOCOM 2016-The 35th Annual IEEE International Conference on Computer Communications*, 1–9. IEEE. (cited on page 17)

Lee, I. and Lee, K., 2015. The internet of things (iot): Applications, investments, and challenges for enterprises. *Business horizons*, 58, 4 (2015), 431–440. (cited on page 2)

Li, M. and Lin, H.-J., 2015. Design and implementation of smart home control systems based on wireless sensor networks and power line communications. *IEEE Transactions on Industrial Electronics*, 62, 7 (2015), 4430–4442. (cited on page 2)

Li, Y.; Liang, W.; Xu, W.; and Jia, X., 2020. Data collection of iot devices using an energy-constrained uav. In *2020 IEEE International Parallel and Distributed Processing Symposium (IPDPS)*, 644–653. IEEE. (cited on pages 18, 42, 52, 86, 90, 91, and 104)

Liang, Y.; Xu, W.; Liang, W.; Peng, J.; Jia, X.; Zhou, Y.; and Duan, L., 2018. Nonredundant information collection in rescue applications via an energy-constrained uav. *IEEE Internet of Things Journal*, 6, 2 (2018), 2945–2958. (cited on pages 4, 43, and 51)

Lin, C.; Guo, C.; Dai, H.; Wang, L.; and Wu, G., 2019. Near optimal charging scheduling for 3-d wireless rechargeable sensor networks with energy constraints. In *2019 IEEE 39th International Conference on Distributed Computing Systems (ICDCS)*, 624–633. IEEE. (cited on pages 19 and 23)

Liu, J.; Wang, X.; Bai, B.; and Dai, H., 2018. Age-optimal trajectory planning for uav-assisted data collection. In *IEEE INFOCOM 2018-IEEE Conference on Computer Communications Workshops (INFOCOM WKSHPS)*, 553–558. IEEE. (cited on pages 52 and 86)

Liu, X.; Cao, J.; Lai, S.; Yang, C.; Wu, H.; and Xu, Y. L., 2011. Energy efficient clustering for wsn-based structural health monitoring. In *2011 Proceedings IEEE INFOCOM*, 2768–2776. IEEE. (cited on page 85)

Luo, C.; Feng, X.; Chen, J.; Li, J.; Xu, W.; Li, W.; Zhang, L.; Tari, Z.; and Zomaya, A. Y., 2019. Brush like a dentist: accurate monitoring of toothbrushing via wrist-worn gesture sensing. In *IEEE INFOCOM 2019-IEEE Conference on Computer Communications*, 1234–1242. IEEE. (cited on page 17)

Mark, d. B.; Otfried, C.; Marc, v. K.; and Mark, O., 2008. *Computational geometry algorithms and applications*. Spinger. (cited on page 102)

Mavrogiorgou, A.; Kiourtis, A.; Perakis, K.; Pitsios, S.; and Kyriazis, D., 2019. Iot in healthcare: Achieving interoperability of high-quality data acquired by iot medical devices. *Sensors*, 19, 9 (2019), 1978. (cited on page 1)

Mozaffari, M.; Saad, W.; Bennis, M.; and Debbah, M., 2016. Mobile internet of things: Can uavs provide an energy-efficient mobile architecture? In *2016 IEEE global communications conference (GLOBECOM)*, 1–6. IEEE. (cited on pages 7, 8, 18, 21, 52, and 86)

Navarra, A.; Pinotti, C. M.; Di Francesco, M.; and Das, S. K., 2015. Interference-free scheduling with minimum latency in cluster-based wireless sensor networks. *Wireless Networks*, 21, 7 (2015), 2395–2411. (cited on page 51)

Nazib, R. A. and Moh, S., 2021. Energy-efficient and fast data collection in uav-aided wireless sensor networks for hilly terrains. *IEEE Access*, 9 (2021), 23168–23190. doi:10.1109/ACCESS.2021.3056701. (cited on page 6)

Ometov, A.; Masek, P.; Malina, L.; Florea, R.; Hosek, J.; Andreev, S.; Hajny, J.; Niutanen, J.; and Koucheryavy, Y., 2016. Feasibility characterization of cryptographic primitives for constrained (wearable) iot devices. In *2016 IEEE International Conference on Pervasive Computing and Communication Workshops (PerCom Workshops)*, 1–6. IEEE. (cited on page 51)

Othman, M. F. and Shazali, K., 2012. Wireless sensor network applications: A study in environment monitoring system. *Procedia Engineering*, 41 (2012), 1204–1210. (cited on page 2)

Poudel, S. and Moh, S., 2021. Hybrid path planning for efficient data collection in uav-aided wsns for emergency applications. *Sensors*, 21, 8 (2021), 2839. (cited on page 7)

Roy, S.; Ghosh, N.; and Das, S. K., 2019. biosmartsense: A bio-inspired data collection framework for energy-efficient, qoi-aware smart city applications. In *2019 IEEE International Conference on Pervasive Computing and Communications (PerCom*, 1–10. IEEE. (cited on page 51)

Samir, M.; Sharafeddine, S.; Assi, C. M.; Nguyen, T. M.; and Ghrayeb, A., 2019. Uav trajectory planning for data collection from time-constrained iot devices. *IEEE Transactions on Wireless Communications*, 19, 1 (2019), 34–46. (cited on pages 4, 6, 18, 51, and 56)

Say, S.; Inata, H.; Liu, J.; and Shimamoto, S., 2016. Priority-based data gathering framework in uav-assisted wireless sensor networks. *IEEE Sensors Journal*, 16, 14 (2016), 5785–5794. (cited on page 86)

Sfar, A. R.; Chtourou, Z.; and Challal, Y., 2017. A systemic and cognitive vision for iot security: A case study of military live simulation and security challenges. In *2017 International Conference on Smart, Monitored and Controlled Cities (SM2C)*, 101–105. doi:10.1109/SM2C.2017.8071828. (cited on page 1)

Shahanaghi, A.; Yang, Y.; and Buehrer, R. M., 2019. On the stochastic link modeling of static wireless sensor networks in ocean environments. In *IEEE INFOCOM 2019-IEEE Conference on Computer Communications*, 1144–1152. IEEE. (cited on page 85)

Sun, M.; Xu, X.; Qin, X.; and Zhang, P., 2021. Aoi-energy-aware uav-assisted data collection for iot networks: A deep reinforcement learning method. *IEEE Internet of Things Journal*, 8, 24 (2021), 17275–17289. doi:10.1109/JIOT.2021.3078701. (cited on page 6)

Sutar, S. H.; Koul, R.; and Suryavanshi, R., 2016. Integration of smart phone and iot for development of smart public transportation system. In *2016 international conference on internet of things and applications (IOTA)*, 73–78. IEEE. (cited on page 1)

Theunissen, J.; Xu, H.; Zhong, R. Y.; and Xu, X., 2018. Smart agv system for manufacturing shopfloor in the context of industry 4.0. In *2018 25th International Conference on Mechatronics and Machine Vision in Practice (M2VIP)*, 1–6. IEEE. (cited on pages 42 and 77)

Trotta, A.; Di Felice, M.; Bononi, L.; Natalizio, E.; Perilli, L.; Scarselli, E. F.; Cinotti, T. S.; and Canegallo, R., 2019. Bee-drones: Energy-efficient data collection on wake-up radio-based wireless sensor networks. In *IEEE INFOCOM 2019-IEEE Conference on Computer Communications Workshops (INFOCOM WKSHPS)*, 547–553. IEEE. (cited on page 52)

Tse, D. and Viswanath, P., 2005. *Fundamentals of wireless communication*. Cambridge university press. (cited on page 90)

Đurišić, M. P.; Tafa, Z.; Dimić, G.; and Milutinović, V., 2012. A survey of military applications of wireless sensor networks. In *Embedded Computing (MECO), 2012 Mediterranean Conference on*, 196–199. IEEE. (cited on page 2)

Wang, J.; Liu, Y.; and Das, S. K., 2010. Energy-efficient data gathering in wireless sensor networks with asynchronous sampling. *ACM Transactions on Sensor Networks (TOSN)*, 6, 3 (2010), 1–37. (cited on page 51)

Xiao, B.; Cao, J.; Zhuge, Q.; He, Y.; and Sha, E.-M., 2004. Approximation algorithms design for disk partial covering problem. In *7th International Symposium on Parallel Architectures, Algorithms and Networks, 2004. Proceedings.*, 104–109. IEEE. (cited on pages 62 and 100)

Xiong, R. and Shan, F., 2018. Dronetank: Planning uavs' flights and sensors' data transmission under energy constraints. *Sensors*, 18, 9 (2018), 2913. (cited on pages 90, 103, and 104)

Yi, M.; Wang, X.; Liu, J.; Zhang, Y.; and Bai, B., 2020. Deep reinforcement learning for fresh data collection in uav-assisted iot networks. In *IEEE INFOCOM 2020 - IEEE Conference on Computer Communications Workshops (INFOCOM WKSHPS)*, 716–721. doi:10.1109/INFOCOMWKSHPS50562.2020.9162896. (cited on page 7)

Zhan, C.; Zeng, Y.; and Zhang, R., 2017. Energy-efficient data collection in uav enabled wireless sensor network. *IEEE Wireless Communications Letters*, 7, 3 (2017), 328–331. (cited on page 18)

Zhang, J.; Li, Z.; Xu, W.; Peng, J.; Liang, W.; Xu, Z.; Ren, X.; and Jia, X., 2021. Minimizing the number of deployed uavs for delay-bounded data collection of iot devices. In *IEEE INFOCOM 2021-IEEE Conference on Computer Communications*, 1–10. IEEE. (cited on pages 52 and 86)